FABRICATION OF POLYMERIC MICROGELS USING MICROFLUIDICS: APPLICATIONS IN BIOLOGICAL SENSING AND DRUG DELIVERY

by

Sinem ORBAY

B.S., in Biomedical Engineering, Erciyes University, 2012

M.S., in Bioengineering, Pennsylvania State University, 2016

Submitted to the Institute of Biomedical Engineering

in partial fulfillment of the requirements

for the degree of

Doctor

of

Philosophy

Boğaziçi University

2024

FABRICATION OF POLYMERIC MICROGELS USING MICROFLUIDICS: APPLICATIONS IN BIOLOGICAL SENSING AND DRUG DELIVERY

APPROVED BY:

Prof. Amitav Sanyal (Thesis Supervisor)	.....
Prof. Bora Garipcan	.....
Prof. Rana Sanyal	.....
Assoc. Prof. Mehmet Arslan	.....
Assist. Prof. Özgül Gök Özatay	.....

DATE OF APPROVAL: 03.01.2024

ACKNOWLEDGEMENTS

I would like to express my appreciation to my thesis advisor Prof. Amitav Sanyal, for the opportunities and for his consistent guidance, support, encouragement, and advice.

I want to show my gratitude to Prof. Rana Sanyal, Prof. Bora Garipcan, Assoc. Prof. Mehmet Arslan, and Assist. Prof. Özgül Gök Özatay for their dedicated service on my committee. I highly appreciate their insightful questions and comments, which added significant value to my work.

I want to thank the members of the Sanyal Group for their collaborative spirit, friendship, and support. Special thanks to Nora Ejderyan for her friendship and continuous support. Thanks to Yavuz Öz for the mentorship, Meltem Alkış and Rüveyda Kılıç Boz for the synthesis of monomers and Aysun Değirmenci for the dyes used in the thesis, and Damla Kayhan for the cell studies. I also want to acknowledge Bogazici University Research Fund (Project Code: 50009, Boun Code: 23BYOKADP1) for the financial support towards the completion of this thesis. I want to thank Erzincan Binali Yıldırım University for allowing me to complete my Ph.D. studies in Bogazici University.

I thank my friends for their unwavering support, attentive ears, and significant contribution in making my Ph.D. journey considerably smoother.

I extend my deepest gratitude to my family members— Ayşe Orbay, Ali Orbay, Buket Orbay Öztürk, and Seçkin Öztürk —for standing by me, offering unwavering support through all circumstances, and, above all, for their boundless love and care.

ACADEMIC ETHICS AND INTEGRITY STATEMENT

I, Sinem Orbay, here by certify that I am aware of the Academic Ethics and Integrity Policy issued by the Council of Higher Education(YÖK) and I fully acknowledge all the consequences due to its violation by plagiarism or any other way.

Name :

Signature:

Date:

Dedicated to my dad...

ABSTRACT

FABRICATION OF POLYMERIC MICROGELS USING MICROFLUIDICS: APPLICATIONS IN BIOLOGICAL SENSING AND DRUG DELIVERY

This thesis focuses on developing polymeric microgels designed to serve various biomedical applications. The fabrication involves microfluidics technology, where unique microchannels are designed and manufactured to produce these microgels. One notable aspect of polymeric microgels is their chemistries, allowing further functionalization to suit specific applications. Using microfluidics technology in the fabrication process ensures precise control and scalability, enhancing these polymeric microgels' potential applications and significant influence in the biomedical field. In the first chapter, we demonstrated monodispersed non-degradable microgels produced by flow-focusing microfluidics channels for protein *catch-and-release* studies. Following, we synthesized microgels of varying porosities using a Y-shaped microfluidic channel and identified the most porous material for comprehensive in vitro drug delivery studies. The succeeding chapter demonstrates degradable microgels that undergo cross-linking as they traverse the serpentine channels within the microfluidics device. These degradable polymeric materials were accompanied by another reducing agent carrying microgels system. The final chapter is about another kind of polymeric material, imprinted polymers, which were fabricated using different polymerization methods. Obtained materials with different sizes were evaluated by their biomarker-catching performances. In summary, this thesis explores various polymeric microgel systems fabricated by distinct microfluidics channel designs. Each has unique features to be functionalized for multiple biomedical applications.

Keywords: Polymeric Microgels, Microfluidics, Droplet-based Microfluidics, Protein Catch&Release, Therapeutic Delivery, Molecularly Imprinted Polymers

ÖZET

MİKRO AKIŞKANLAR KULLANARAK POLİMERİK MİKROJEL ÜRETİMİ: BİYOLOJİK ALGILAMA VE İLAÇ TESLİMİ UYGULAMALARI

Bu tez, biyomedikal alanındaki çeşitli uygulamalarda kullanılmak üzere polimerik mikrojellerin tasarlanması ve üretilmesine odaklanmaktadır. Polimerik mikrojellerin üretimi için özel mikrokanalların tasarlanıp üretildiği mikroakışkanlar teknolojisi kullanılmıştır. Polimerik mikrojellerin dikkate değer bir özelliği, özel uygulamalara uygun hale getirilmelerini sağlayan kimyasal yapılarıdır. Mikroakışkanlar teknolojisinin kullanımı, üretim sürecinde hassas kontrol ve ölçeklenebilirlik sunarak bu polimerik mikrojellerin potansiyel uygulamalarını artırmakta ve biyomedikal alanındaki etkilerini güçlendirmektedir. Tezin ilk bölümünde, akış odaklı mikroakışkan kanallar aracılığıyla monodispers mikrojeller üretilmiş ve protein *yakalama ve salım* çalışmaları için kullanılmıştır. Daha sonra, bir Y-şekilli mikroakışkan kanal kullanılarak farklı gözenekli yapılara sahip mikrojeller sentezlenmiş ve en gözenekli malzeme belirlenerek kapsamlı in vitro ilaç teslim çalışmalarında kullanılmıştır. Bir sonraki bölüm, mikroakışkan cihaz içinde dolaşırken çapraz bağ oluşturan, bozulabilir mikrojellerin üretilmesini ele almaktadır. Bu bozulabilir polimerik malzemelere, başka bir indirgeyici ajan taşıyan mikrojel sistemleri eşlik etmektedir. Son bölüm, farklı boyutlarda üretilmiş polimerik malzemeleri ve bunların biyobelirteç yakalama performanslarını içeren bir diğer polimerik malzeme olan moleküler baskılı polimerlerin üretimine odaklanmaktadır. Özetle, bu tez, farklı mikroakışkan tasarımlarını kullanarak üretilen çeşitli polimerik mikrojel sistemlerini incelemektedir. Her bir mikrojel sistemi, çeşitli biyomedikal uygulamalar için tasarlanabilir ve benzersiz özelliklere sahip olabilir.

Anahtar Kelimeler: Polimerik Mikrojeller, Mikroakışkanlar, Damla-tabanlı Mikroakışkanlar, Protein Yakalama&Salma, Terapötik Teslimat, Moleküler Baskılı Polimerler

TABLE OF CONTENTS

ACKNOWLEDGEMENTS . . . iii
ACADEMIC ETHICS AND INTEGRITY STATEMENT . . . iv
ABSTRACT . . . vi
ÖZET . . . vii
LIST OF FIGURES . . . xii
LIST OF TABLES . . . xvii
LIST OF ACRONYMS/ABBREVIATIONS . . . xviii
1. INTRODUCTION . . . 1
1.1 Polymeric Materials used in Biomedical Applications . . . 1
1.1.1 Polymeric Microgels . . . 2
1.1.2 Fabrication of Polymeric Microgels . . . 8
1.2 Microfluidics for Biomedical Applications . . . 11
1.2.1 Microfluidics . . . 11
1.2.2 Fabrication of Droplet-based Microfluidics Channels . . . 12
1.2.3 Photolithography-Master Mold Fabrication . . . 13
1.2.3.1 Mask Design . . . 13
1.2.3.2 Photoresist . . . 13
1.2.3.3 Soft-baking . . . 14
1.2.3.4 Photo Mask Alignment and UV Exposure . . . 15
1.2.3.5 Post-baking . . . 16
1.2.3.6 Development . . . 16
1.2.4 Soft Lithography-PDMS Casting, Replica Molding and Bonding 16
1.2.5 Microfluidics for Polymeric Microgels Synthesis . . . 17
1.2.6 Overview of the Droplet-based Microfluidics Channels . . . 19
2. MICROFLUIDICS ASSISTED MICROGELS FABRICATION: UTILIZING THIOL-DISULFIDE EXCHANGE FOR REVERSIBLE PROTEIN CAPTURE . . . 21
2.1 Introduction . . . 21
2.2 Experimental . . . 23
2.2.1 Materials and Characterization . . . 23

2.2.2 Fabrication of Flow-focusing Droplet-based Microfluidics Channel 24
2.2.3 Preparation of PDS-group containing Polymeric Microgels . . . 25
2.2.4 Pyridothione Release Studies 25
2.2.5 Conjugation and Release of Bodipy-SH 25
2.2.6 Conjugation and Release of a Protein 27
2.2.7 Extravidin Selectivity-Catch&Release from the Protein Mixture 27
2.2.8 Incorporation of PEG 10kDa 28
2.3 Results and Discussion 28
2.3.1 PDS-group-containing Polymeric Microgels 28
2.3.2 Functionalization of PDS-group-containing Microgels 29
2.3.3 Catch&release of TRITC-extravidin and Selectivity Study . . . 31
2.3.4 Catch&release of TRITC-extravidin from Porous and Non-porous Microgels 35
2.4 Conclusion 38
3. POROUS MICROGELS FOR DELIVERY OF CURCUMIN: MICROFLUIDICS-BASED FABRICATION AND CYTOTOXICITY EVALUATION 39
3.1 Introduction 39
3.2 Experimental 42
3.2.1 Materials and Characterization 42
3.2.2 Y-shaped Droplet-based Microfluidics Channel Fabrication . . . 43
3.2.3 Microgels Synthesis via Microfluidics 44
3.2.4 Morphological Analysis Using Scanning Electron Microscopy (SEM) 46
3.2.5 Curcumin + HP-β-CD Complexation 46
3.2.6 Curcumin Loading and Release 46
3.2.7 Drug Release Kinetic Models 46
3.2.8 Antioxidant Activity 47
3.2.9 In Vitro Cytotoxicity and Internalization 47
3.3 Results and Discussion 48
3.3.1 Microgels Synthesis and Characterization 48
3.3.2 Curcumin Loading and Release 53
3.3.3 Drug Release Kinetic Models 56
3.3.4 Antioxidant Activity of Curcumin-Loaded Microgels 58

3.3.5 In Vitro Studies . . . 59
3.4 Conclusion . . . 61
4. MICROFLUIDICS-ASSISTED FABRICATION OF DEGRADABLE POLYMERIC MICROGELS . . . 62
4.1 Introduction . . . 62
4.2 Experimental . . . 64
4.2.1 Materials and Characterization . . . 64
4.2.2 Microfluidics Channels Fabrication . . . 65
4.2.3 Degradable Microgels Fabrication via Microfluidics . . . 66
4.2.4 Reducing Agent Carrier Microgels Fabrication via Microfluidics 68
4.2.5 Degradation of Microgels . . . 68
4.2.6 Encapsulation and Release of Protein . . . 69
4.3 Results and Discussion . . . 69
4.3.1 Degradable Microgels Fabrication via Microfluidics . . . 69
4.3.2 HP-β-CD-containing Microgels Production via Microfluidics . . 72
4.3.3 Degradation of Microgels . . . 75
4.3.4 FITC-BSA Encapsulation and Release Studies . . . 78
4.4 Conclusion . . . 80
5. MOLECULARLY IMPRINTED POLYMERS FOR BIOMARKER DETECTION . . . 81
5.1 Introduction . . . 81
5.2 Experimental . . . 84
5.2.1 Materials and Characterization . . . 84
5.2.2 Molecularly Imprinted Polymers (MIPs) Synthesis . . . 84
5.2.3 Rebinding the Target Molecule . . . 85
5.2.4 Different Fabrication Methods for Dopamine-Imprinted Polymeric Materials . . . 86
5.3 Results and Discussion . . . 86
5.3.1 Molecularly Imprinted Polymers (MIPs) Design for Dopamine Template . . . 86
5.3.1.1 Bulk Polymerization . . . 86
5.3.1.2 Precipitation Polymerization . . . 87

5.3.1.3 W/O Emulsion Polymerization in Microfluidics 87
5.3.2 Template Removal 90
5.3.3 Dopamine Rebinding 90
5.3.4 Imprinting Factor (IF) Calculations 92
5.4 Conclusion 92
6. CONCLUSION 94
REFERENCES 95
APPENDIX A. SUPPLEMENTARY DATA 107
APPENDIX B. COPYRIGHT NOTICES 111

LIST OF FIGURES

Figure 1.1	Polymeric materials employed in biomedical applications.	1
Figure 1.2	Polymeric microgels and their biomedical applications.	3
Figure 1.3	The double cross-linked PNIPAM microgel dots exhibit a reversible redox-responsive feature, with permanent cross-linking through BIS and reversible cross-linking via the disulfide bonds of BAC.	5
Figure 1.4	(a) Illustration of KGN-loaded liposomes and the GelMA-liposome interactions established through non-covalent bonding, (b) demonstration of the fabrication of KGN-loaded GelMA@Lipo hybrid microgel (GelMA@Lipo@KGN) via microfluidics, (c) illustration of KGN release from GelMA@Lipo microgels.	6
Figure 1.5	Schematic representation of the glucose-imprinted poly(NIPAM-AAm-VPBA)-CDs microgels for glucose detection.	7
Figure 1.6	Fabrication methods of polymeric microgels, (a) mechanical crushing, (b) emulsion polymerization, (c) lithography methods, (d) microfluidics emulsion.	9
Figure 1.7	Microfluidics for biomedical applications.	11
Figure 1.8	Schematic demonstration of photolithography process.	13
Figure 1.9	A sample mask design rendered in AutoCAD illustrations.	14
Figure 1.10	Spin Speed vs Thickness (Microchem SU-8 datasheet).	15
Figure 1.11	Schematic illustration of PDMS casting and replica molding processes.	17
Figure 1.12	Different microchannel configurations for microgels fabrication: (a) T-junction/Y-junction, (b) flow-focusing, (c) co-flow configuration.	18
Figure 1.13	Illustration of droplet-based microfluidics channels.	20
Figure 2.1	General scheme of the concept.	22
Figure 2.2	General and chemical scheme of PDS-group containing microgels fabrication via microfluidics.	26

Figure 2.3 (a) A fluorescence image of monodisperse PDS-group containing microgels (Scale 200 μm), (b) SEM image of the PDS-group containing microgel, (c) size distribution of the microgels. 29

Figure 2.4 (a) Functionalization of the microgels with DTT, (b) associated pyridothione release profiles of various amount PDS-group containing microgels. 30

Figure 2.5 (a) Functionalization of the microgels with Bodipy-SH, (b) fluorescence microscopy images of Bodipy-SH conjugated microgels (Scale 200 μm). 32

Figure 2.6 (a) Illustration of TRITC-extravidin capture by the Biotin-SH conjugated microgels and subsequent release, (b) fluorescence microscopy images of TRITC-extravidin immobilization onto the mirogels with the comparison of control group (Scale 100 μm). 33

Figure 2.7 (a) Illustration of TRITC-extravidin capture by the Biotin-SH conjugated microgels in a protein mixture and subsequent release, (b) fluorescence microscopy images of selectivity profile of the microgels (Scale 100 μm). 34

Figure 2.8 (a) General demonstration of incorporation of PEG 10 kDa into microgels system, (b) SEM images of porous microgel. 36

Figure 2.9 Fluorescence microscopy images of TRITC-extravidin immobilization onto the microgels with the comparison of porosity (Scale 100 μm). 37

Figure 2.10 Quantification of protein amounts for catch&release process in both porous and non-porous microgels. 37

Figure 3.1 General demonstration of the concept. 41

Figure 3.2 (a) General illustration of microfluidics fabrication of polymeric microgels, (b) chemical scheme of microgel formation, (c) real droplet generator in operation, (d) optical image of monodispersed microgels at dry stage produced via microfluidics (Scale 200 μm). 45

Figure 3.3 Size distribution of microgels. (a) Microgels with PEGMEMA, (b) microgels without PEGMEMA (Scale 200 μm). 50

Figure 3.4	SEM images of microgels. (a) Microgels with PEGMEMA, (b) microgels without PEGMEMA.	51
Figure 3.5	(a) Volume changes of microgels, (b) P-PEGMEMA-PEGDA microgels swelling profile video images (Scale 200 μm).	52
Figure 3.6	(a) Curcumin and β-cyclodextrin (HP-β-CD) complexation and solubilities in DI water, (b) the differences of only curcumin-loaded and inclusion complex-loaded microgels under the same exposure (Scale 200 μm).	54
Figure 3.7	Curcumin loading to different microgel systems.	55
Figure 3.8	Curcumin Release from P-PEGMEMA-PEGDA microgels in DI Water + Tween20 (0.5%) and cell medium (Scale 200 μm).	55
Figure 3.9	Model fitting of curcumin release kinetics. (a) Zero order model, (b) first order model, (c) Higuchi model, and (d) Korsmeyer-Peppas model.	57
Figure 3.10	(a) Curcumin reaction with DPPH, (b) DPPH radical color change in the presence of curcumin, (c) DPPH radical scavenging UV spectroscopy result.	59
Figure 3.11	(a) Cell viability, (b) internalization of curcumin released from microgels (Scale 100 μm).	60
Figure 4.1	General demonstration of the concept.	64
Figure 4.2	(a) Droplet-based microfluidics channel for degradable microgels production, (b) chemical demonstration of the degradable microgels and a fluorescence image of dye-conjugated degradable microgels (Scale 200 μm).	67
Figure 4.3	Illustration of microfluidics fabrication of HP-β-CD containing non-degradable microgels (Scale 200 μm).	68
Figure 4.4	Optical microscopy images capturing various degradable microgels were taken immediately upon exiting the outlet tube, along with size distribution graphs. (a) MG1, (b) MG2, (c) MG3 (Scale 200 μm).	70
Figure 4.5	SEM images of the degradable gels (MG1 and MG2).	71

Figure 4.6	(a) Size changes of degradable microgel from dry to wet stage, (b) volume change graph, (c) time-lapse optical microscopy images showing the swelling process (Scale 200 μm).	71
Figure 4.7	Optical images and size distribution of different amount of HP-β-CD containing microgels as reducing agent carrier. (a) 10%, (b) 30%, (c) 50% (Scale 200 μm).	73
Figure 4.8	(a) HP-β-CD containing microgels at dry stage, (b) HP-β-CD containing microgels in water, (c) size changes from dry to wet stage, (d) percentage change in volume (Scale 200 μm).	74
Figure 4.9	SEM images of 50% HP-β-CD-containing microgels.	75
Figure 4.10	Degradation profile of bodipy-maleimide conjugated microgels in the presence of reducing agent-carrier microgels (Scale 200 μm).	76
Figure 4.11	Control experiments without loading reducing agent to microgels (Scale 200 μm).	77
Figure 4.12	Fluorescence images of FITC-BSA encapsulated microgels (Scale 200 μm).	78
Figure 4.13	Degradation profile of FITC-BSA encapsulated microgels (MG1) in the presence of DTT-loaded microgels (Scale 200 μm).	79
Figure 5.1	Schematic representation for the preparation of the molecularly imprinted polymer.	81
Figure 5.2	Illustration of various fabrication techniques for MIPs.	83
Figure 5.3	Images of the DA-imprinted and non-imprinted bulk polymers.	87
Figure 5.4	(a) Pre-polymer solution, (b) DA-imprinted nanogels produced via precipitation polymerization.	88
Figure 5.5	(a) DA-imprinted microgels produced via microfluidics (Scale 200 μm), (b) size distribution graph of DA-imprinted microgels.	88
Figure 5.6	SEM images of DA-imprinted polymeric materials synthesized by different methods.	89
Figure 5.7	Dopamine rebinding results of polymers prepared via different polymerization methods.	91
Figure 5.8	Dopamine rebinding results of polymers prepared via different polymerization methods with control groups.	91

Figure A.1	FT-IR spectra of the components of the Curcumin-HP-β-CD complex inclusion.	107
Figure A.2	H-NMR spectrum of the components of the curc/HP-β-CD complex inclusion in DMSO-d6. (a) Curcumin, (b) HP-β-CD and (c) curc/HP-β-CD inclusion complex.	108
Figure A.3	Microscopy images of microgels after release in cell medium (Scale 200 μm).	109
Figure A.4	(a) DPPH solutions introduced to the curcumin and curc/HP-β-CD complex, (b) UV-vis spectra of DPPH solution and DPPH radical scavenging.	109
Figure A.5	UV spectra of dopamine solution after 24 h.	110
Figure B.1	Copyright permission for Figure 1.3.	111
Figure B.2	Copyright permission for Figure 1.4.	112
Figure B.3	Copyright permission for Figure 1.5.	112
Figure B.4	Copyright permission for Figure 1.6.	113
Figure B.5	Copyright permission for Figure 1.7.	114
Figure B.6	Copyright permission for Figure 1.12.	115
Figure B.7	Copyright permission for Chapter 3.	116

LIST OF TABLES

Table 2.1	Microgels fabricated with varying amounts of PDS-PEGMA.	28
Table 3.1	Properties of microgels with varying monomers. While P signifies porous, NP signifies non-porous.	49
Table 4.1	Different equivalents for degradable microgels. MG signifies microgel.	69
Table 4.2	Various ratios for reducing agent carrier microgels.	72
Table 5.1	Various ratios of functional monomers and cross-linkers used for the dopamine imprinted polymer synthesis.	85
Table 5.2	Imprinting factor values of MIPs prepared by different methods.	93

LIST OF ACRONYMS/ABBREVIATIONS

AAm	Acrylamide
BAC	N,N'-bis (acryloyl) Cystamine
BIOTIN-SH	Biotinylated-hexa(ethylene glycol) Undecane Thiol
BIS	N,N'-methylenebis (acrylamide)
BSA	Bovine Serum Albumin
CD	Cyclodextrin
DA	Dopamine
DAPI	4′,6-diamidino-2-phenylindole
DMEM	Dulbecco's Modified Eagle's Medium
DMPA	2,2-Dimethoxy-2-phenylacetophenone
DMSO	Dimethyl sulfoxide
DTT	Dithiothreitol
DPPH	2,2-diphenyl-1-picrylhydrazy
EGDMA	Ethylene Glycol Dimethacrylate
ETOH	Ethanol
FITC	Fluorescein Isothiocyanate
FT-IR	Fourier-transform Infrared Spectroscopy
GSH	Glutathione
HCl	Hydrochloric Acid
HEPES	4-(2-hydroxyethyl)-1-piperazineethanesulfonic Acid
HMDS	Hexamethyldisilane
HP-β-CD	2-hydroxypropyl-β-cyclodextrin
HPLC	High Performance Liquid Chromatography
IPA	Isopropyl Alcohol
KGN	Kartogenin
LAP	Lithium phenyl-2,4,6-trimethylbenzoylphosphinate
LCST	Lower Critical Solution Temperature
NMR	Nuclear Magnetic Resonance

MEOH	Methanol
MIPs	Molecularly Imprinted Polymers
NIPs	Non-imprinted Polymers
PD	Parkinson's Disease
PBS	Phosphate-buffered Saline
PDMS	Polydimethylsiloxane
PDS	Pyridyl Disulfide
PDS-PEGMA	Pyridyl Disulfide Poly(ethylene glycol) Methacrylate
PEG	Poly(ethylene glycol)
PEGDA	Poly(ethylene glycol) Diacrylate
PEGMEMA	Poly(ethylene glycol) Methyl Ether Methacrylate
PGMEA	Propylene Glycol Monomethyl Ether Acetate
PNIPAM	Poly(N-isopropylacrylamide)
PTFE	Polytetrafluoroethylene
PP	Phenolphthalein
SEM	Scanning Electron Microscopy
SI	Silicon
SPAN 80	Sorbitan Monooleate
TRITC	Tetramethyl Rhodamine
UV-Vis	Ultraviolet-visible Spectroscopy
VPBA	Vinylphenylboronic Acid
V-501	4,4′-Azobis (4-cyanovaleric Acid)
β-CD	Beta-cyclodextrin
O/W	Oil-in-Water
W/O	Water-in-Oil

1. INTRODUCTION

1.1 Polymeric Materials used in Biomedical Applications

Polymeric materials have gained significant attention in biomedical applications due to their superb physical and chemical features, as well as their adaptability to adapt diverse functionalities tailored for specific purposes [1–4]. Commonly used polymeric materials, including hydrogels, microgels, nanogels, nanofibers, polymeric aggregates, and micelles in the biomedical field, are illustrated in Figure 1.1.

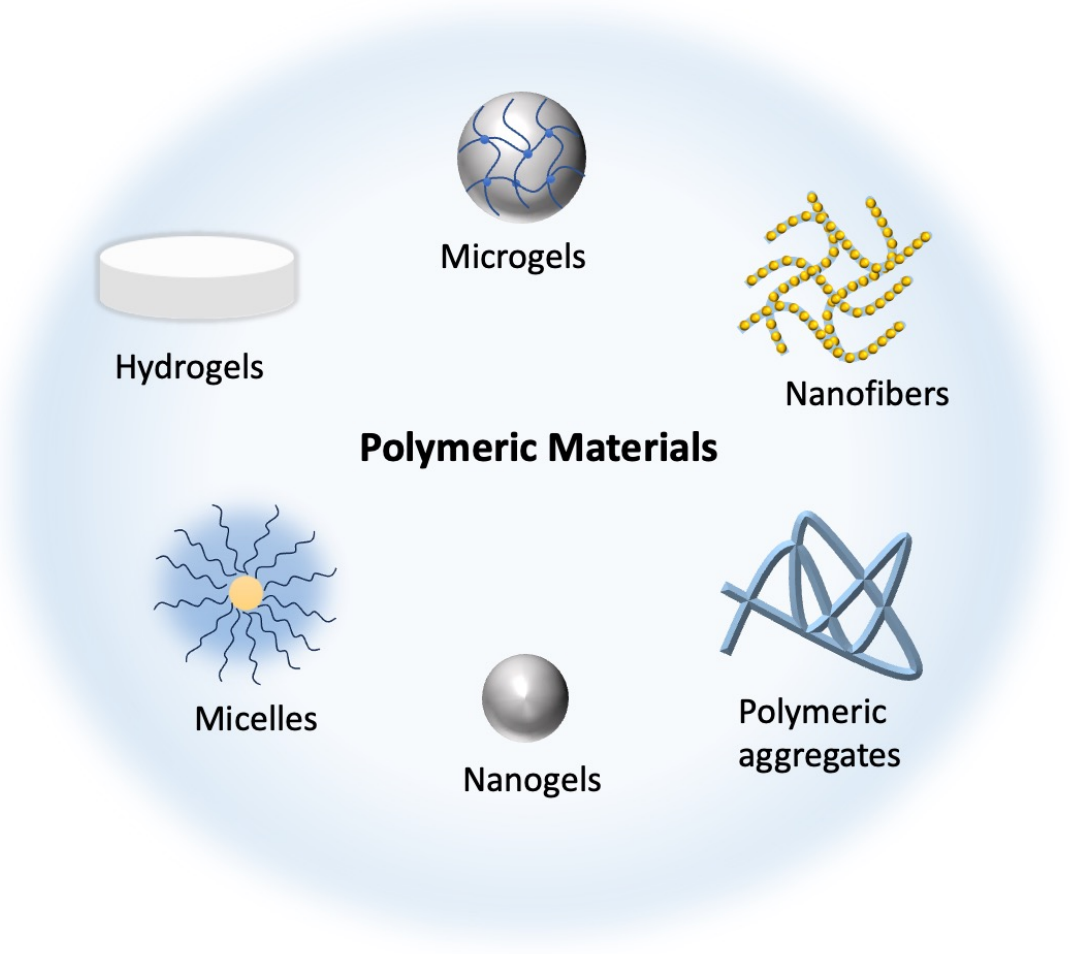

Figure 1.1 Polymeric materials employed in biomedical applications.

Polymeric materials are commonly employed in the assembly of medical devices, such as artificial joints [5], vascular grafts [6], and sutures [7], owed to their robust mechanical features and compatibility with the human body. Additionally, polymeric materials play an essential role in drug delivery systems [8, 9], enabling the controlled release of pharmaceuticals to target specific tissues or organs. Their ability to mimic the extracellular matrix makes them suitable for tissue engineering, providing a scaffold for cell growth and tissue regeneration [10]. Moreover, polymers are crucial in diagnostic tools, such as microfluidics devices [11] and biosensors [12, 13], enhancing the accuracy and sensitivity of medical tests. Polymeric materials intended for biomedical research should meet specific criteria for effectiveness and efficiency. They must exhibit minimal non-specific interactions with biomolecules, ensuring stability under physiological conditions. Furthermore, biocompatibility is critical to guarantee their compatibility with biological systems, preventing systemic toxicity. Functional polymers should also be bio-orthogonal, meaning they don't disrupt critical biochemical processes in the body. Finally, they should possess high drug-loading capabilities and the ability to ensure controlled, on-demand drug release for delivery purposes.

The introductory section of this thesis provides a concise overview of micron-sized polymeric materials and their production methods utilizing microfluidics-based methods. This section outlines these materials' significance and fundamental concepts, setting the stage for more detailed exploration in the subsequent chapters.

1.1.1 Polymeric Microgels

Polymeric microgels are colloidal materials of a three-dimensional macro-molecular network formed by cross-linked polymer chains [14]. These particles absorb large amounts of solvent, which causes them to swell and increase in size. Synthetic conditions, including monomer selection and cross-linker/initiator concentrations, offer control over properties like surface charge, size, cross-linking density, amphiphilicity, porosity, degradability, and softness [15]. Due to the solvent within, microgels resemble soft matter, exhibiting a fuzzy surface with grafting chains. Therefore, there has

been a growing interest in polymeric microgels, both in theoretical investigations on soft matter [16, 17], and in various practical applications, particularly in the field of materials science and biomedicine [18].

The fascinating interaction between their structural properties and their responsiveness to environmental changes has made polymeric microgels a subject of extensive research and innovation in fields including drug delivery [19], sensing [20], photonic crystals creation [21], bioimaging [22], as well as separation and purification technologies [23]. Figure 1.2 illustrates the different polymeric microgel systems and their biomedical applications.

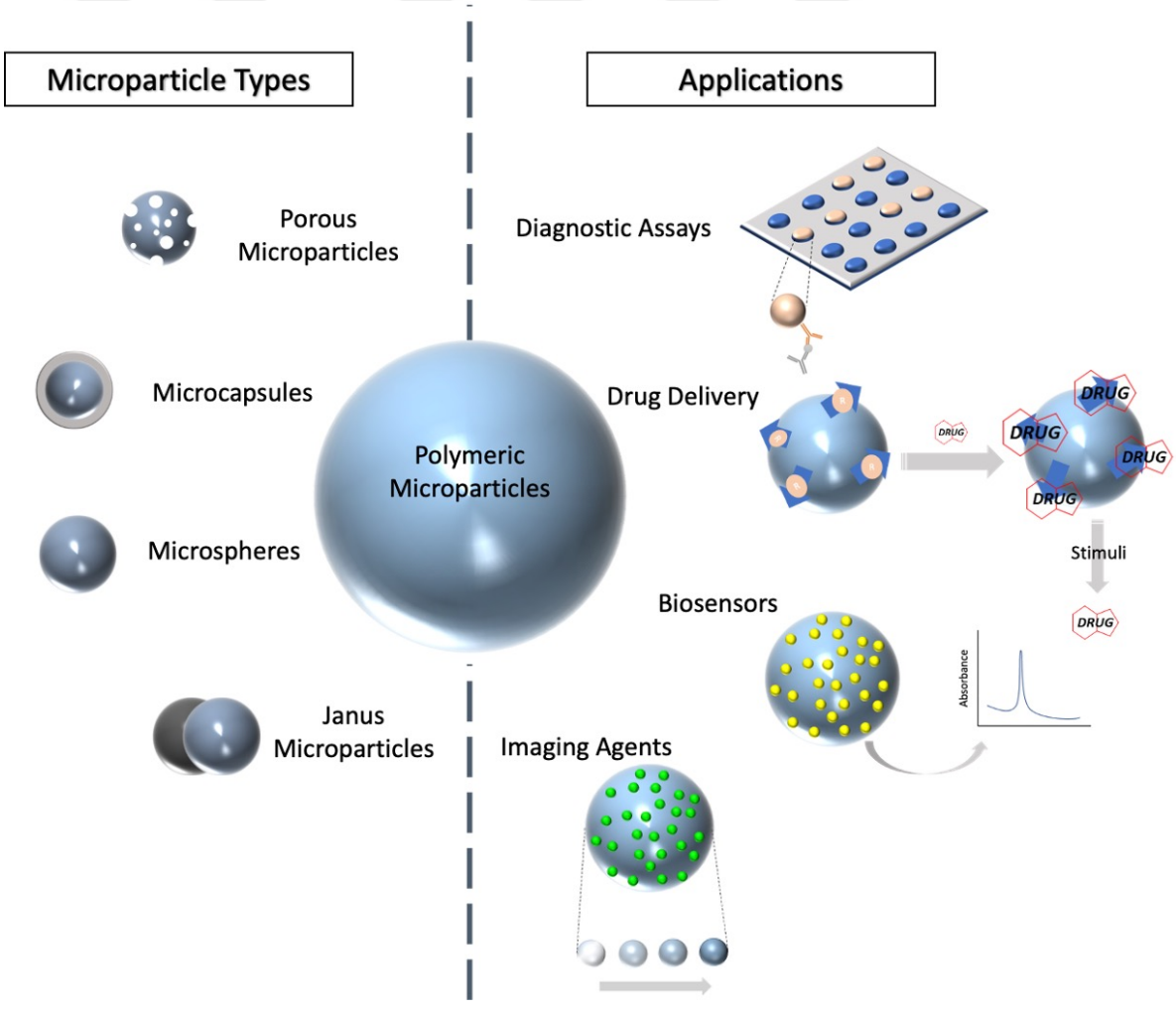

Figure 1.2 Polymeric microgels and their biomedical applications.

Microgels are classified into two primary groups based on their cross-linking methods: chemically or physically cross-linked microgels. Within microgels formed through chemical cross-linking, the junction points are permanent. In contrast, physically cross-linked microgels are held together by transient junctions formed through physical interactions like hydrogen bonding [24], ionic [25], or hydrophobic interactions [26]. Covalently cross-linked microgels can be synthesized using various methods, including free radical cross-linking and chemistry such as azide-alkyne cycloaddition [27], thiol-ene [28], and Diels-Alder reactions [29]. Chemically cross-linked microgels are typically more stable because they are formed by creating covalent bonds, unlike physically cross-linked microgels, which rely on weaker physical interactions for their network.

Chemically cross-linked microgels can be further classified by their distinct responsive properties to external or internal stimuli like pH, temperature, light, reducing agent, etc. [30]. The nature of these responsive attributes is determined by the particular functional groups present in the particles and the composition of the polymer. This strategic polymer choice or incorporation of dynamic covalent linkages enables the creation of microgels responsive to pH [31], temperature [32], mechanical force [33], as well as electric/magnetic fields [34, 35]. Among various responses to stimuli, temperature sensitivity has captured the greatest attention. PNIPAM is the extensively researched and widely employed temperature-responsive polymer, which demonstrates an LCST at approximately 32°C, aligning closely with physiologically relevant values. Recently, photothermally responsive poly(N-isopropylacrylamide-co-acrylic acid) microgels were used in cancer chemotherapy studies by Lee and co-workers [36]. On the other hand, pH-responsive microgels are extensively utilized as a smart drug delivery and release system in cancer studies [37, 38]. This is attributed to the well-established fact that cancer cells exhibit a more acidic pH (around 5.5) than healthy cells (pH 7.4). This acidic environment provides an optimal setting for triggering the release of chemotherapy drugs from the microgel network.

Microgels responsive to redox conditions can be created by utilizing dynamic disulfide-based cross-linkers, which undergo cleavage in the presence of thiol-bearing

reducing agents like DTT and GSH [39]. Voit and co-workers [40] demonstrated the incorporation of PNIPAM hydrogel into a microfluidics device by utilizing both a permanent cross-linker (BIS) and a redox-responsive reversible cross-linker (BAC) through photo-polymerization (Figure 1.3). They introduced the disulfide bonds by BAC facilitated alterations in the cross-linking densities of the micron-sized dots into the microfluidics channel. They further confirmed the endurance of microdots under the continuous flow through rheological assessments. Upon implementation, the thiol-disulfide exchange facilitated the efficient capture and release of BSA from the micron-sized dots.

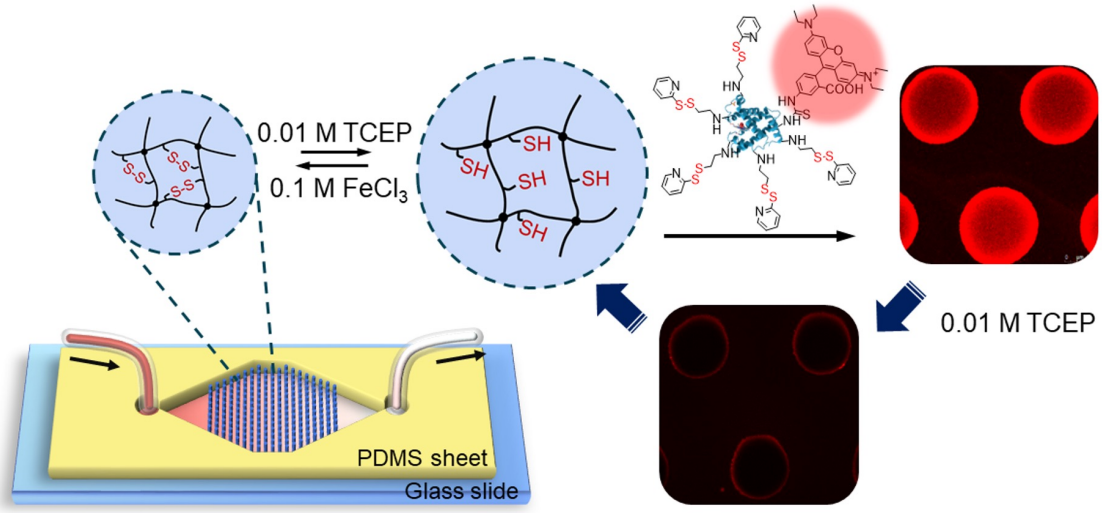

Figure 1.3 The double cross-linked PNIPAM microgel dots exhibit a reversible redox-responsive feature, with permanent cross-linking through BIS and reversible cross-linking via the disulfide bonds of BAC. Adapted with the permission of [40] © 2022 MDPI.

Microgels can be purposely designed to be biodegradable, making them highly adaptable for various applications, particularly in delivering therapeutic agents [41, 42] and proteins [43]. The delivery system within the microgels can involve either chemical cross-linking or encapsulation of the therapeutic agents or protein. Chemically cross-linked microgels, drugs/proteins are covalently attached through suitable linkers. It offers a controlled and sustained release, avoiding undesired burst releases commonly observed in physically cross-linked microgels containing encapsulated delivery agents. Cui and co-workers [44] fabricated GelMA@Lipo hybrid microgels via microfluidics fabrication to deliver KGN for osteoarthritis treatment (Figure 1.4). They achieved the

extended KGN release over time, ultimately leading to the differentiation of chondrocytes. Subsequently, in vitro studies delved into examining the degradation dynamics and release profile of microgels.

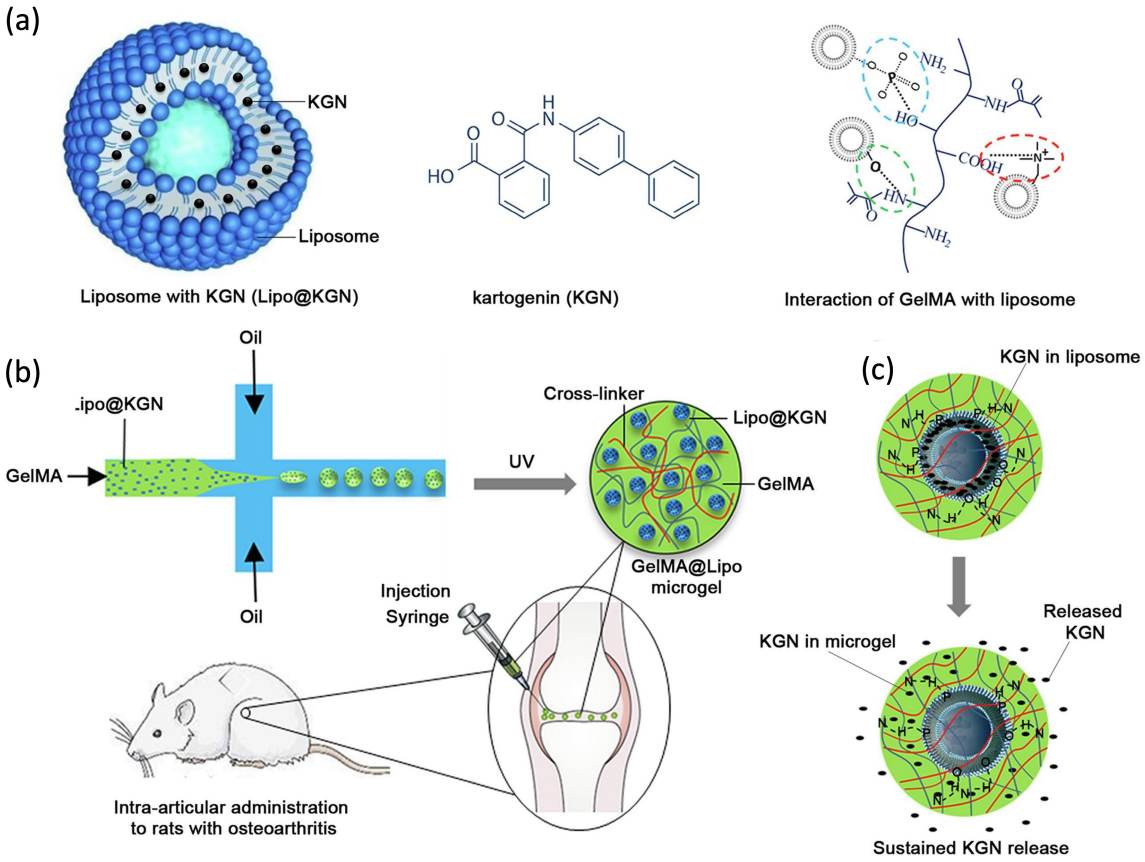

Figure 1.4 (a) Illustration of KGN-loaded liposomes and the GelMA-liposome interactions established through non-covalent bonding, (b) demonstration of the fabrication of KGN-loaded GelMA@Lipo hybrid microgel (GelMA@Lipo@KGN) via microfluidics, (c) illustration of KGN release from GelMA@Lipo microgels. Adapted with the permission of [44] © 2020 Elsevier.

In the advanced polymeric microgel systems category, molecularly imprinted microgels stand out as a unique and promising category, smoothly progressing beyond traditional microgel technologies. [45]. Molecularly imprinted microgels are synthesized through a process where a specific target molecule, called the template, guides the polymerization of monomers and cross-linkers around it. Once the template is removed, it leaves the chemical and physical cavities that precisely match the features of the original template. These microgels possess a unique feature: a molecular memory to bind specific target molecules with precision selectively. This exceptional characteristic

puts them in a different place from traditional microgels since they possess inherent and tailored specificity toward the target molecule. It opens up possibilities in various applications, from advanced drug delivery systems to the sensing and molecular separation processes [46]. Molecularly imprinted microgels can be employed independently or combined with inorganic nanomaterials to achieve a synergistic enhancement in their performance [47]. As an example, Zhou and co-workers [48] presented the incorporation of fluorescent carbon dots (CDs) and molecularly imprinted polymer microgels for glucose detection (Figure 1.5). The imprinted polymers were synthesized via copolymerization of the VPBA, NIPAM, AAm, and CDs in the presence of glucose and BIS. They provide a selective platform for glucose sensing at physiological conditions compared to the non-imprinted control group.

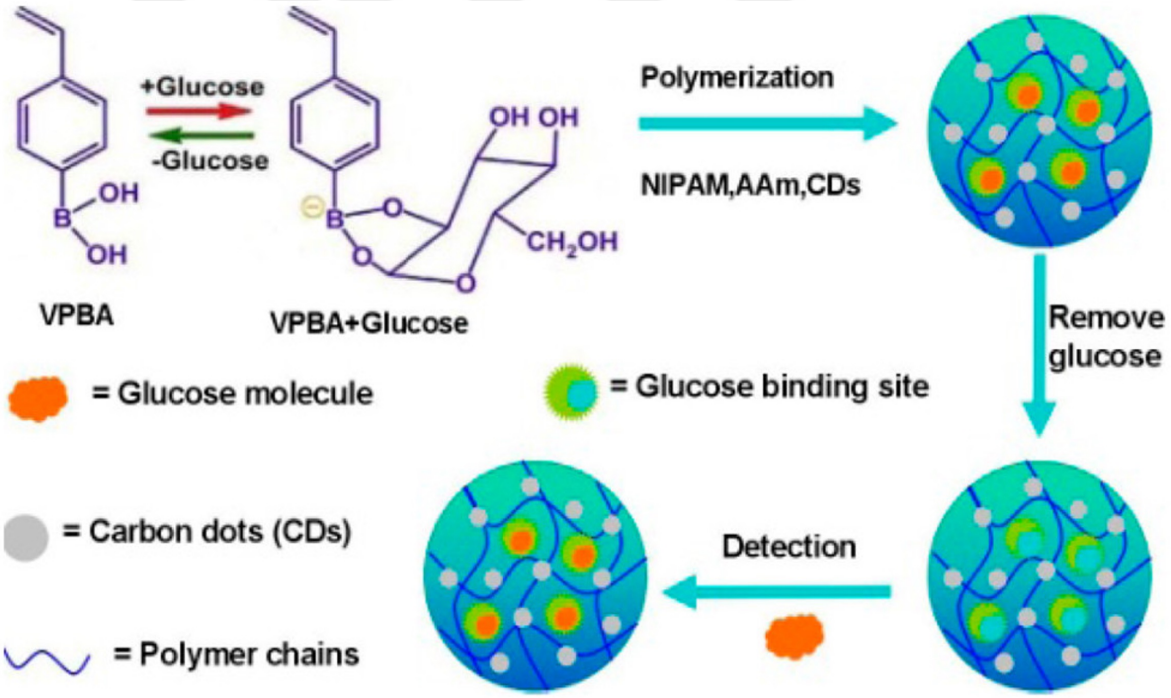

Figure 1.5 Schematic representation of the glucose-imprinted poly(NIPAM-AAm-VPBA)-CDs microgels for glucose detection. Adapted with the permission of [48] © 2015 American Chemical Society.

1.1.2 Fabrication of Polymeric Microgels

Various techniques for microgel fabrication have been developed, including mechanical crushing, emulsion polymerization, microfluidics, and templating, as illustrated in Figure 1.6 [49]. Generally, the fabrication processes involve both the creation and gelation of microgels. The methods for creating micron-sized materials vary depending on the techniques employed. For the gelation step, the monomers within the particles undergo initiation for polymerization and cross-linking, achieved through heating or irradiation. This leads to the formation of microgels with diameters spanning from 100 nm to 1 mm.

The mechanical crushing method involves the physical breakdown of larger hydrogel structures into smaller microgels through mechanical force, often facilitated by techniques such as grinding or milling. The starting material, typically a bulk hydrogel, reduces size until the desired microgel dimensions are achieved. This method is commonly used for molecularly imprinted polymer synthesis [50]. Peeters and coworkers [51] presented an antidepressant detection method using imprinted polymer technology. For the synthesis of microgels approximately 25 μm in size, they used a planetary ball mill device to perform the mechanical grinding method. Mechanical crashing provides a straightforward approach to obtaining polymeric microgels, but the debate often centers around the size distribution and monodispersity of the resulting product.

Emulsion polymerization techniques utilize immiscible oil and aqueous hydrogel precursor solutions to create droplets, which are subsequently cross-linked into microgels [52]. In a single batch, a water-based precursor incorporating the hydrogel pre-polymer with initiator and cross-linker is combined with the oil, potentially introducing a surfactant to maintain the emulsion's stability. By mechanical mixing, the solution undergoes homogenization, giving rise to aqueous droplets encapsulated within an oil phase. The size and uniformity of the resulting droplets are contingent upon the duration and timing of the mixing process. Finally, the droplets undergo cross-linking, and the oil phase is removed through washing, centrifugation, and filtration steps.

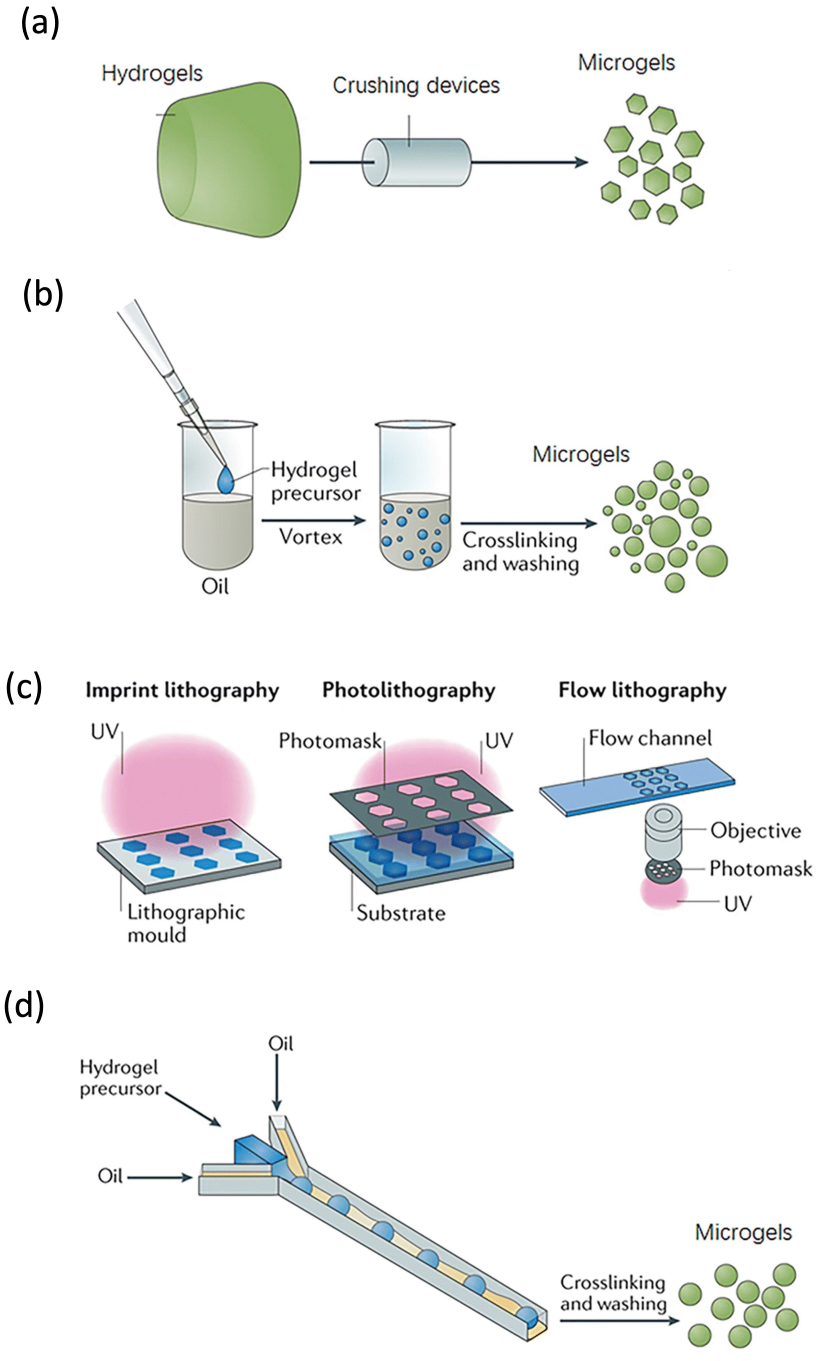

Figure 1.6 Fabrication methods of polymeric microgels, (a) mechanical crushing, (b) emulsion polymerization, (c) lithography methods, (d) microfluidics emulsion. Adapted with the permission of [49] © 2020 Springer Nature.

The main limitation of emulsion polymerization is that inconsistent mixing procedures across batches may result in batch-to-batch variations. Polydispersity is undesirable in specific applications, such as the microgel systems used for growth factor release. In these systems, polydispersity and particle sizes can influence the diffusion process. Studies indicate that microgels fabricated through either batch or microfluidics emulsions with similar mean diameters exhibit distinct release profiles [53]. Batch emulsion preparations show more significant variability in the release of encapsulated drugs, characterized by an earlier burst release. Moreover, in cell studies, the polydispersity of microgels poses challenges in controlling cell numbers within each particle.

Another method for microgel fabrication is the lithography. This process offers a highly controllable and repeatable approach compared to previously mentioned techniques. The lithographic synthesis of microgels involves transferring pre-designed template patterns onto hydrogel precursors, followed by polymerization and/or crosslinking, leading to the formation of distinct microgels [54]. Microgels with desired shapes can be fabricated using a photo mask, offering limitless possibilities for tunability to suit various applications [55]. However, a significant drawback of the lithography methods is their comparatively lower throughput when compared to alternative methods. The dimensions of the molds or photo masks limit the rate of particle production.

The microfluidics technique is widely used for continuously preparing microgels, ensuring consistent and adjustable particle dimensions, shapes, compositions, and pore sizes. This is accomplished by adjusting various parameters, including flow rates and channel features such as diameters, shapes, size, and architecture. The detailed exploration of this technique will be covered in the following section, as it serves as the primary method employed in this thesis for fabricating polymeric microgels.

1.2 Microfluidics for Biomedical Applications

1.2.1 Microfluidics

Microfluidics technology refers to a precision-based approach for manipulating small amounts of fluid ranging from 10^{-9} to 10^{-18} liters within microscale devices featuring channels ranging from tens to hundreds of micrometers [56]. Microfluidics offers important benefits such as minimal reagent usage, excellent repeatability, rapid reaction rates, and precise manipulation of both physical and chemical properties.

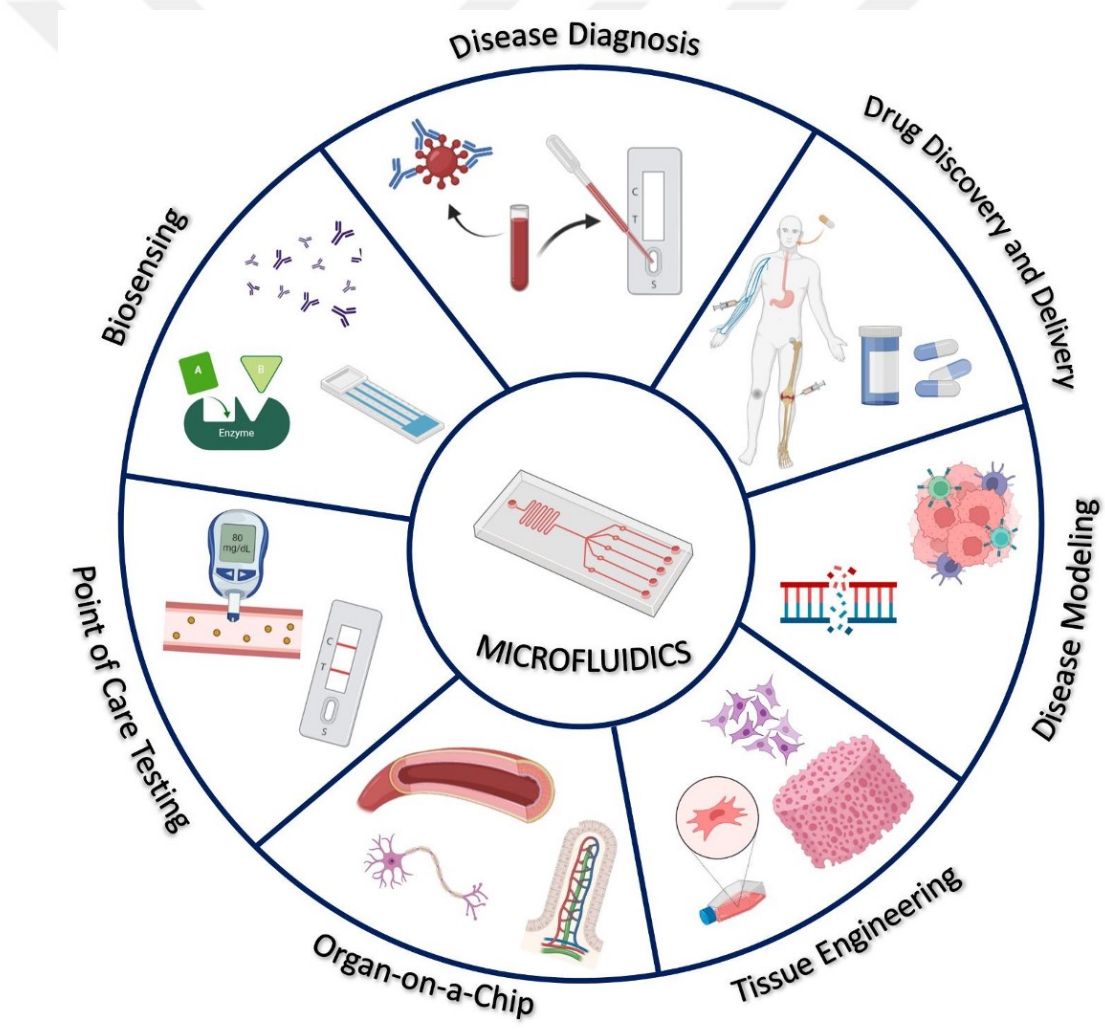

Figure 1.7 Microfluidics for biomedical applications. Adapted with the permission of [57] © 2022 MDPI.

As illustrated in Figure 1.7, microfluidics technology is advancing significantly [57]. It's playing a crucial role in diverse fields, from diagnostics to drug delivery and *organ-on-a-chip* applications. It highlights the versatile and impactful nature of microfluidics, reshaping how we approach challenges and enabling innovative solutions in diagnostics, treatment delivery, and the simulation of physiological systems on a small scale to do further analysis. Another great feature of microfluidics technology is its exceptional capability in facilitating the fabrication of polymeric materials. Its offers in the production of diverse polymeric materials are virtually limitless. By making simple adjustments to compositions, flow rates, or channel designs, microfluidics fabrication enables the formation of a wide array of polymeric materials, showcasing the remarkable flexibility and potential inherent in this technology.

1.2.2 Fabrication of Droplet-based Microfluidics Channels

Microfluidics channel fabrication techniques can be divided into two main categories: traditional and rapid prototyping methods [58]. Traditional approaches are well-suited for glass or silicon wafers and involve complex processes such as photolithography and etching. Photolithography utilizes light to precisely transfer desired patterns from a photo mask onto photosensitive materials, achieving high-resolution micro-structures. Complementary to this, etching further refines the substrate patterns. On the other hand, rapid prototyping techniques, known as soft lithography and hot-embossing, provide a more prompt approach. These methods leverage flexible and cost-effective polymer materials, particularly polydimethylsiloxane (PDMS), to transfer micro-patterns onto diverse substrates. PDMS enables rapid micro-structure replication, facilitating quick prototyping across various microfluidics, biotechnology, and materials science applications.

This thesis explores the creation of various droplet-based microfluidics channels using photolithography and replica molding methods. The design of these channels is tailored to specific applications, allowing for a customized approach based on the intended use.

1.2.3 Photolithography-Master Mold Fabrication

Photolithography utilizes optical radiation to imprint geometric patterns onto a silicon wafer. This process involves using a photo mask and can be applied to either negative or positive photoresist-coated silicon wafers. The photolithography fabrication process involves six main steps: surface cleaning of Si wafer, application of photoresist, conducting a soft bake (pre-bake), aligning the mask and exposure, development, and performing a hard bake (post-bake), as illustrated in Figure 1.8.

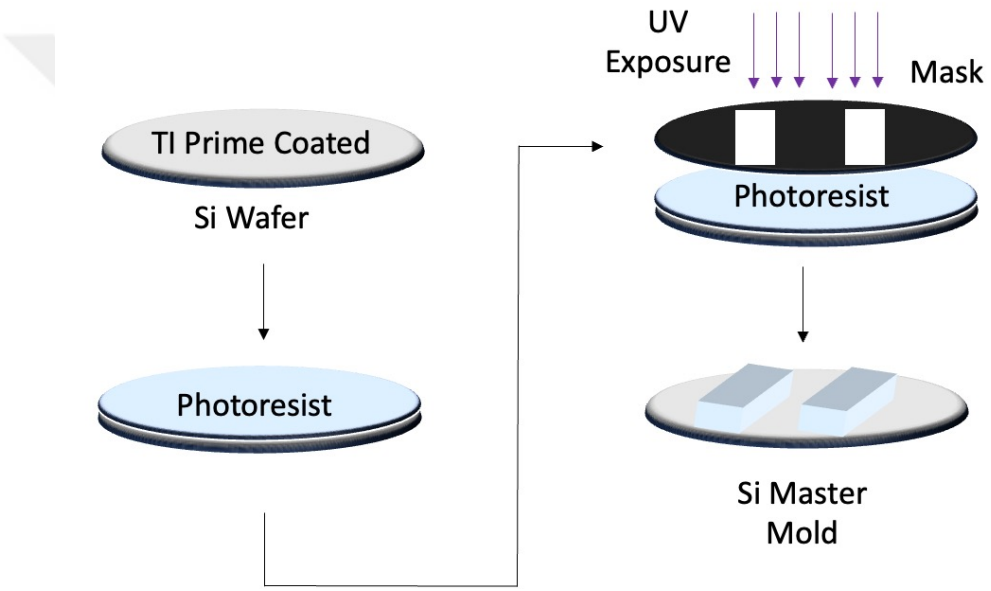

Figure 1.8 Schematic demonstration of photolithography process.

1.2.3.1 Mask Design. The masks were created using AutoCAD software (Autodesk, Inc., California, USA) and subsequently printed onto transparent plastic film, referred to as photo masks. An example of a photo mask used in studies of this thesis can be seen in Figure 1.9.

1.2.3.2 Photoresist. Positive and negative photoresists represent distinct types of light-sensitive materials. While both resist UV light, their reactions to it are opposite. Regarding positive photoresists, UV light exposure alters the chemical structure of

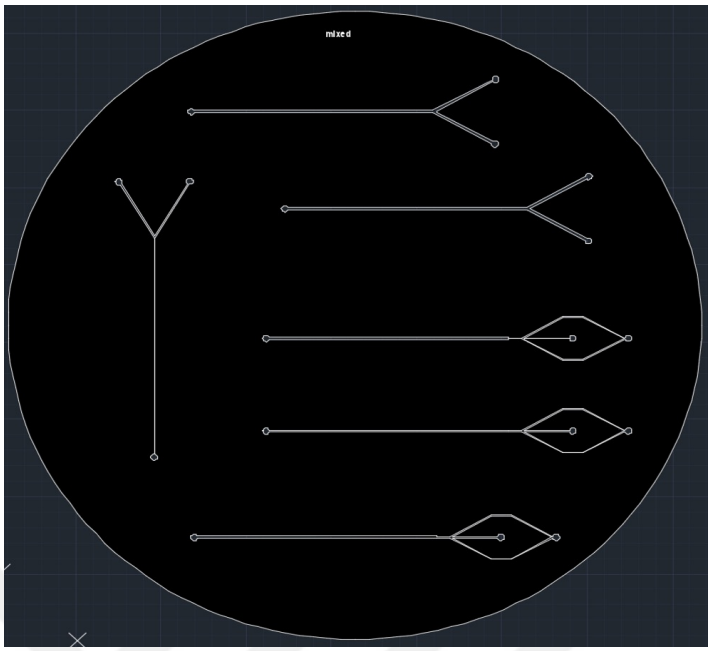

Figure 1.9 A sample mask design rendered in AutoCAD illustrations.

the coated material, making it more soluble. As a result, the UV-exposed areas are removed, leaving the unexposed regions intact, effectively replicating the mask pattern. Conversely, negative photoresists operate oppositely. When exposed to UV light, the negative photoresist polymerizes and adheres to the surface. Subsequent treatment with a developer solution removes the portions not exposed to UV light, creating an inverse pattern. Designing masks should consider this fundamental distinction in behavior between positive and negative photoresists.

In this thesis, we utilized a negative photoresist, SU-8 2050, to craft our master molds. As illustrated in Figure 1.10, applied photoresist thickness on the substrate can be adjusted, relying on the spin speed, as provided in the Microchem product datasheet.

1.2.3.3 Soft-baking. The primary objective of the soft baking step is to dry the photoresist, eliminating excess solvent to establish a stable resist film on the wafer's surface. Excess solvent removal occurs through evaporation, necessitating careful mon-

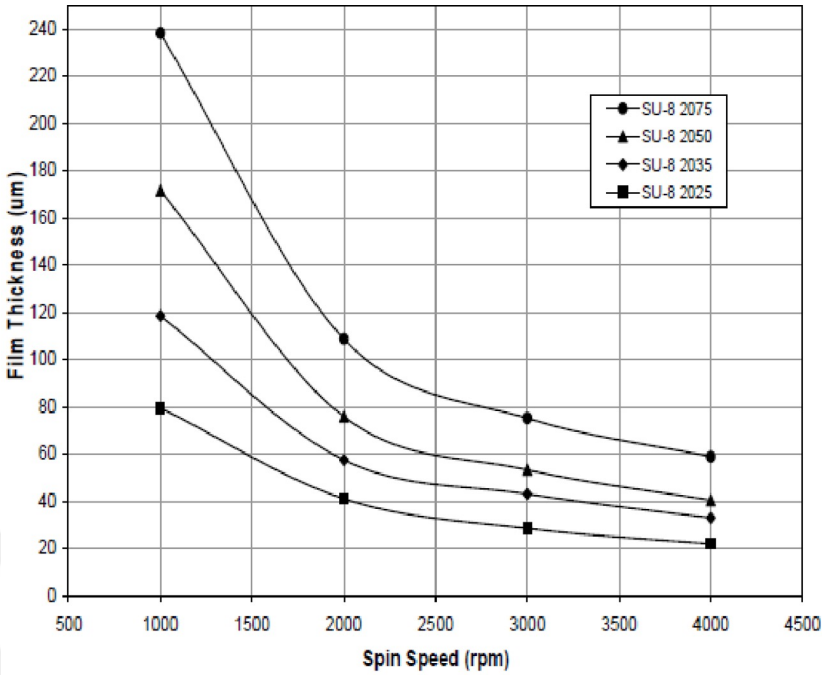

Figure 1.10 Spin Speed vs Thickness (Microchem SU-8 datasheet).

itoring of the evaporation rate to achieve the desired resist thickness. The significance of the soft baking part lies in rendering the photoresist layer photosensitive. Hot plates or ovens can be employed for the soft baking process, with the time and temperature settings tailored to the conduction methods, photoresist type, and desired thickness.

1.2.3.4 Photo Mask Alignment and UV Exposure. An EVG 620 semiautomatic contact photolithographic alignment and exposure device with a 1000-watt light source was used for the silicon master mold fabrication (EV Group, Sankt Florian am Inn, Austria). In this process, UV light, integrated into the mask alignment system, illuminates the wafer, exposing specific areas of the photoresist to UV light. The photo mask obstructs certain portions, preventing light transmission to those areas of the wafer. Utilizing SU-8 2050, a negative photoresist, the exposed areas undergo cross-linking to form distinct patterns, while the unexposed regions are subsequently removed through a developing process.

The alignment system comprises a stage for securing the wafer, a stage for

holding the photo mask, and a UV illumination system. The illumination system utilizes a high-pressure mercury plasma arc discharge lamp known for emitting UV light (365 nm) onto the photo mask. Enhanced resolution is achieved when the mask is in direct contact with the wafer. The exposure duration depends on the photoresist type and the UV lamp's power.

1.2.3.5 Post-baking. The post-baking step involves heating the wafer for a specific time to enhance the stability and durability of the photoresist patterns. Post-baking improves adhesion to the substrate, reduces pattern distortion, and ensures the overall strength of the micro-structures. Post-baking time and temperature are chosen based on the photoresist type, the final products' thickness, and desired characteristics.

1.2.3.6 Development. The development step involves using specific developer solutions specific to the type of photoresist employed. These solutions allow for the elimination of unpolymerized photoresist transferred onto the wafer. In the case of positive photoresist, the exposed areas wash away during the development step. Conversely, for negative photoresists, the unexposed areas wash away in this stage. The choice of developer solution is essential for achieving the desired pattern and functionality in the subsequent stages of the microfabrication process.

1.2.4 Soft Lithography-PDMS Casting, Replica Molding and Bonding

A soft lithography technique, replica molding, was employed to craft the microchannel on a silicone elastomer, PDMS. The fabrication involved pouring a mixed PDMS and a curing agent with a 10:1 ratio onto the mold mounted in a petri dish. After placing the petri dish in a vacuum chamber for approximately 90 minutes to eliminate bubbles, the mold underwent a 2 h curing process in an oven at 65 °C. The cured PDMS was then carefully peeled from the mold, as illustrated in Figure 1.11. Inlets and outlets of the PDMS channel were opened using a hand-operated puncher. Subsequently, the PDMS channel was affixed to a glass slide by a corona discharge

plasma treatment machine. The surfaces of the PDMS channel and the glass slide were subjected to a 3 minutes of oxygen plasma to provide strong bonding. The obtained microchannels were left in an oven overnight at 65 °C.

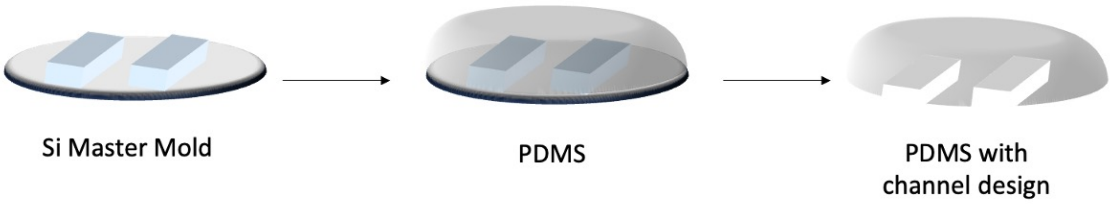

Figure 1.11 Schematic illustration of PDMS casting and replica molding processes.

1.2.5 Microfluidics for Polymeric Microgels Synthesis

Microfluidics is an impressive tool in fabricating polymeric microgels, offering precise control over their size, structure, and functionality [59–61]. In this innovative approach, microfluidics devices manipulate minute volumes of fluids within micron-sized channels, enabling droplet formation in *water-in-oil(W/O)* or *oil-in-water(O/W)* systems. The ability to fine-tune the parameters of these microfluidics systems enables the production of microgels with desired properties, such as tunable porosity, drug-loading capabilities, or controlled release kinetics. Microfluidic-based polymeric microgels represent a frontier in biomaterials science, offering the potential to address diverse biomedical challenges with exceptional precision and versatility [62].

Microfluidics-based microgel fabrication was performed in droplet-based channel configurations. Due to the distinctive configuration of the microfluidics channels, an aqueous/water phase undergoes shearing within an oil phase, resulting in the production of consistently sized droplets enveloped by oil (for the W/O systems). These designs may include T-junctions, flow-focusing configurations, or co-flow geometries, as illustrated in Figure 1.12 [63]. In the T-junction/Y-junction configuration, droplets

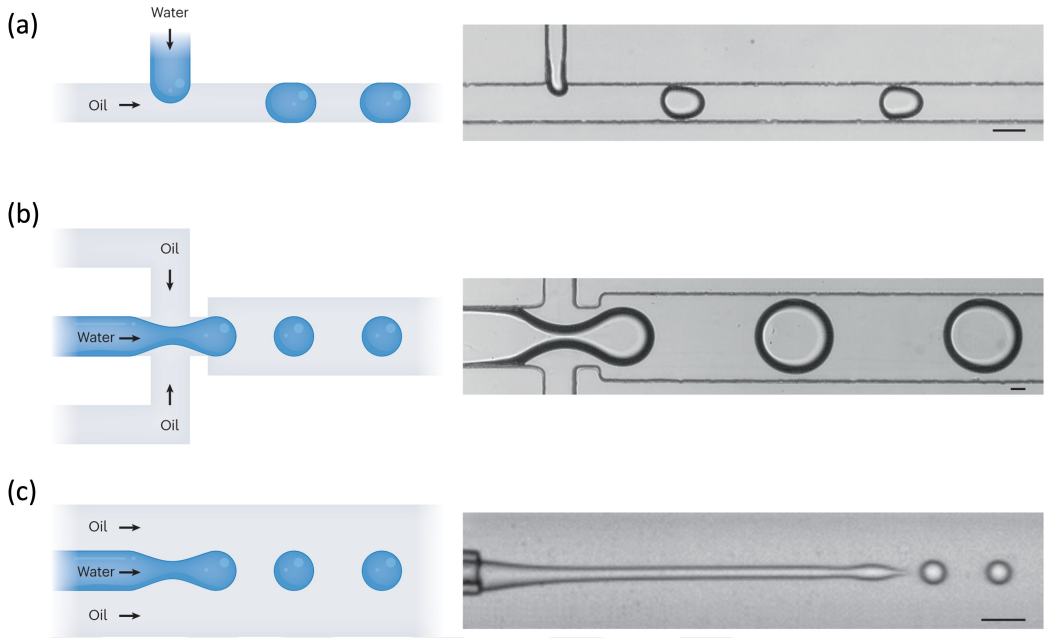

Figure 1.12 Different microchannel configurations for microgels fabrication: (a) T-junction/Y-junction, (b) flow-focusing, (c) co-flow configuration. Adapted with the permission of [63] © 2023 Springer Nature.

are formed as the perpendicular flow of the water phase undergoes shearing by the surrounding oil. The flow-focusing design generates droplets by subjecting the aqueous stream to shearing forces from side directions. In the co-flow design, the water phase is directed through a smaller capillary channel coaxially positioned inside a larger one, through which immiscible oil is injected, compelling the generation of droplets.

In a W/O system, the continuous phase should meet specific criteria, including a strong affinity for the channel surface and low viscosity, to avoid issues related to excessive back pressure. Various oil phases have been tested for diverse applications, with hydrocarbon and fluorocarbon oils emerging as the most commonly employed options [64, 65]. To achieve emulsion stability, selecting a proper surfactant is crucial, considering factors such as biocompatibility, emulsion stability, and possible micellar transport [66]. Surfactants, acting primarily at the interface between oil and water, play a key function by reducing surface tension, thereby improving the emulsions' stability. In the absence of surfactants, minimizing the surface area becomes energetically favorable, resulting in the coalescence of droplets.

1.2.6 Overview of the Droplet-based Microfluidics Channels

In this thesis, we designed and fabricated three different droplet-based microfluidic channels as illustrated in Figure 1.13.

The preceding sections provide the significant role played by cross-linked polymeric materials, specifically microgels, in effectively playing a role in diverse biomedical fields, spanning diagnostics to enhanced delivery. Creating polymeric microgel materials tailored for specific applications and their fabrication methods necessitates the development of novel methodologies and chemistries. Despite notable advancements, as outlined in the mentioned examples, the design of intelligent microgel materials is still in its nascent stages. This thesis endeavors to advance the existing state of the art by fabricating various novel microgel systems specifically for therapeutic and biomolecular protein sensing applications.

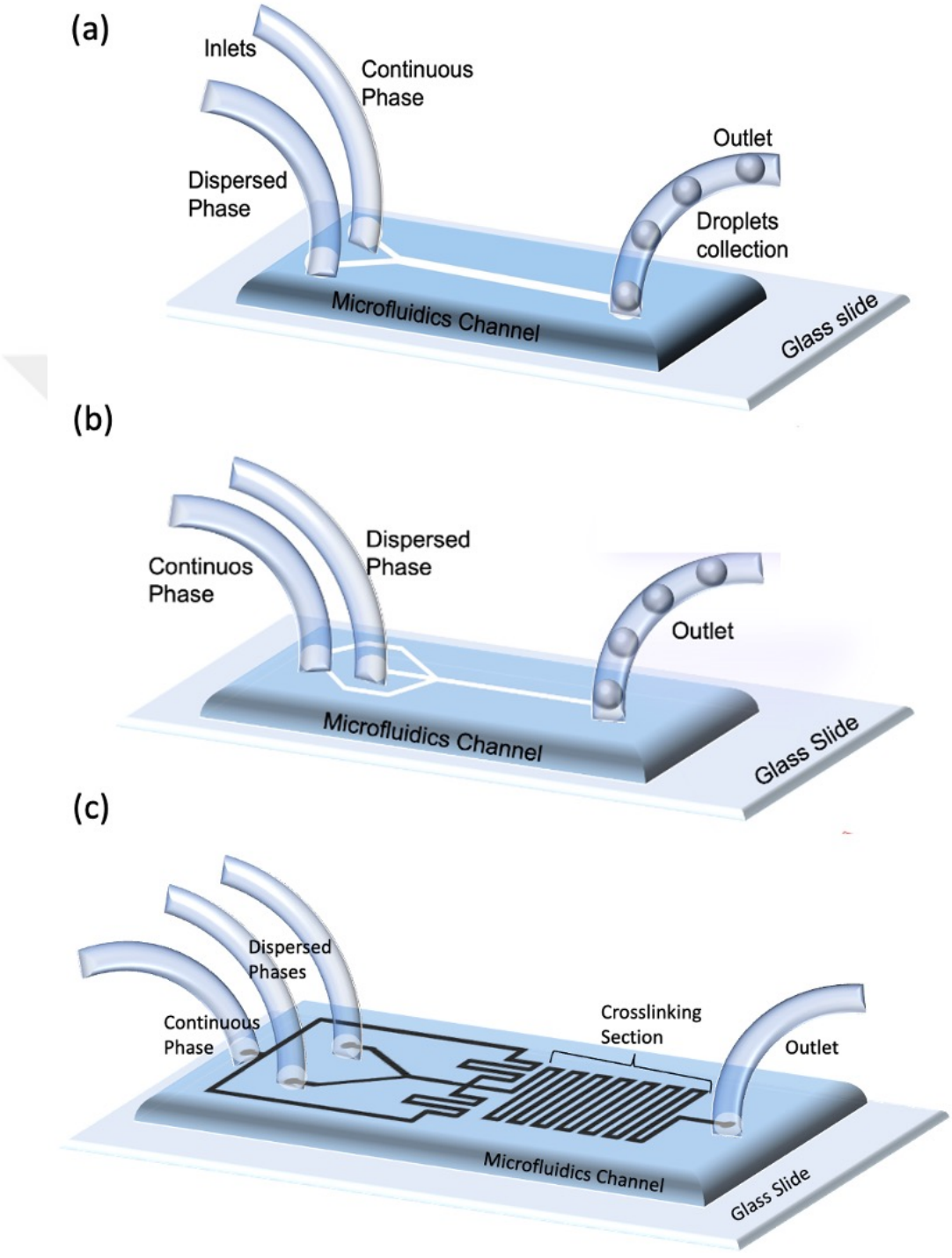

Figure 1.13 Illustration of droplet-based microfluidics channels.

2. MICROFLUIDICS ASSISTED MICROGELS FABRICATION: UTILIZING THIOL-DISULFIDE EXCHANGE FOR REVERSIBLE PROTEIN CAPTURE

2.1 Introduction

In diagnostics, it's crucial to selectively capture various substances, ranging from tiny molecules to large biomolecules, at device interfaces [67]. Once the analyte selectively interacts at the interface, generally by non-covalent molecular recognition events such as protein-ligand interactions [68], the detection of this interaction involves optical [48], spectroscopic [69] or electrochemical [70] readouts. The development of innovative polymeric materials for capturing bioentities has hugely taken place in the literature [71–73]. These applications require the creation of novel and efficient methodologies, facilitating the seamless engineering of interfaces for the selective attachment and *on-demand* release of analytes. Therefore, redox-responsive functional groups containing microgels have emerged as promising candidates for *catch-and-release* applications [74]. These microgels, composed of cross-linked polymers with tunable properties, exhibit unique responsiveness to changes in redox conditions. This distinctive characteristic allows for precise control over the immobilization and *on-demand* release of biomolecules.

Numerous conjugation strategies utilize thiol-based reactions since the thiol groups are either naturally present or can be incorporated into a biomolecule by nucleophilic or radical thiol-ene reactions [75, 76]. Despite their efficiency, the non-reversible attribute of these conjugations restricts their applicability in designing *catch-and-release* platforms. An alternative thiol-based approach based on the thiol-disulfide exchange chemistry arises due to its reversible nature. The disulfide linkage is a highly responsive redox-functional group. It can exchange reactions with thiol groups, where the thiolate acts as a nucleophile, attacking the disulfide linkage. This chemistry has taken place in applications as stimuli-responsive polymeric materials, which ultimately

undergo *on-demand* cleavage as introduced to thiol-bearing reducing agents, including GSH or DTT. It can be commonly seen in examples of polymer-drug conjugates [77], micelles [78], or protein-encapsulated gel systems [79]. On the other hand, the microfluidic fabrication of polymeric microgels, incorporating the versatile PDS group for *catch-and-release*, is relatively new [80]. Recently, Voit and co-workers demonstrated an on-chip microgel dot design that utilizes thiol-disulfide exchange reaction for bovine serum albumin (BSA) *catch-and-release* studies [40]. However, as opposed to embedding microgel system into a microfluidic channel, using them outside after the microfluidic cross-linking offers advantages including simplified handling, greater flexibility in experimental setups, easier accessibility for characterization techniques, scalability for larger quantities, and reduced complexity in fabrication.

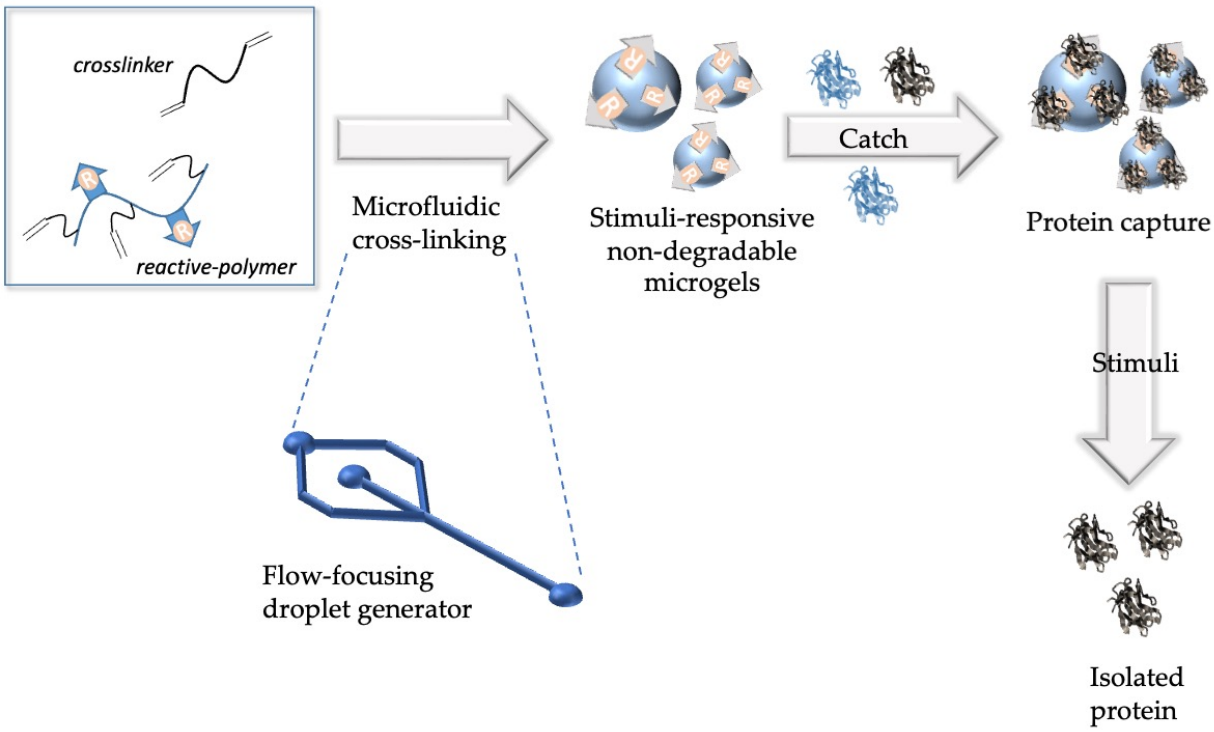

Figure 2.1 General scheme of the concept.

Herein, we show the synthesis of the PDS-group carrying monodisperse polymeric microgels via microfluidics techniques and UV-induced polymerization as seen in Figure 2.1. The microgels, equipped with thiol-reactive groups, were synthesized with PEG-based monomers, enabling the conjugation of thiol-containing molecules through thiol-disulfide exchange reactions. Various microgels featuring different amounts of reactive groups were fabricated. The best microgel system is further conjugated with biotin-containing ligands to allow specific determination of extravidin in a protein mixture. Furthermore, the release of bound proteins was successfully achieved in a DTT solution. To enhance the catching performance of the microgel system, we further introduce porosity into the polymeric network and highlight the differences between porous and non-porous structures.

2.2 Experimental

2.2.1 Materials and Characterization

PDS-PEGMA monomer (was synthesized by Rüveyda Kılıç Boz) [81], biotin-SH [82] and bodipy-SH [83] (was synthesized by Aysun Değirmenci) were synthesized according to the reported procedures. PEGMEMA (300 g/mol), PEGDA (700 g/mol), LAP, TRITC-extravidin, and DTT were obtained from Sigma Aldrich (Sigma, St. Louis, MO, USA). Mineral oil (0.880 kg/l) was purchased from AppliChem.

For the microfluidics system, we procured essential materials from Sigma Aldrich, including PDMS, HMDS, chlorotrimethylsilane, a negative photoresist (SU-8 2050), PGMEA, glass slides, a biopsy punch (Harris Uni-Core 0.75 mm, USA), and Span 80. Mineral oil (0.880 kg/L) was sourced from AppliChem, and the TI prime was acquired from MicroChemicals. PTFE tubes for the microfluidic channels' inlets and outlets were obtained from Microfluidic ChipShop (Jena, Germany). The silicon master mold was fabrication by using the EVG 620 aligner (EV Group, Sankt Florian am Inn, Austria). Plasma treatment of the PDMS device and glass slide was conducted using a laboratory corona treater. In situ photopolymerization was performed using a UV

light source (36-watt, 365 nm). UV-vis spectra data were collected on a Cary Varian spectrometer (Santa Clara, CA, USA). Microgels were visualized using fluorescence microscopy (HBO100 ZEISS Fluorescence Microscopy, Carl Zeiss., Jena, Germany), and fluorescence images were processed using the Zeiss AxioVision software. SEM images were obtained using a JCM-5000 NeoScop Tabletop SEM with an accelerating voltage of 10 kV.

2.2.2 Fabrication of Flow-focusing Droplet-based Microfluidics Channel

For the fabrication of a PDMS flow-focusing microfluidics channel, as demonstrated in Figure 2.2, photolithography and PDMS molding methods were performed. For the master mold fabrication, the Si wafer (4-inch) was cleaned and treated with HMDS for 1 h. Later, the water was coated with TI prime to obtain better adhesion for the following steps. The TI prime-coated wafer was baked on a hotplate at 95 °C for 1 min. The negative photoresist, SU-8 2050, was spun coated onto the wafer depending on the desired channel thickness. The pre-bake was performed at 65 °C for 1 minute and then at 95 °C for 20 minutes. The photo mask with the flow-focusing channel design was placed face-down on the mask aligner device. The photoresist-coated wafer was aligned with the photo mask and brought into the desired contact for UV exposure. Following the exposure step, the post-bake step was achieved at 65 °C for 5 minutes and then, 95 °C for 10 minutes. PGMEA was utilized to remove excess/uncured photoresist, followed by rinsing with IPA and DI water.

Before the PDMS casting step, the master mold underwent a silane vapor treatment in a vacuum desiccator. Silicone elastomer base with a curing agent was mixed in a dust-free environment with a ratio of 10:1. The PDMS mixture was poured over the master mold, degassed, and cured at 65 °C for 2 h. The baked PDMS was peeled off from the master mold, and each microchannel was cut with a razor. Using a hand-operated biopsy puncher, the inlets and outlets of the channels were opened. The final step is the oxygen plasma treatment of the PDMS and glass slide surfaces for 3 min. The bonding was achieved at 65 °C for a night. Lastly, PTFE tubes were inserted into

the inlets and outlets of the microfluidics channel to conduct experiments.

2.2.3 Preparation of PDS-group containing Polymeric Microgels

PDMS flow-focusing microfluidics channel was designed with two inlets and one outlet. Microspheres were synthesized using mineral oil containing nonionic surfactant Span 80 (10wt%) as a continuous phase in a W/O system (Figure 2.2). A range of PDS-PEGMA monomer concentrations was prepared in pre-polymer solutions for the dispersed phase. W/O droplet emulsions were easily formed in the microfluidic channel, and generated droplets traveled along the channel. When they arrived at the tubing, they were exposed to UV light to perform in situ polymerization. Produced microparticles were gathered in a vial or directly on a coverslip for visualization. Polymerized particles were washed with hexane and MeOH to eliminate the unreacted liquid portion and surfactant residues from the polymerized droplet core. Before lyophilization, microparticles were washed with DI water and frozen.

2.2.4 Pyridothione Release Studies

Microparticle samples containing a different amount of PDS-PEGMA monomer (2 mg) were introduced into a DTT solution (1 mL, 100 mM, 1xPBS) and subjected to incubation at 37 °C. Following a 3 h incubation period, the UV-vis spectrum of the solutions was analyzed to quantify the absorbance at 343 nm, indicative of the freed pyridothione fragment.

2.2.5 Conjugation and Release of Bodipy-SH

Microparticles containing various ratios of PDS were subjected to incubation in a MeOH solution containing Bodipy-SH for 18 h with a catalytic amount of acetic acid. Subsequently, the microparticles underwent multiple washes with MeOH to eliminate unbound dye. As part of a control experiment, microparticles without PDS-group

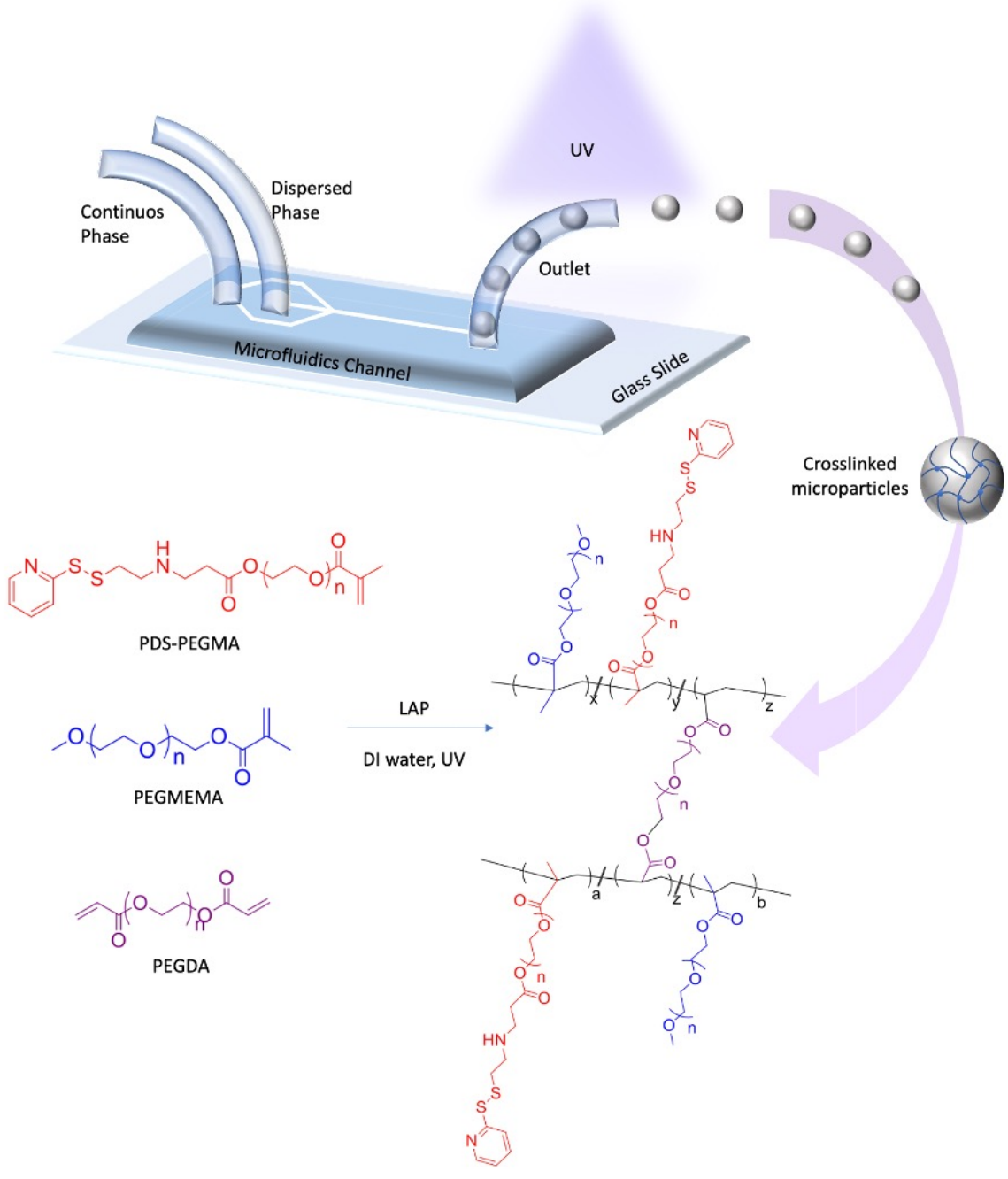

Figure 2.2 General and chemical scheme of PDS-group containing microgels fabrication via microfluidics.

containing monomer were fabricated and treated using a comparable procedure. The thoroughly washed microparticles were then examined using fluorescence microscopy.

2.2.6 Conjugation and Release of a Protein

Microparticles with PDS-group (2 mg) underwent incubation with a MeOH solution of Biotin-SH (1 mg/mL) with a trace amount of acetic acid for 18 h at 37 °C. Following multiple washes of the biotinylated microparticles with MeOH, they were exposed to a TRITC-extravidin solution for 30 minutes. The particles with immobilized proteins were purified through multiple water washes, and following analysis involved fluorescence microscopy examination of the samples. Microparticles lacking the PDS-PEGMA monomer underwent a similar treatment and examination for control experiments. For the release of protein, microspheres were subjected to incubation in a 100 mM DTT solution (3 mL) at room temperature for 3 h. Finally, microgels were visualized again under fluorescence microscopy to observe the release performance.

2.2.7 Extravidin Selectivity-Catch&Release from the Protein Mixture

A mixture comprising 1 mg of TRITC-extravidin and 1 mg of FITC-albumin in 0.5 mL of 1x PBS was prepared, and 20 μL of this solution was applied to biotin-conjugated microgels, allowing for a 30-minute incubation. Following the removal of excess solution, fluorescence microscopy images were acquired using distinct filter sets corresponding to the different dyes. Additional fluorescence microscopy images were obtained after removing unbound proteins by washing them with water. The microgels were subsequently immersed in a 100 mM DTT solution for 3 h and observed through fluorescence microscopy. Control experiments were carried out following the similar procedure with microgels lacking the PDS-group.

2.2.8 Incorporation of PEG 10kDa

Upon noting that protein binding predominantly occurs on the microgels' surface, we aimed to enhance the porosity within the polymeric network of the microgels. Various proportions of PEG 10 kDa were introduced into the dispersed phase to achieve this. After gelation, the microgels were washed with hexane, MeOH, and water to eliminate the PEG 10 kDa and unreacted residues. After obtaining the more porous microgels with the PDS-group, the protein catch&release experiments were performed to visualize the differences between porous and non-porous polymeric materials under fluorescence microscopy.

2.3 Results and Discussion

2.3.1 PDS-group-containing Polymeric Microgels

Various microgels with different PDS-group concentrations, as seen in Table 2.1 were produced through microfluidics cross-linking. The chosen procedure for the synthesis of polymeric microgels is as follows: PDS-PEGMA (21.6 mg, 0.036 mmol), PEGMEMA (84 mg, 0.28 mmol), PEGDA (112 mg, 0.16 mmol), and LAP (2wt%) were dissolved in DI water (0.8 mL).

Table 2.1

Microgels fabricated with varying amounts of PDS-PEGMA.

	PEGDA eq.	**PEGMEMA eq.**	**PDS-PEGMA eq.**
2.5%	1	1.75	0.075
5%	1	1.75	0.15
7.5%	1	1.75	0.225

Higher amounts of thiol-reactive PDS-group-containing microgels were used for further functionalization. For the fabrication of microgels, flow rates of oil and water

phases were fixed at 18 μL/min and 3 μL/min, respectively, to obtain microspheres with the size of approximately 230 μm as depicted in Figure 2.3a,c. The SEM images of the 7.5% PDS-containing microgels can be observed in Figure 2.3b.

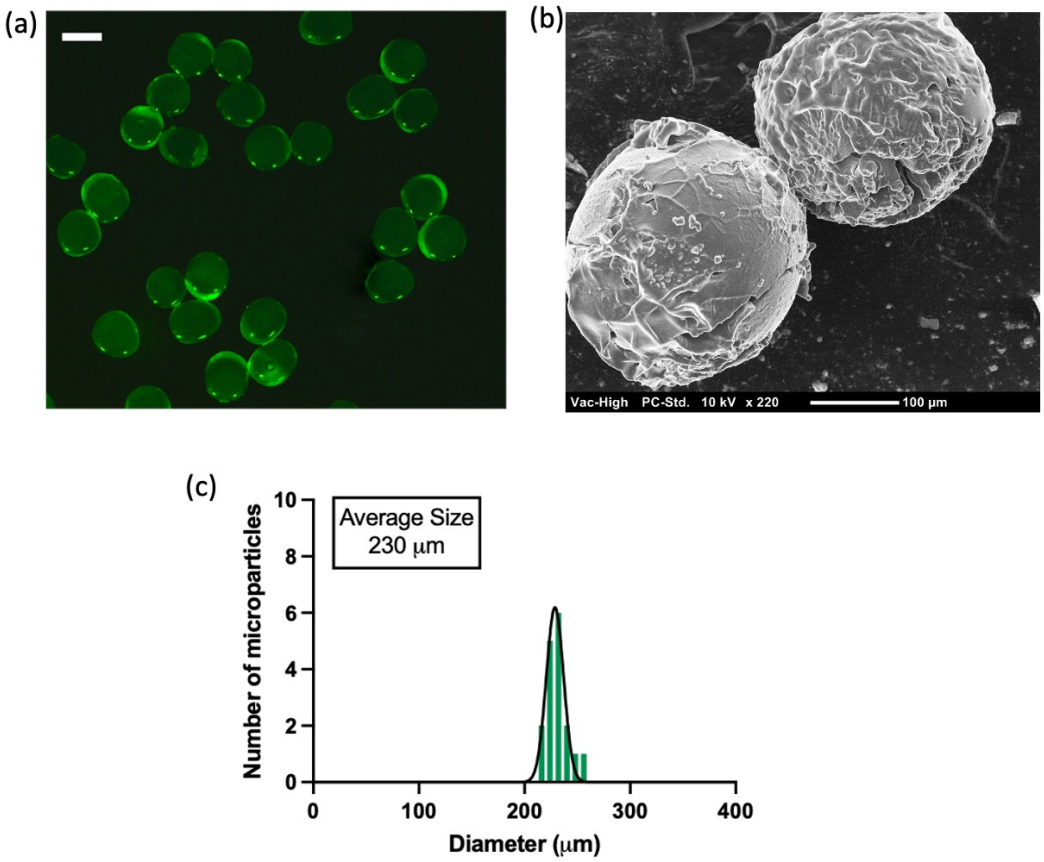

Figure 2.3 (a) A fluorescence image of monodisperse PDS-group containing microgels (Scale 200 μm), (b) SEM image of the PDS-group containing microgel, (c) size distribution of the microgels.

2.3.2 Functionalization of PDS-group-containing Microgels

It was observed that an elevated amount of PDS groups in the network resulted in a higher functionalization efficiency. The microgels containing PDS and exhibiting thiol-reactive properties were evaluated for their efficacy in functionalization in mild environments. DTT initiated the reduction, and the subsequent liberation of pyridothione from the microgels was tracked using UV-vis spectroscopy, as illustrated in Figure 2.4a,b. It was concluded that an increased amount of PDS-groups in the microgel

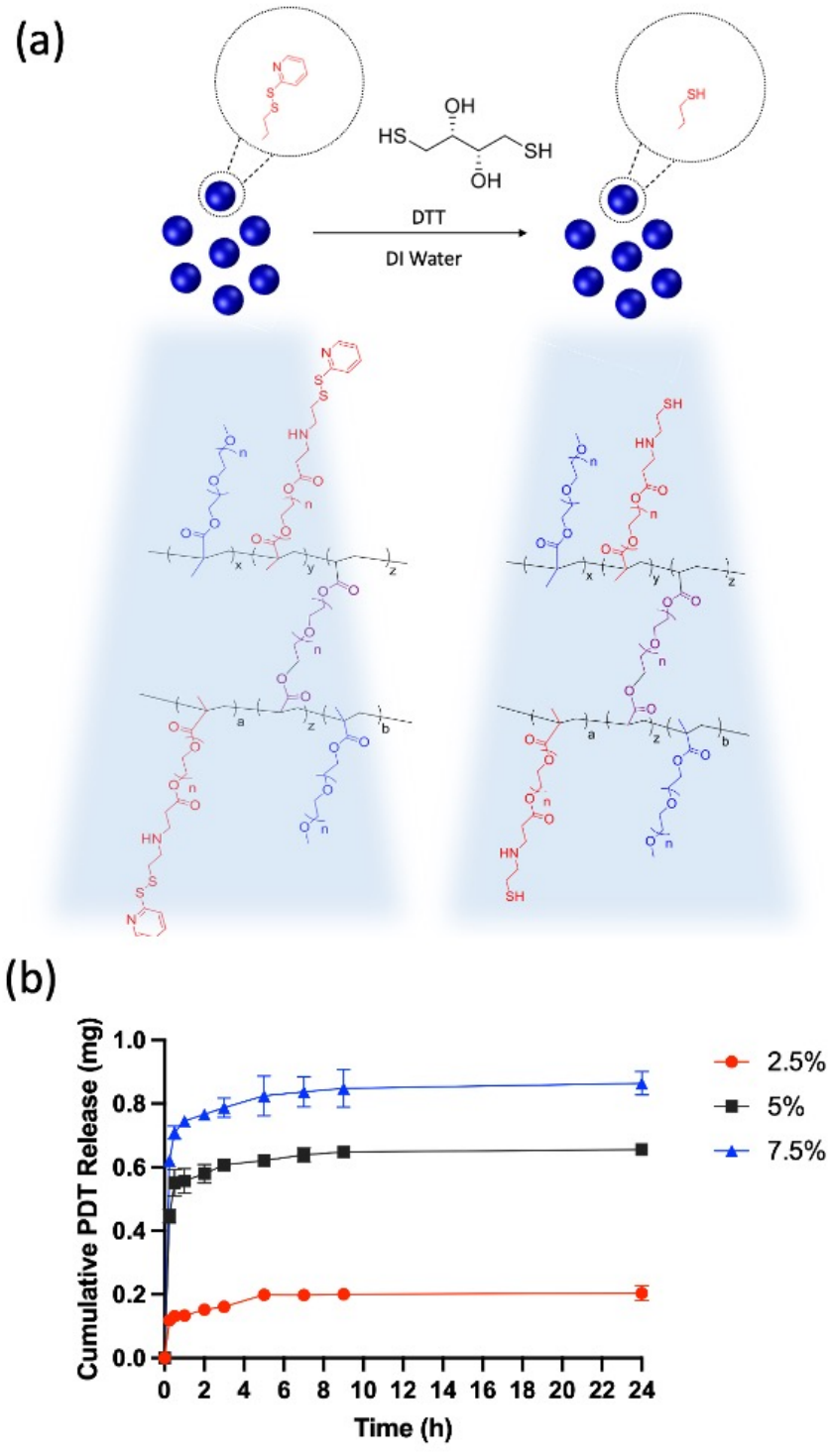

Figure 2.4 (a) Functionalization of the microgels with DTT, (b) associated pyridothione release profiles of various amount PDS-group containing microgels.

network resulted in a higher functionalization efficiency.

Thiol reactive microgels were subjected to functionalize with Bodipy-SH, as illustrated in Figure 2.5a. For dye conjugation, a control group lacking a reactive monomer and various concentrations of the reactive group-containing microgels were employed. As anticipated, fluorescence microscopy analysis demonstrated the absence of noticeable fluorescence in microgels without the reactive PDS monomer (Figure 2.5b). Conversely, microgels containing the PDS group exhibited heightened fluorescence, aligning with the escalation in the amount of the reactive monomer. Before capturing fluorescence images, all samples underwent sonication using a fresh solvent to eliminate dye physically trapped in the gel network and images captures under the same exposure.

2.3.3 Catch&release of TRITC-extravidin and Selectivity Study

Biotin and extravidin are recognized for exhibiting one of the most robust non-covalent biological interactions. Beyond their exceptional affinity, the binding of extravidin to biotin offers distinct advantages, including high specificity, rapid binding kinetics, and resilience to variations in pH or temperature. These attributes make the biotin-extravidin interaction a widely utilized model system for studying protein-ligand interactions. To showcase its applicability in microgel systems, microgels were employed for the immobilization and release of the protein (Figure 2.6a). First, PDS functional microgels were conjugated with thiol-bearing biotin (Biotin-SH). The resulting biotinylated microgels, were subjected to TRITC-extravidin, confirming the effective binding of the protein to the microgel through fluorescence microscopy analysis (Figure 2.6b). Subsequent treatment of the protein-immobilized microgels with DTT aimed to isolate the bound protein. Fluorescence microscopy images of DTT-treated microgels indicated a notable decrease in red fluorescence, suggesting the release of the protein from the microgels. The control group of microgels without the reactive group was treated the same way and evaluated under fluorescence microscopy.

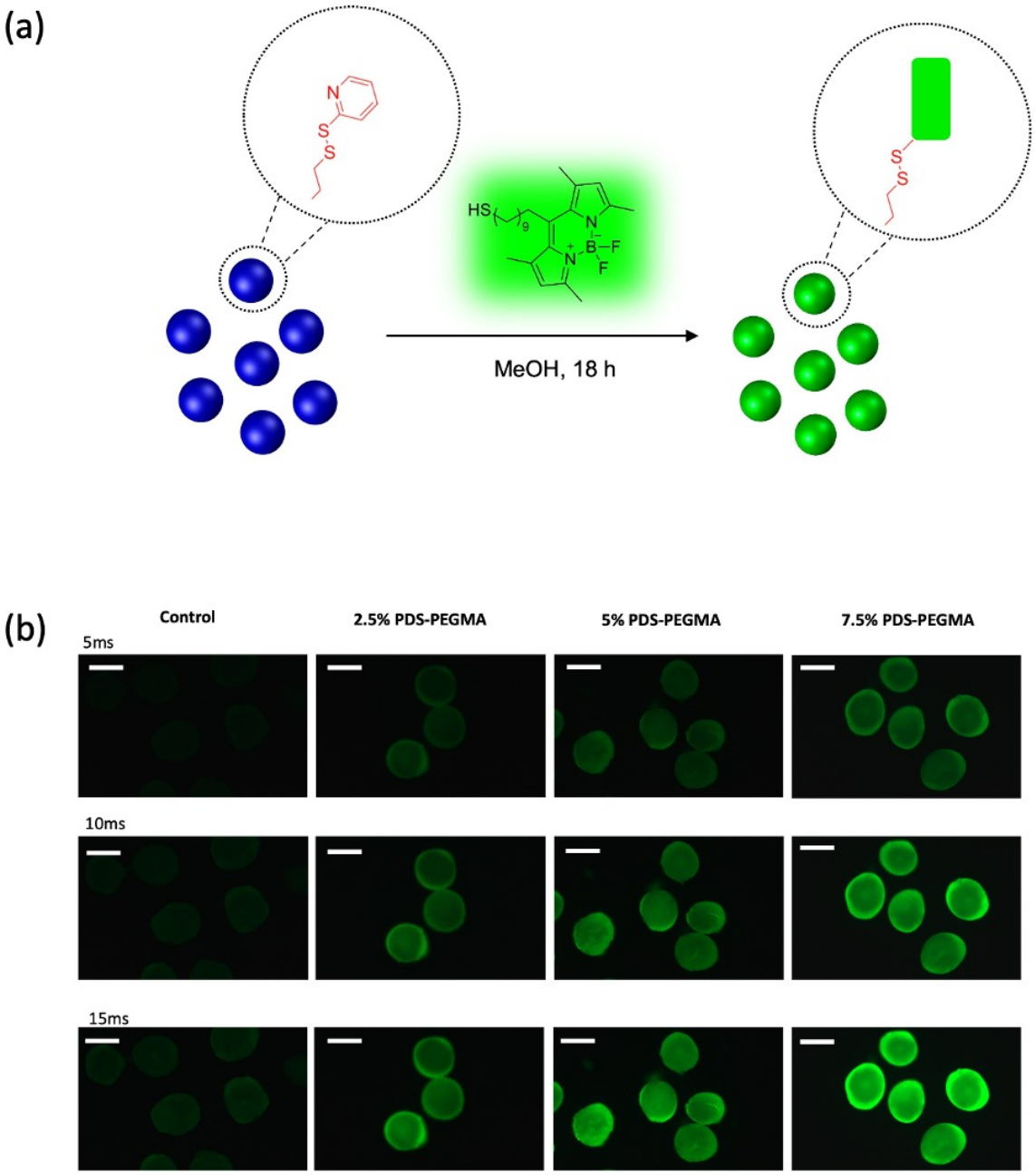

Figure 2.5 (a) Functionalization of the microgels with Bodipy-SH, (b) fluorescence microscopy images of Bodipy-SH conjugated microgels (Scale 200 μm).

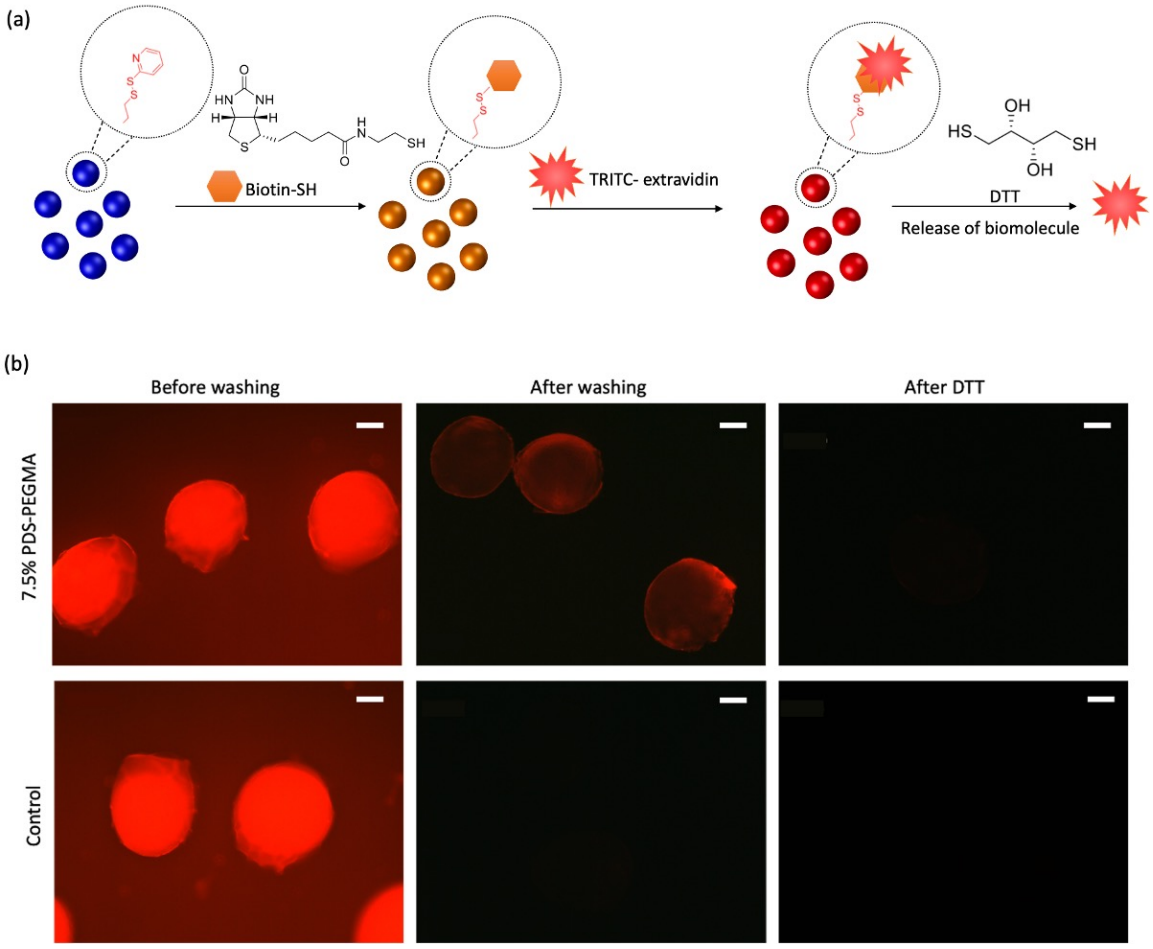

Figure 2.6 (a) Illustration of TRITC-extravidin capture by the Biotin-SH conjugated microgels and subsequent release, (b) fluorescence microscopy images of TRITC-extravidin immobilization onto the mirogels with the comparison of control group (Scale 100 μm).

After straightforward attachment and detachment of proteins on these microgels, we investigated the selective capture and release of a specific biomolecule in the presence of another protein. To assess this capability, the biotinylated microgels underwent incubation with a mixture of TRITC-extravidin and FITC-albumin (Figure 2.7a).

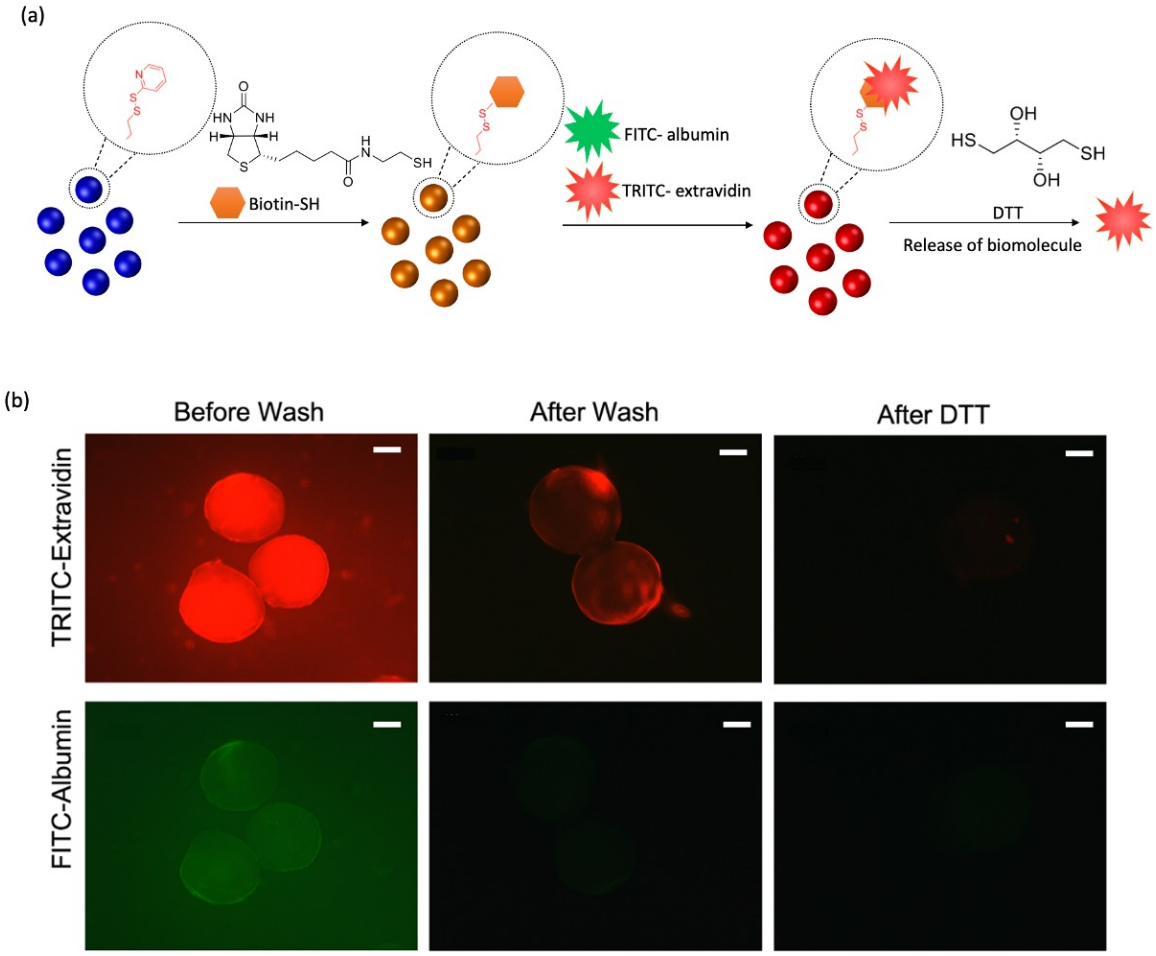

Figure 2.7 (a) Illustration of TRITC-extravidin capture by the Biotin-SH conjugated microgels in a protein mixture and subsequent release, (b) fluorescence microscopy images of selectivity profile of the microgels (Scale 100 μm).

The protein mixture treatment to microgels followed the washing steps and fluorescence microscopy analysis. Since FITC and TRITC give different green and red fluorescence, we can characterize the selective binding of extravidin through fluorescence images as shown in Figure 2.7b. Images captured before washing clearly show the

protein mixture in the environment. Following the washing process, the fluorescence in the green channel was removed, whereas the fluorescence in red channel persisted due to the strong binding of biotin and extravidin. Later, protein-conjugated microgels were exposed to DTT to perform *on-demand* release. The release performance was also observed under fluorescence microscopy since red fluorescence was significantly reduced.

2.3.4 Catch&release of TRITC-extravidin from Porous and Non-porous Microgels

The final material's porosity enhancement, as depicted in Figure 2.8a, was achieved by incorporating PEG 10kDa into the gel system. The porosity facilitated the functionalization of the PDS group, not only on the surface of the microgels but throughout the entire polymeric network. The SEM images presented in Figure 2.8b visually capture the resulting porous structure of the microgels. These images represent the extended reach of PDS functionalization within the polymeric network, emphasizing the uniformity of the modification across the microgel material.

Later, protein *catch-and-release* studies conducted a comparative analysis between porous and non-porous microgels. Following the initial procedure, biotin-SH was conjugated to the microgels via a thiol-disulfide exchange reaction. Finally, TRITC-extravidin catch experiments were executed. Fluorescence images were captured for porous and non-porous materials under identical exposure conditions, as depicted in Figure 2.9. The captured images serve as a qualitative representation of the protein *catch-and-release* capabilities and offer insights into the spatial distribution and extent of protein binding on the microgel surfaces. This meticulous examination contributes valuable data for understanding how the porosity of the microgels influences their performance in protein interactions.

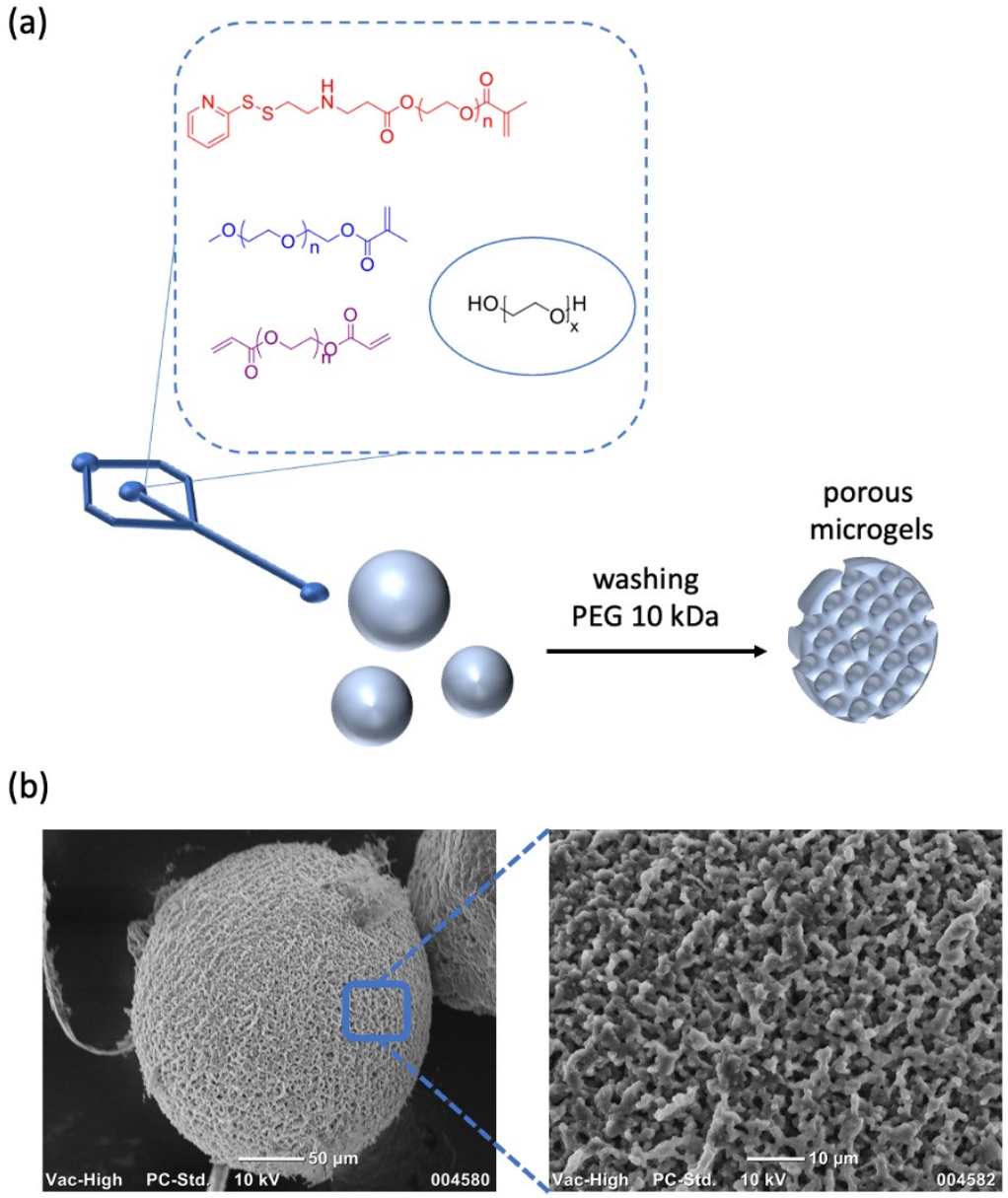

Figure 2.8 (a) General demonstration of incorporation of PEG 10 kDa into microgels system, (b) SEM images of porous microgel.

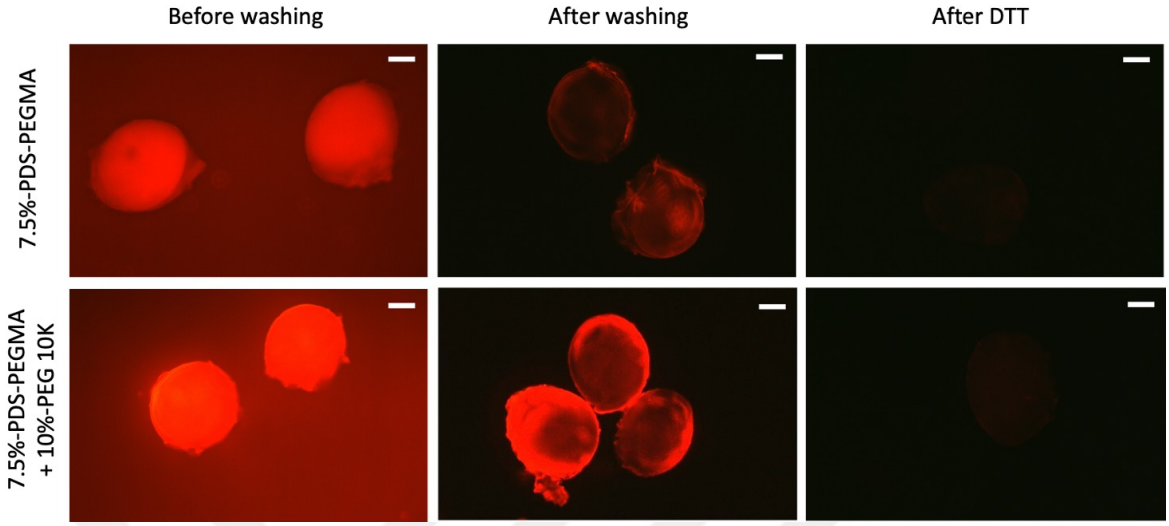

Figure 2.9 Fluorescence microscopy images of TRITC-extravidin immobilization onto the microgels with the comparison of porosity (Scale 100 μm).

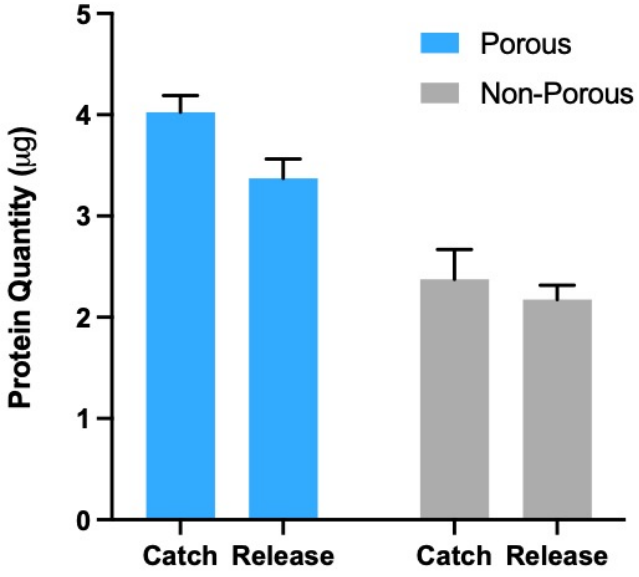

Figure 2.10 Quantification of protein amounts for catch&release process in both porous and non-porous microgels.

The quantitative analysis of the caught and released protein was determined using the same amount of porous and non-porous microgels. First, Biotin-SH conjugated to the microgels. Then, the biotinalyted porous and non-porous microgels (2 mg) were incubated in a TRITC-extravidin solution for 30 minutes. The quantities of the captured and released protein were determined through UV-spectroscopy, with results provided by TRITC-extravidin at 450 nm. Figure 2.10 demonstrated the caught and released quantity of the protein from 1 mg porous and non-porous microgels as can be concluded that the incorporation of the porosity into microgels' network increased the amount of isolated protein from the environment.

2.4 Conclusion

In conclusion, droplet-based microfluidics and photopolymerization methods fabricated thiol-reactive PDS groups containing microgels. Different amounts of PDS groups were employed in the fabrication process, and the highest quantity was chosen, reaching the point where the microdroplets lost their stability for demonstration. The PDS group was finally activated with thiol-containing biotin using a thiol-disulfide exchange reaction, and successful immobilization of TRITC-extravidin was demonstrated. The *on-demand* release and selectivity from the protein mixture was performed. Later, to enhance the performance of the microgel system, we augmented its porosity by incorporating PEG. The SEM characterizations of the porous and non-porous materials were done. The following experiments effectively demonstrated the protein *catch-and-release* capabilities, providing valuable insights into isolating proteins from the environment. These findings hold significant promise for biomedical applications, showcasing the system's potential to interact with proteins in a controlled and selective manner.

3. POROUS MICROGELS FOR DELIVERY OF CURCUMIN: MICROFLUIDICS-BASED FABRICATION AND CYTOTOXICITY EVALUATION

The materials in this chapter have been adapted from the following article: Orbay, S.; Sanyal, R.; Sanyal, A. *"Porous Microgels for Delivery of Curcumin: Microfluidics-Based Fabrication and Cytotoxicity Evaluation"*, Micromachines., Vol. 14, No. 10, pp.1969, October 2023 [84].

3.1 Introduction

Polymeric microgels, produced via the microfluidics technique, have emerged as a fascinating area of research in materials science and biotechnology [85–87]. These miniature hydrogel particles, typically ranging from hundreds of nanometers to a few micrometers in size, impart unique properties that make them vital in a wide range of applications [61, 88, 89]. Microfluidics, a technology that manipulates fluids in micro scale channels, allows precise control over the synthesis process, resulting in well-defined and uniform polymeric microgels [90]. Fabricating microgels using microfluidics offers numerous advantages compared to traditional methods. The precise control over size and shape enabled by microfluidic devices ensures the production of monodisperse microgels, providing uniformity in their properties. Microfluidics devices enable high-throughput production, allowing the rapid generation of large quantities in a short time, thus facilitating scalability for mass production [91]. Moreover, the tunable properties of microgels, such as porosity and drug release kinetics, can be finely adjusted by manipulating the fabrication parameters. With reduced reagent consumption, ease of automation, and the seamless integration of other functionalities, microfluidics-fabricated microgels emerge as a versatile and cost-effective solution to advance biomedical research and enable cutting-edge technologies [92, 93].

Due to their versatile and multifunctional nature, soft materials like hydro-

gels [94–96], microgels [97–99], and nanogels [100–102] are finding increasing use in applications such as drug delivery and diagnostics. Microgels are being explored as promising candidates for drug delivery systems due to their remarkable features, such as substantial loading capacity, compatibility with biological systems, and biostability [88,103–105]. The cross-linked network of microgels plays a crucial role in preventing the breakdown of long molecular chains, thereby contributing to its stability [106]. The viscoelastic characteristics of microgels add to their appeal by demonstrating structural changes in response to environmental changes. Additionally, stimuli-responsive microgels [107,108] exhibit a faster response to stimuli than bulk gels, proving their efficiency in drug delivery systems [109–112]. Another aspect is that modulating the porosity of microgels through precise adjustments in monomer compositions has a significant influence on drug delivery. By tailoring the monomer constituents, it becomes possible to engineer microgels with varying degrees of porosity. This, in turn, directly impacts the performance and efficacy of the drug delivery process.

The fabrication of microgels with a porous morphology enables control over the diffusion of drugs from within the gel matrix [113,114]. Microgels with higher porosity exhibit larger interstitial spaces, facilitating the faster diffusion and release of encapsulated drugs. Moreover, the porosity of microgels influences their loading capacity. Microgels with increased porosity can accommodate a larger quantity of drugs, enhancing the total payload that they can deliver. This is particularly valuable when aiming to administer therapeutic agents in precise amounts over extended periods. Additionally, porosity impacts the interaction between microgels and their environment. Microgels with higher porosity tend to be more responsive to external stimuli [115], leading to more pronounced changes in their size and structure. This responsiveness can be harnessed to trigger accelerated drug release when desired, providing an on-demand delivery mechanism.

Curcumin, a naturally occurring polyphenolic compound sourced from the rhizome of turmeric (curcuma longa), exhibits a wide array of biological and health-enhancing attributes. These encompass antioxidant, antimicrobial, anti-inflammatory, anti-proliferative, and anti-cancer activities, making it a versatile and valuable com-

pound [116–118]. However, its potential for clinical applications remains limited due to curcumin's challenges in terms of low bioavailability, limited absorption, aqueous solubility, and rapid metabolism. Therefore, curcumin has been explored using a variety of delivery techniques. These include liposomes [119], micelles [110, 120], lipid-based nanoparticles [121], and polymer–drug conjugates [122], often involving physical encapsulation or chemical conjugation for its incorporation. Curcumin beta-cyclodextrin inclusion complexes represent a solution to the inherent limitations of curcumin, including poor solubility, low bioavailability, and susceptibility to degradation.

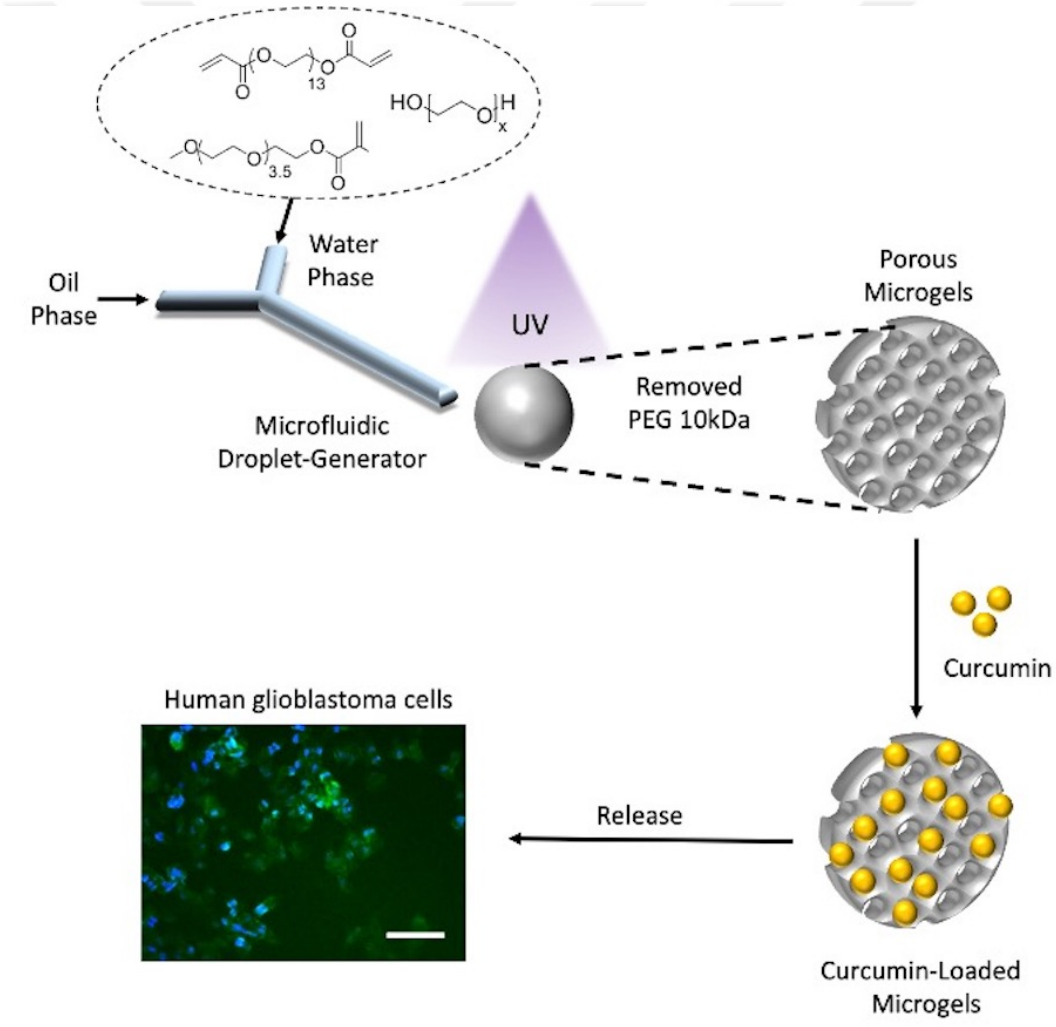

Figure 3.1 General demonstration of the concept.

Through the complexation of curcumin with beta-cyclodextrin, its solubility is significantly improved, ensuring better absorption in the body and increased bioavailability [123, 124]. Furthermore, these complexes play a pivotal role in bolstering curcumin's stability, shielding it from detrimental environmental factors like light, heat, and oxygen, which can cause degradation. Additionally, the capacity to regulate release rates enables the sustained and controlled delivery of curcumin over time [125]. Therefore, curcumin beta-cyclodextrin inclusion complexes offer a versatile and potent solution to unlock the therapeutic potential of curcumin.

Herein, we fabricate non-porous and porous microgels using a microfluidics platform and demonstrate the effective loading of a curcumin cyclodextrin complex into these microgels. We show that the fine tuning of the monomer composition and porosity has a profound effect on the efficiency of these microgels as drug delivery vehicles. General concept of this chapter can be seen in Figure 3.1. This study delves into the intricate relationship between microgel morphologies, drug encapsulation and release, and cytotoxicity, thus providing valuable insights into the future of the microfluidics-based tailoring of drug delivery systems.

3.2 Experimental

3.2.1 Materials and Characterization

All solvents were purchased from Merck and used as obtained without further purification. Ultrapure water was obtained from a Milli-Q Water Purification System (Milli-pore, Billerica, MA, USA). PEGDA, PEGMEMA, PEG 10kDa, DPPH, LAP, HP-β-CD, and curcumin were obtained from Sigma Aldrich (Sigma, St. Louis, MO, USA).

For the microfluidics setup, PDMS, HMDS, chlorotrimethylsilane, a negative photoresist (SU-8 2050), PGMEA, glass slides and a biopsy punch (Harris Uni-Core 0.75 mm, USA), and Span 80 were purchased from Sigma Aldrich. Mineral oil (0.880

kg/L) was purchased from AppliChem. Adhesion promoter TI prime was purchased from MicroChemicals. PTFE tubes for the inlets and outlets of microfluidic channels were obtained from Microfluidic ChipShop (Microfluidic ChipShop, Jena, Germany).

An EVG 620 semiautomatic contact photolithographic alignment and exposure tool with a 1000-watt light source was used for the silicon master mold fabrication (EV Group, Sankt Florian am Inn, Austria). Plasma treatment of the PDMS device and a glass slide was performed using a laboratory corona treater (BD-20AC, Electro-Technic Products Inc., Chicago, IL, USA).

In situ photopolymerization was performed using a UV light source (36-watt, 365 nm). UV-vis spectra were collected on a Cary Varian spectrometer (Santa Clara, CA, USA). Curcumin-loaded polymeric microgels were visualized using fluorescence microscopy (HBO100 ZEISS Fluorescence Microscopy, Carl Zeiss., Jena, Germany), and fluorescence images were processed using the Zeiss AxioVision software. Syringe pumps were purchased from maviTeknik (Mersin, Turkiye).

Cell viability experiments were performed with a plate reader (Multiscan FC, Thermo Scientific, Waltham, MA, USA) using Cell Counting Kit-8 (CCK-8, Fluka, Sigma, St. Louis, MO, USA). Images of drug internalized cells were obtained using a Zeiss Observer Z1 fluorescence microscope with an Axiocam MRc5 camera. The U87 MG cell line was purchased from ATCC (LGC Standards, Wesel, Germany) and grown according to the culture method requirements of the manufacturer. All the chemicals used in cell experiments were purchased from Sigma Aldrich.

3.2.2 Y-shaped Droplet-based Microfluidics Channel Fabrication

To create a single-layer microfluidic channel of PDMS with dimensions measuring 400 μm in width, 300 μm in-depth, and 3 mm in length, as illustrated in Figure 3.2a, the initial step involved crafting a replication mold using a conventional lithography technique. To produce the master mold, a 4-inch silicon wafer underwent a

meticulous cleaning process, followed by silane vapor treatment utilizing HMDS for 1 h. After applying a coating of TI prime to serve as an adhesion promoter, a brief one-minute pre-bake was carried out on a hotplate at 95 °C. Subsequently, a layer of SU-8 2050 was spun onto the wafer and subjected to a baking process at 65 °C for one minute, followed by 20 minutes at 95 °C before the exposure stage. The photo mask, bearing the desired pattern, was positioned pattern side up on a 5 × 5-inch soda-lime glass substrate, which was then placed face-down on a mask aligner. The silicon wafer coated with a photoresist was precisely aligned with the mask and brought into contact to enable exposure. After exposure, the wafer was post-baked at 65 °C for 5 minutes and 95 °C for 10 minutes. A subsequent immersion in an organic SU-8 developer solvent (PGMEA) for 10 minutes facilitated the removal of excess photoresist. The wafer underwent sequential rinsing with IPA and DI water, followed by nitrogen drying. To enable the reuse of the mold, the wafer's surface was treated with chloro trimethylsilane vapor within a vacuum desiccator. The next phase involved mixing a silicone elastomer base with a curing agent in a 10:1 ratio within a controlled environment devoid of dust. This mixture was then cured at 65 °C for 2 h, leading to the replication of PDMS channels. Once complete curing was achieved, the PDMS was extracted from the master mold, and each microchannel was individually cut. The inlet and outlet points were established using a manually operated biopsy puncher. Both the PDMS channel and the glass slide surfaces underwent oxygen plasma treatment for 3 minutes to enhance bonding. The bonding itself was performed at 65 °C for a night. Lastly, PTFE tubes were inserted into the inlets and outlets of the PDMS microfluidics channel in preparation for conducting experiments.

3.2.3 Microgels Synthesis via Microfluidics

Microgels of varying porosities were fabricated using the W/O emulsion technique within a droplet-based microfluidics setup. Briefly, a Y-shaped microfluidic channel was employed to generate consistently sized droplets, as seen in Figure 3.2a,c, and d. The oil phase was pumped to create a continuous phase, and the aqueous phase, including monomer solution and initiator, was injected into the channel to form a dis-

persed phase. The dispersed phase was then broken off when it met the continuous phase at the intersection of the channel. After the microdroplet formation, the droplets traversed the channel and reached the outlet tubing, where UV polymerization was initiated. The microgels were collected in a container to undergo thorough washing steps to eliminate residuals, unreacted monomers, and PEG.

PEGDA, PEGMEMA, and PEG (10 kDa) were dissolved in DI water to prepare the dispersed phase. To catalyze the polymerization, a photoinitiator, LAP (constituting 2% of the total monomers), was introduced into this solution. This aqueous solution was then utilized as the dispersed phase in the microfluidics process, while the mineral oil with 10% SPAN 80 was employed as the continuous phase can be seen in Figure 3.2b.

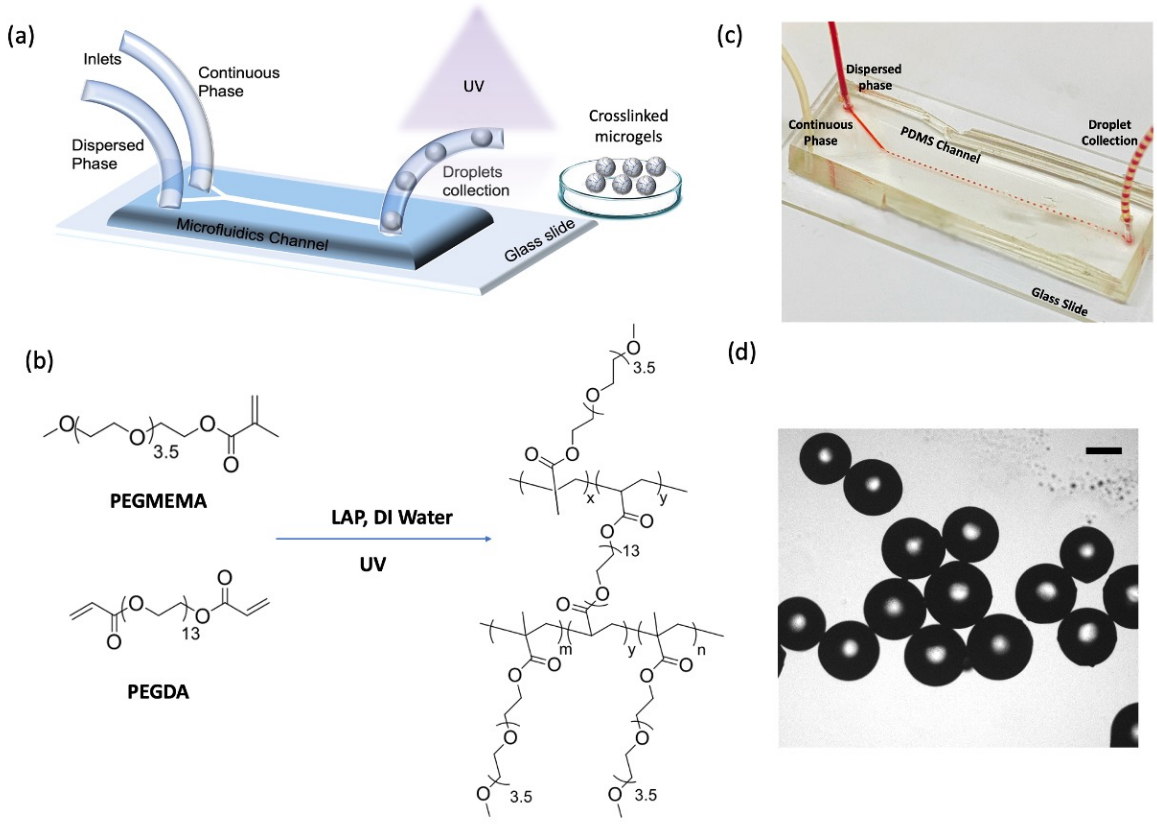

Figure 3.2 (a) General illustration of microfluidics fabrication of polymeric microgels, (b) chemical scheme of microgel formation, (c) real droplet generator in operation, (d) optical image of monodispersed microgels at dry stage produced via microfluidics (Scale 200 μm).

3.2.4 Morphological Analysis Using Scanning Electron Microscopy (SEM)

SEM studies were conducted to characterize the microgels' morphologies. SEM images were obtained from dried microgel samples using a JCM-5000 NeoScop Tabletop SEM with an accelerating voltage of 10 kV.

3.2.5 Curcumin + HP-β-CD Complexation

The complexation of curcumin and HP-β-CD was achieved through solvent evaporation methods, as described in previous reports [126, 127]. Curcumin and HP-β-CD were dissolved in a 1:2 ratio in ethanol and stirred at 40°C until the ethanol completely evaporated. The resulting mixture was re-dissolved in water, filtered, and subjected to lyophilization. Subsequently, the sample was stored at 4°C for further analysis.

3.2.6 Curcumin Loading and Release

Curcumin was loaded into the microgels using a solution absorption method. Microgels (5 mg) were soaked in 1 mg/ml curcumin-HP-β-CD complex aqueous solution at 37 °C with 100-rpm mechanical shaking for 1 h. The curcumin loading was monitored by analyzing the curcumin concentration in the soaking solution with a UV-Vis spectrometer at 425 nm. Later, the curcumin-loaded microgels were gently washed with water, and 1 ml release medium was added. The release experiments were done at 37 °C with a 100-rpm shaking. At predetermined time intervals, the concentration of the drug in the collected media was monitored using a UV-Vis spectrometer.

3.2.7 Drug Release Kinetic Models

Various kinetic models, including zero-order, first-order, Higuchi, and Korsmeyer-Peppas, have been employed to validate and elucidate the underlying mechanism of drug release. To predict the release behavior of the drug, it is imperative to analyze

diverse outcomes derived from fitting data into a range of validated mathematical models [128,129]. These kinetic models elucidate whether the drug release is contingent on dissolution or diffusion. They also distinguish whether the release aligns with fickian, non-fickian, or super case-II drug release models.

3.2.8 Antioxidant Activity

The antioxidant activities of curcumin-loaded microgels were measured using the DPPH radical scavenging activity test. It involves exposing a purple-colored DPPH radical to a sample containing potential antioxidants. Antioxidants reduce the DPPH radical, causing it to change color from purple to yellow, which is quantified by measuring the decrease in absorbance at a specific wavelength using a UV spectrophotometer [130]. The extent of color change reflects the antioxidant capacity of the tested compound. To assess the antioxidant activity of the curcumin-loaded microgels, we prepared curcumin-loaded and non-loaded microgels. We measured the absorbance at 517 nm to demonstrate the inhibition of the DPPH radical.

3.2.9 In Vitro Cytotoxicity and Internalization

Cytotoxicity of drug-loaded microgels was determined using CCK-8 viability assay. U87 MG human glioma cell line (purchased from ATCC (LGC Standards, Germany) was used for cytotoxicity experiments. Cells were grown in DMEM supplemented with 10% fetal bovine serum and incubated at 37 °C. U87 MG cells (4000 cells/well) were seeded in a 96-well plate in 100 μL DMEM and incubated at 37 °C for 24 h to adhere completely. Cell-adhered plates were treated with the aliquots of drug-loaded microgels at 37 °C for 24 h and 48 h. After 48 h, a CCK-8 solution (10%) was introduced into each well. Following a 2 h incubation period, the absorbance values were quantified using a plate reader (Multiscan FC, Thermo Scientific, USA) set at 450 nm. The cell viability of the treated cells was assessed based on the percentage relative to control cells (cells in media only). The results were analyzed using GraphPad Prism

software employing a nonlinear regression model.

To facilitate cellular internalization, we initially seeded U-87 MG glioblastoma cells (50,000 cells per well) into a 24-well plate, triplicating the setup, with each well containing 1 mL of DMEM culture media. These cell cultures were then incubated at 37°C for 24 h. The cells were then subjected to three consecutive washes with 500 μL of PBS each time. Afterward, the cells were fixed by exposure to a 4% formaldehyde solution at 37°C for 10 min. Following another three rounds of PBS washing, the cells underwent a 15-min incubation at 37°C for DAPI nuclei staining. We employed a Zeiss Observer Z1 fluorescence microscope to visualize and document the cellular state and processed the obtained images using AxioVision software (Version 4.8.2.0).

3.3 Results and Discussion

3.3.1 Microgels Synthesis and Characterization

Through a photo-initiated polymerization process using PEGDA, PEGMEMA, and PEG 10 kDa, polymeric microgels were successfully synthesized using microfluidics, as illustrated in Figure 3.2d. The gelation was accomplished under UV irradiation at 365 nm in the presence of the photoinitiator, LAP. This approach harnessed the precise manipulation of fluid dynamics within microchannels by adjusting flow rates forming mono-dispersed microdroplets. The dispersed phase consisted of PEG monomers, which were delivered by one of the inlets, as summarized in Table 3.1. The continuous phase consisted of 10 wt% Span 80. All components were pumped into the microfluidics channel via tubing attached to the tip of 1 ml syringes. Pumping into the channel was done using a syringe pump at a flow rate of 10 μL/min for the continuous phase and 5 μL/min for the dispersed phase. Droplet formation was observed once a steady flow of both phases had been established. These microdroplets underwent photopolymerization while traversing the outlet tubing.

After the microgel formation, microgels were collected into eppendorf tubes.

Table 3.1

Properties of microgels with varying monomers. While P signifies porous, NP signifies non-porous.

	PEGMEMA eq.	**PEGDA eq.**	**PEG 10kDa eq.**
P-PEGMEMA-PEGDA	1.3	1	0.1
NP-PEGMEMA-PEGDA	1.3	1	-
P-PEGDA	-	1	0.1
NP-PEGDA	-	1	-

Microgels were washed with hexane, methanol, DI water, and methanol, respectively, to remove excess oil. Then, microgels were dried overnight at room temperature under vacuum. The resulting microgels were weighed prior to use in trials. The synthesized microgels underwent examination using an optical microscope, allowing for the acquisition of size distributions (Figure 3.3a,b). Thereafter, SEM was utilized to probe the surface micro-structures of the microgels. The microgels were dried before the analysis. It is known that porogens, often PEG-based, can be introduced during fabrication to increase porosity [131–133].

From the SEM images, morphologies with increased pore size were observed upon adding the chain length of PEG 10 kDa. Additionally, we inferred that enhanced porosity was obtained upon the incorporation of PEGMEMA as the monomer, along with the linear PEG (10 kDa). The comparison of Figure 3.4a,b indicates that the utilization of PEGMEMA resulted in a significant augmentation in the microgels' porosity. The impact of incorporating PEG (10 kDa) into the polymeric network was explored within both PEGMEMA-containing and PEGMEMA-free microgels to elucidate the effect of individual components in terms of porosity and drug-loading capacities.

To obtain further insights, water-induced swelling was employed to investigate the relationship between the volume change of dry microgels and their porosity. Dry microgels were first prepared and characterized for their initial size and structure. Then, a known amount of water was gradually introduced to the microgels, and their volume changes were meticulously recorded using an optical microscope. As water

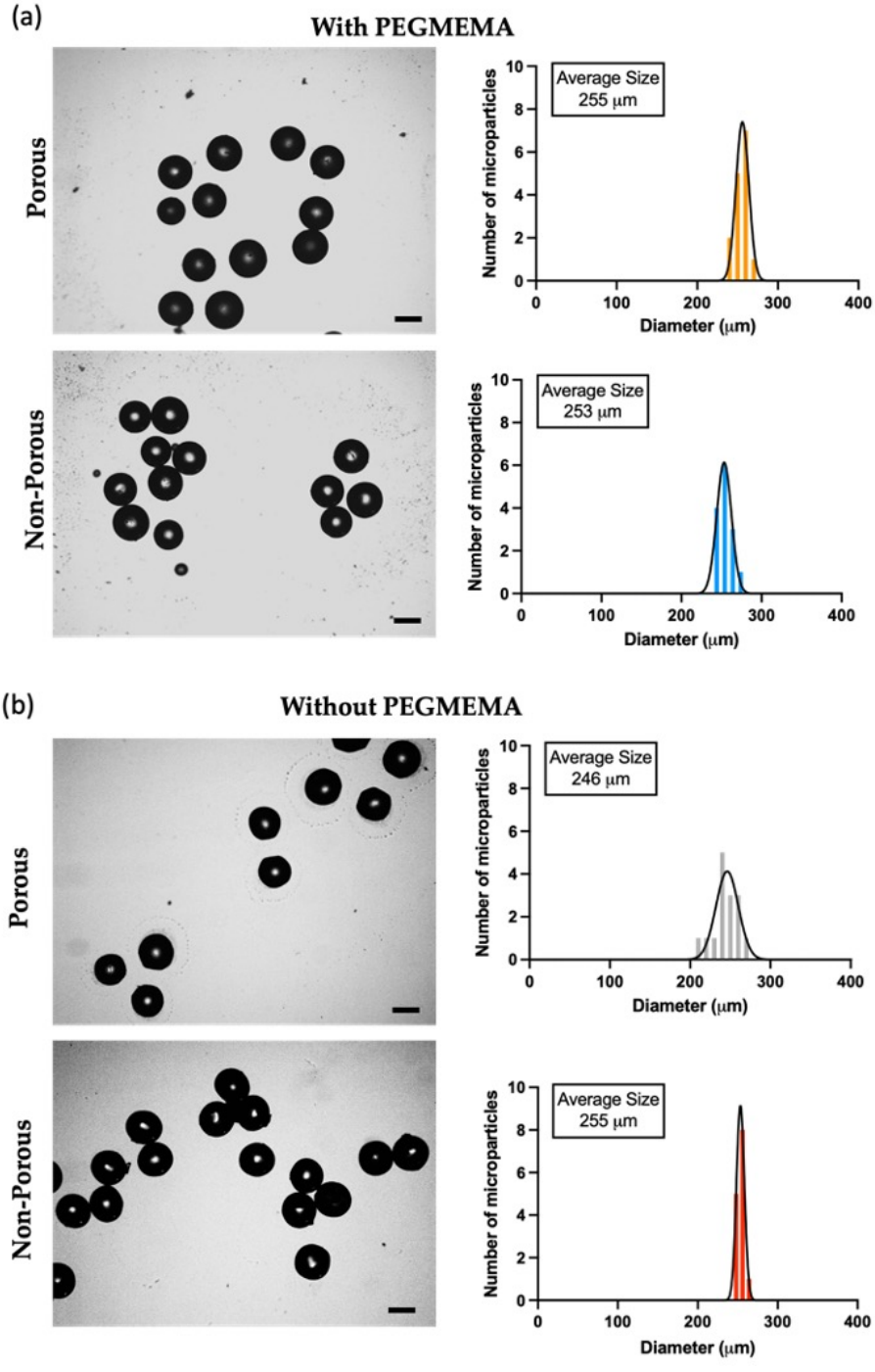

Figure 3.3 Size distribution of microgels. (a) Microgels with PEGMEMA, (b) microgels without PEGMEMA (Scale 200 μm).

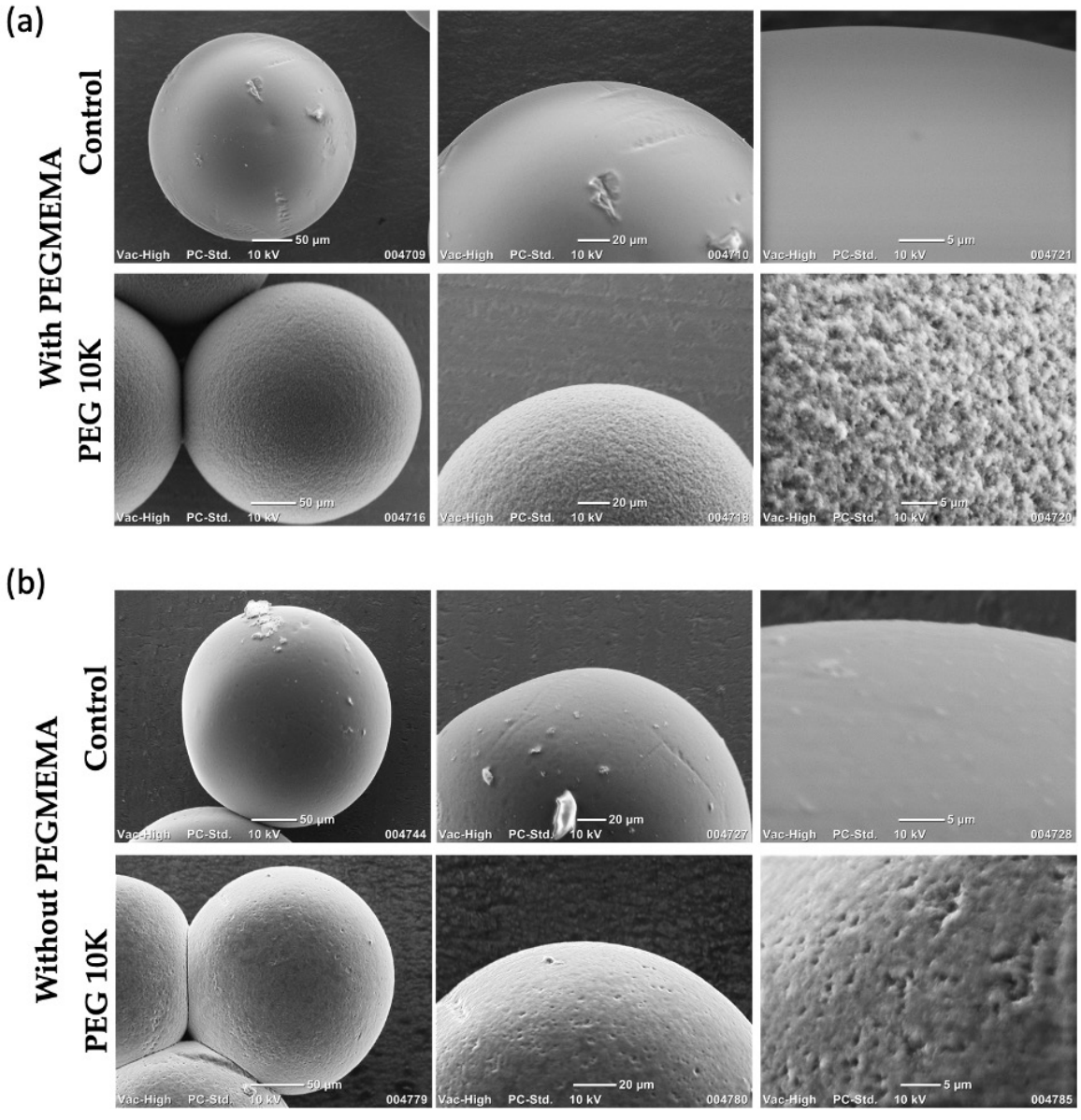

Figure 3.4 SEM images of microgels. (a) Microgels with PEGMEMA, (b) microgels without PEGMEMA.

permeated the microgel network, the polymer chains within the microgels adsorbed water molecules, expanding the microgel structure.

The volume change was directly proportional to the porosity of the microgels (Figure 3.5a), with more porous microgels (P-PEGMEMA-PEGDA) exhibiting larger volume increases due to the greater accessibility of water molecules to the internal void spaces. Figure 3.5b displays optical microscopy images capturing the swelling behavior of porous microgels upon the addition of 100 μL of water to the initially dry gels.

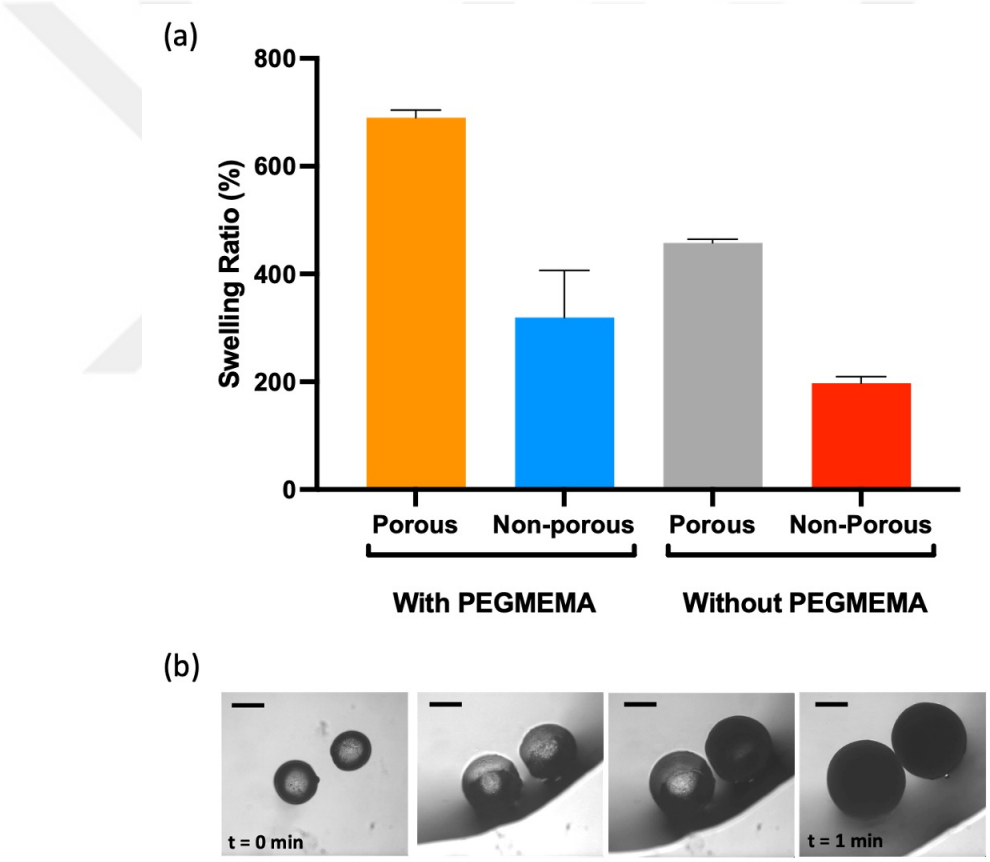

Figure 3.5 (a) Volume changes of microgels, (b) P-PEGMEMA-PEGDA microgels swelling profile video images (Scale 200 μm).

3.3.2 Curcumin Loading and Release

Microgels' drug loading and release characteristics were examined using a hydrophobic drug, curcumin. Loading of the drug onto the microgel samples was accomplished through a solution absorption technique. Curcumin loading trials were conducted in DI water, and given curcumin's hydrophobic nature, a curcumin HP-β-CD complex was employed to enhance the drug's solubility to obtain better loading, as seen in Figure 3.6a. Figure 3.6b demonstrates that using curcumin alone for loading, without incorporating the complex, does not yield effective results. This suggests that the supramolecular complex plays a crucial role in enhancing the loading performance, which will be important in obtaining sufficient release to induce cytotoxicity. An additional analysis was conducted to establish the formation of inclusion complexes between CUR and HP-β-CD through the analysis of FTIR (Figure A.1) and 1H NMR (Figure A.2) spectra.

For loading studies, the curcumin–CD complex was dissolved in water (1 mg/mL). A predetermined amount of dry microgel was weighed and placed in separate vials for each microgel system. A calculated volume of the curcumin–CD solution was added to each vial, and the microgels were allowed to adsorb the complex at 37 °C with 100 rpm gentle mechanical shaking for 1 h. After adsorption, the microgels were separated from the solution, and the concentration of curcumin in the supernatant was measured using UV spectrophotometry at 425 nm. It enabled the calculation of the loaded curcumin by subtracting the initial concentration from the measured concentration. This loading process was repeated for microgels of varying porosity, and the data were analyzed to understand the influence of porosity on the curcumin adsorption efficiency (Figure 3.7).

The optimal microgel system with the highest loading performance was employed to monitor the release profile of curcumin. The curcumin-loaded microgels were carefully washed with distilled water before introduction into the release medium. Release studies were conducted in both DI water with 0.5% Tween 20 and cell medium. At specific time intervals, the release medium was examined using a UV spectropho-

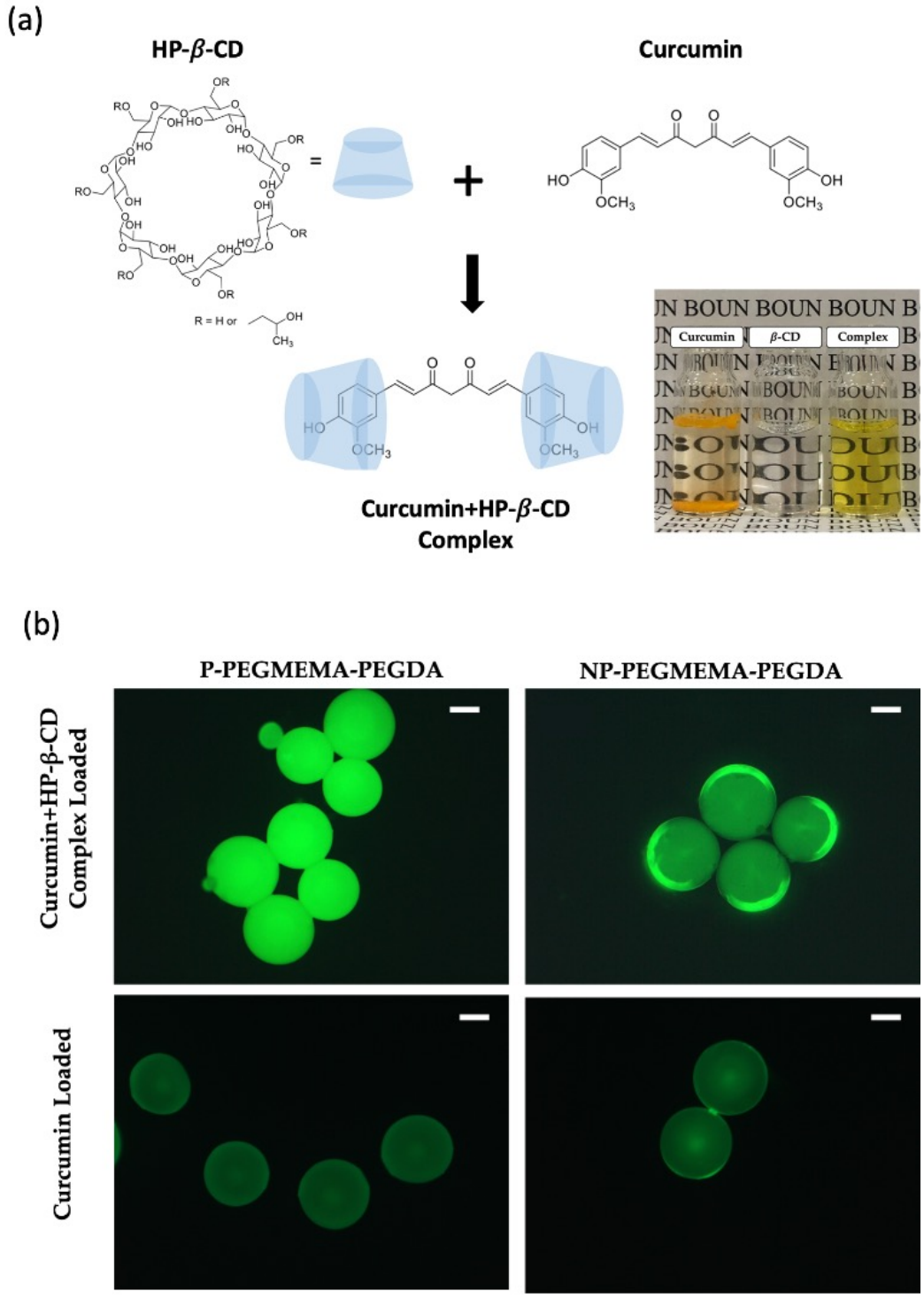

Figure 3.6 (a) Curcumin and β-cyclodextrin (HP-β-CD) complexation and solubilities in DI water, (b) the differences of only curcumin-loaded and inclusion complex-loaded microgels under the same exposure (Scale 200 μm).

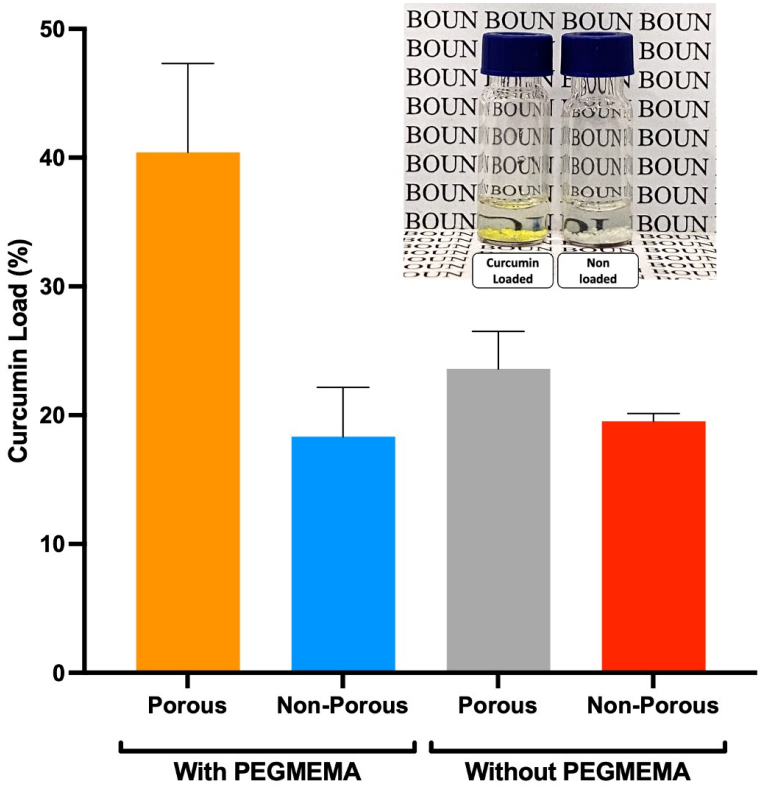

Figure 3.7 Curcumin loading to different microgel systems.

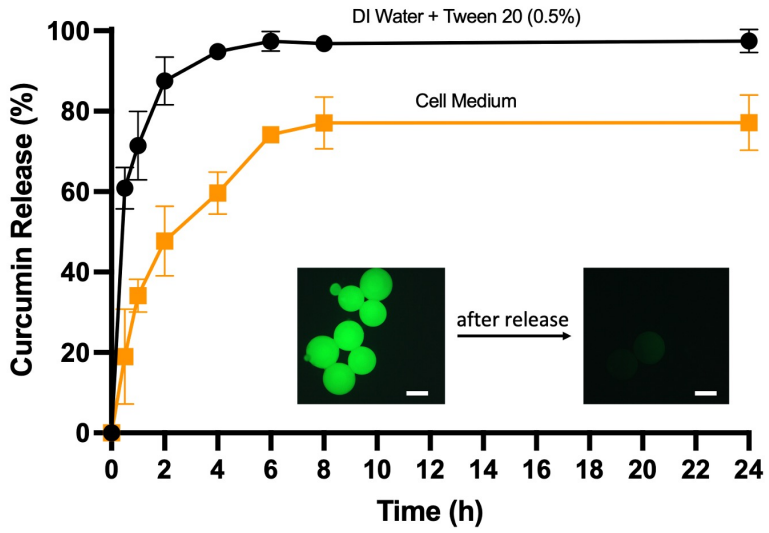

Figure 3.8 Curcumin Release from P-PEGMEMA-PEGDA microgels in DI Water + Tween20 (0.5%) and cell medium (Scale 200 μm).

tometer to monitor drug release. The obtained release profiles demonstrated an initial rapid drug release from microgels (Figure 3.8). The microgels were captured under both optical and fluorescence microscopy after the release completed and the results can be seen in Figure A.3.

3.3.3 Drug Release Kinetic Models

The most suitable kinetic model for predicting the release of curcumin from spherical microgels was determined through curve fitting and calculation of correlation coefficients. These models help us understand and predict how drugs are released over time, influencing their efficacy. Various models, such as zero-order (constant release rate)(Eq.3.1), first-order (proportional to remaining drug)(Eq. 3.2), Higuchi (diffusion-based release) (Eq. 3.3), and Korsmeyer-Peppas (complex release mechanisms)(Eq. 3.4), were investigated for curcumin release by fitting experimental data to these models using the equations following:

$$\mathbf{M}_t \div \mathbf{M} = \mathbf{k}_0\mathbf{t} \tag{3.1}$$

$$\mathbf{M}_t \div \mathbf{M} = \mathbf{1} - \mathbf{e}^{(-k_1\ t)} \tag{3.2}$$

$$\mathbf{M}_t \div \mathbf{M} = \mathbf{k}_h\mathbf{t}^{0.5} \tag{3.3}$$

$$\mathbf{M}_t \div \mathbf{M} = \mathbf{k}\mathbf{t}^n \tag{3.4}$$

The drug release dynamics of the composite hydrogel were investigated using the Korsmeyer–Peppas model, which characterizes drug release kinetics based on alterations in diffusion coefficients of both water and the drug. The diffusion index (n) obtained from the Korsmeyer–Peppas model was 0.4857, indicative of non-Fickian

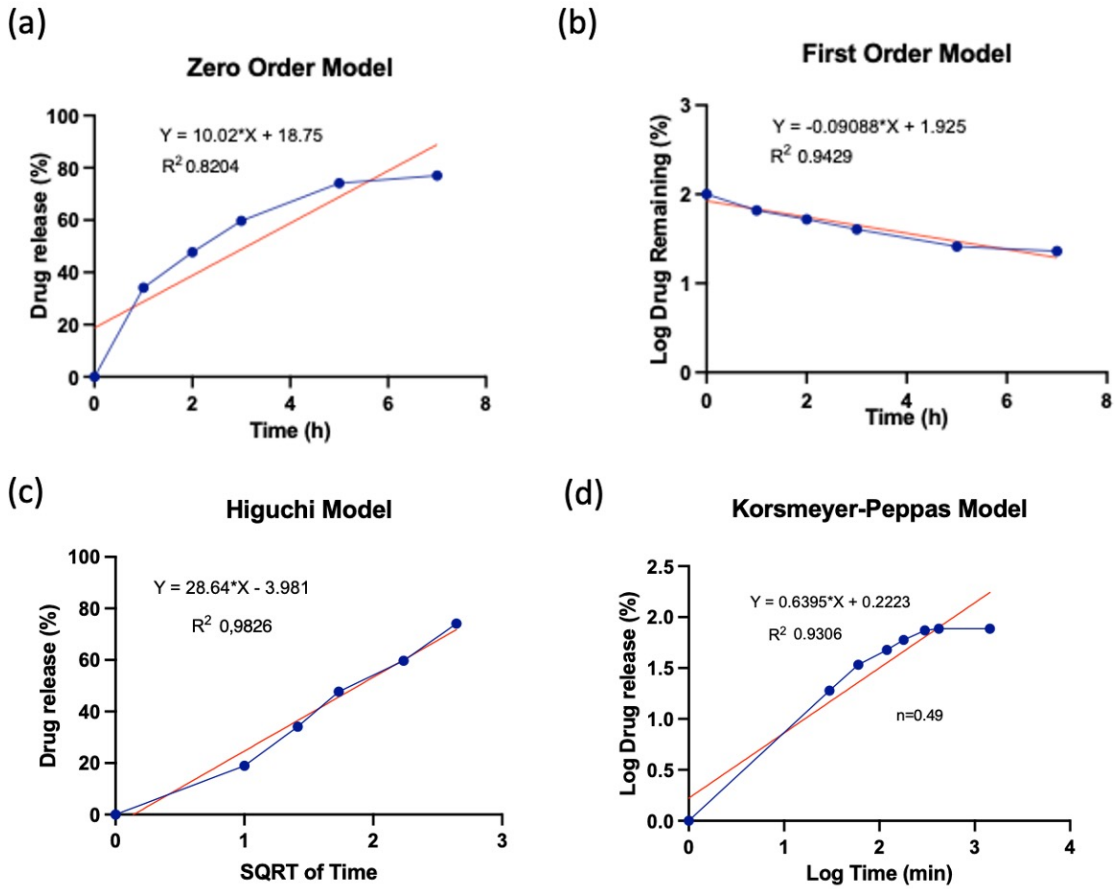

Figure 3.9 Model fitting of curcumin release kinetics. (a) Zero order model, (b) first order model, (c) Higuchi model, and (d) Korsmeyer-Peppas model.

(anomalous) diffusion in the range of 0.45 to 0.89. Anomalous transport encompasses a spectrum of behaviors that lie between simple Fickian diffusion and more intricate processes like erosion, swelling, relaxation, or chemical reactions.

The fitting curves' correlation coefficients for the release of curcumin from the spherical microgels were found 0.8204, 0.9429, 0.9826, and 0.9306, as seen in Figure 3.9. Among these, the Higuchi model exhibited the highest correlation coefficient. The Higuchi model had the highest correlation coefficient when fitting the release data of curcumin from the spherical microgels; it suggests that the release mechanism for curcumin from these microgels is consistent with diffusion-based release, where the amount released increases with the square root of time.

3.3.4 Antioxidant Activity of Curcumin-Loaded Microgels

The DPPH radical scavenging activity of curcumin-loaded and non-loaded microgels was evaluated to assess their potential antioxidant properties. For the DPPH radical scavenging test, curcumin-loaded and non-loaded microgels were combined with 1 mL of an ethanolic DPPH solution (0.2 mmol/L).

Subsequently, the resultant mixtures were left to stand for 30 min at room temperature in the dark (Figure 3.10). The absorbance of the resulting supernatants was then measured spectrophotometrically at 517 nm. The DPPH radical is a stable free radical with a deep purple color in solution, and it changes color to yellow when it is reduced by an antioxidant compound, which can be observed in UV spectroscopy, as seen in Figure 3.10c.

These results clearly indicate that incorporating curcumin into the microgels does not compromise its antioxidant activity. A slight delay in the quenching of the radical is observed for the curcumin-loaded microgels as compared to the free and complexed drug, presumably due to the slower release of the drug from the microgels (Figure A.4).

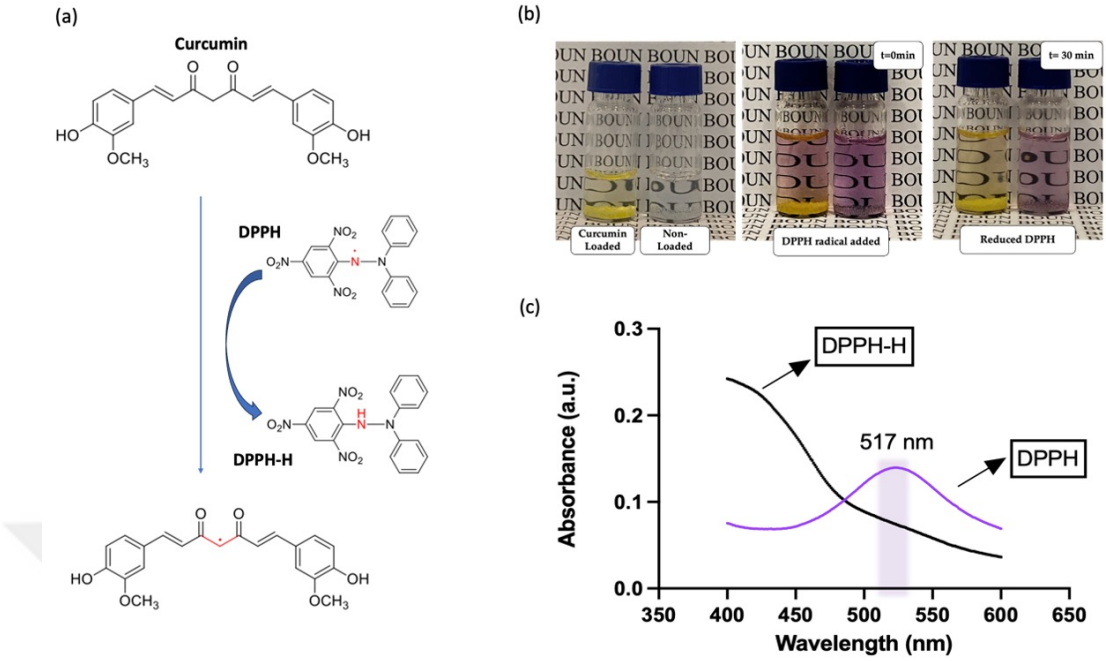

Figure 3.10 (a) Curcumin reaction with DPPH, (b) DPPH radical color change in the presence of curcumin, (c) DPPH radical scavenging UV spectroscopy result.

3.3.5 In Vitro Studies

This study aims to design microgels to evaluate their potential as biomaterials for delivering curcumin. Hence, it is crucial to assess the cytotoxicity of these microgels and their resultant drug-release products. Therefore, we evaluated the anticancer activity of curcumin-loaded microgels (P-PEGMEMA-PEGDA) against U-87 MG human glioblastoma cells by assessing their cytotoxicity using the CCK-8 assay. In Figure 3.11a, it can be observed the cell viability percentages after a 48-h treatment with various curcumin concentrations.

At the lowest concentration of 10 μg/mL, there was a modest reduction in cell viability, with approximately 85% of cells remaining viable. As the concentration of curcumin was increased to 30 μg/mL and 45 μg/mL, cell viability decreased progressively to 65% and 40%, respectively. These findings suggest that curcumin exerts a significant inhibitory effect on U87MG cell proliferation, highlighting its potential as a candidate for further investigation in the context of glioblastoma therapy.

We also investigated the cellular internalization of the drug using fluorescence microscopy, since curcumin is inherently fluorescent. Cancer cells were treated with aliquots from drug loaded microgels for 6 h. We employed DAPI, a fluorescent blue dye, to stain the cell nuclei. The results were analyzed using fluorescence microscopy, as seen in Figure 3.11b. The high level of green fluorescence in these experiments indicated the successful internalization of the hydrophobic drug.

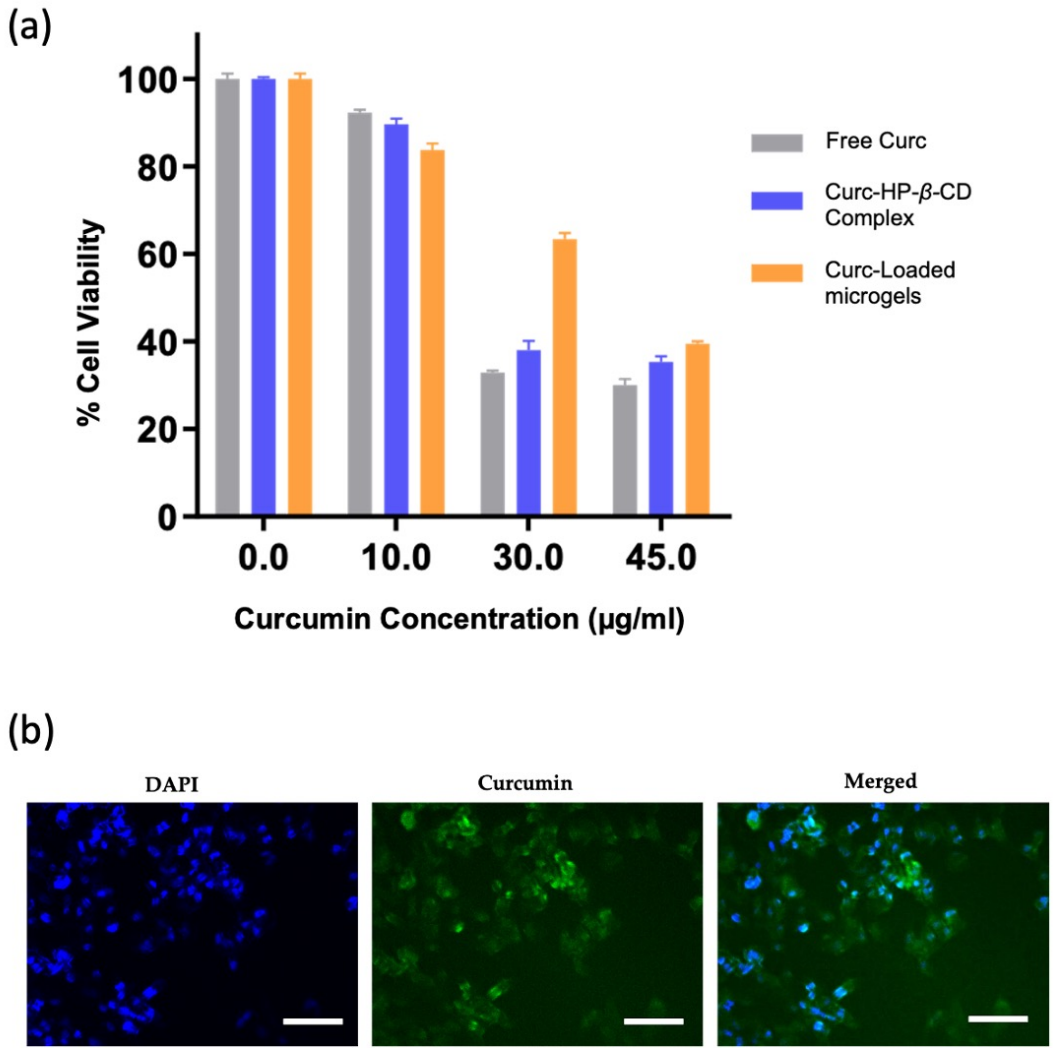

Figure 3.11 (a) Cell viability, (b) internalization of curcumin released from microgels (Scale 100 μm).

3.4 Conclusion

Porous microgels using PEG with a molecular weight of 10 kDa. This approach is achieved through a single-step procedure within a droplet microfluidic system, offering enhanced precision and control over the microgel formation process. By harnessing this technique, we successfully fabricate microgels characterized by their unique porous structure, which holds great potential for various applications. One of the remarkable features of our approach is the ability to adjust the porosity of these microgels by making specific changes to their composition. By modifying factors such as the concentration or ratio of components, we can finely control the extent of porosity within the microgel structure. This tunability provides a versatile platform for tailoring the structural properties of the microgels to meet the requirements of specific applications.

Introducing porosity into microgels is a significant advancement, as it opens doors to a wide range of applications ranging from drug delivery to tissue engineering. The tailored structural characteristics of these porous microgels can influence various factors such as drug release kinetics, cellular interactions, and mechanical properties. Therefore, our study not only introduces a streamlined method for producing such microgels but also highlights the potential impact of their tunable porosity on the broader field of materials science and biomedical engineering.

Our work showcases a novel approach to creating porous microgels using PEG 10 kDa through a simplified single-step process within a droplet microfluidics setup. Controlling the microgel porosity via compositional adjustments offers a versatile avenue for customizing their properties. This achievement contributes to the expanding toolkit of materials with tailored features, holding promise for diverse applications across multiple disciplines.

4. MICROFLUIDICS-ASSISTED FABRICATION OF DEGRADABLE POLYMERIC MICROGELS

4.1 Introduction

Microgels with micron-scale dimensions show considerable capacity in various applications, including drug delivery [134], cell encapsulation [135], microreactors for chemical reactions [136], and biosensing platforms [137]. The success of microgels in these applications is attributed to their high internal void fraction, which facilitates efficient drug encapsulation, as well as the easy transport of proteins, antimicrobial agents, or wastes for entrapped cells for biosensing receptors. Specifically, in delivery applications, microgels in the tens or hundreds of microns, while remaining injectable, can effectively provide phagocytosis avoidance and evasion of the reticuloendothelial system due to their larger size. Unlike nano-sized particles, this characteristic allows them to stay at the injection site, enabling longer-term local drug/biomolecule delivery [138].

Recently, there has been increased interest in microgels composed of *smart* polymeric materials that can undergo swelling and deswelling in response to environmental changes [139]. Stimuli-responsive microgels as *smart* materials, known for their reversibility and triggered deswelling in response to external stimuli like heating [32,140], pH changes [141], electric fields [34], redox reactions [39], or combinations of multiple stimuli [142] have captured considerable attention. When microgels are crafted from biodegradable polymers, the degradation of these gels governs the release of encapsulated biomolecules upon introduction into biological systems. Tailoring the characteristics of the microgels allows for optimizing both the release profile and rate, catering to the specific requirements of the intended application.

Conventional approaches for fabricating these *smart* microgels involve spray drying [143], emulsion techniques [144], or mechanical crushing of bulk hydrogels [86].

However, a significant disadvantage of these methods is the relative polydispersities they yield, which can result in varied outcomes in biomedical applications, mainly due to the observed strong dependence of tissue response on particle size [145]. Additionally, these techniques require drying, direct exposure of cells to solvents, and the application of locally high shear rates. These conditions can significantly compromise the cell viability and the stability of proteins encapsulated within the microgels intended for delivery.

Microfluidics is an innovative alternative to traditional techniques for producing microgels, ensuring monodispersity [49, 61]. This approach has been effectively employed to generate a varied array of polymeric microgels within droplets formed when the two immiscible phases meet at the junction of the microfluidics channel. After droplet formation, gelation typically occurs on-chip, through free radical polymerization of monomers or cross-linkers initiated by initiators [146]. In this case, the cross-linking nature is random and doesn't ensure a homogeneous network's formation. Recently, a growing interest has been in achieving a more uniform and well-defined polymeric network, as these structures exhibit better swelling. Reactions with high efficiency, such as click reactions [147], have grabbed attention for both the fabrication and functionalization of microgels. Compared to random cross-linking, creating redox-responsive networks with well-defined chain connectivity will offer control over the release characteristics of encapsulated agents [148]. The typical approach to producing redox-responsive polymeric materials is employing the thiol-disulfide exchange reaction due to its high efficiency at mild conditions.

In this project, we demonstrate a microfluidic fabrication of degradable microgels using the thiol-disulfide exchange reaction as illustrated in Figure 4.1. The microgels are used as a platform to encapsulate biomacromolecules and facilitate their control release. In particular, a copolymer containing the PDS-group was mixed on-chip with tetra-arm thiol-containing PEG, forming microgels within minutes as the droplets traversed the serpentine section of the microchannel. The obtained microgels were further characterized, and the encapsulation of the bovine serum albumin (BSA) was investigated. Degradation of the obtained microgels was achieved in the

presence of a thiol-containing reducing agent. We employed a different microgel system to encapsulate a reducing agent, enabling precise control over the loaded amount and consequently allowing us to fine-tune the degradation profile.

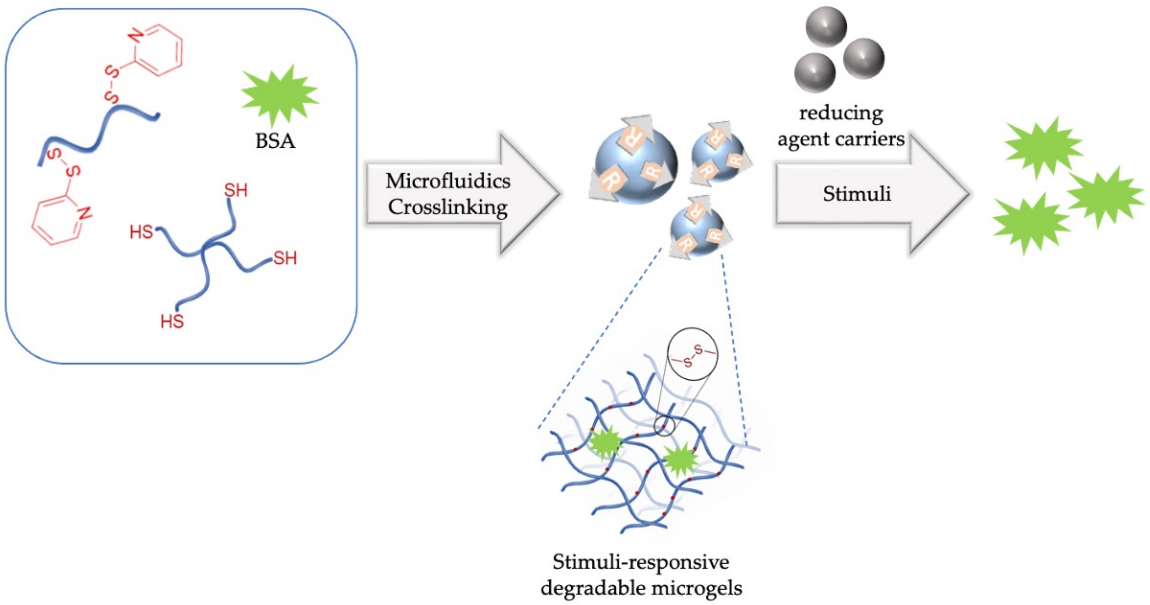

Figure 4.1 General demonstration of the concept.

4.2 Experimental

4.2.1 Materials and Characterization

Tetra-arm PEG thiol [149] and PDS-copolymer [150] (were synthesized by Meltem Alkış), bodipy-maleimide [83] (was synthesized by Aysun Değirmenci) was synthesized according to literature. Merck provided all the organic solvents, which were used without further purification. Ultrapure water from a Milli-Q Water Purification System (Milli-pore, Billerica, MA, USA) was employed. Materials including PEGDA, PEGMEMA, LAP, HP-β-CD were sourced from Sigma Aldrich (Sigma, St. Louis, MO, USA).

For the microfluidics setup, materials such as PDMS, HMDS, chlorotrimethylsilane, a negative photoresist (SU-8 2050), PGMEA, glass slides, a biopsy punch (Harris Uni-Core 0.75 mm, USA), and Span 80 were procured from Sigma Aldrich. Mineral oil (0.880 kg/L) was obtained from AppliChem, and the adhesion promoter TI prime was acquired from MicroChemicals. PTFE tubes for the microfluidic channels' inlets and outlets were sourced from Microfluidic ChipShop (Microfluidic ChipShop, Jena, Germany). The silicon master mold fabrication utilized an EVG 620 semiautomatic contact photolithographic alignment and exposure tool from EV Group (Sankt Florian am Inn, Austria). Plasma treatment of the PDMS device and glass slide was conducted using a laboratory corona treater (BD-20AC, Electro-Technic Products Inc., Chicago, IL, USA).

In situ photopolymerization employed a UV light source (36-watt, 365 nm). UV-vis spectra were recorded on a Cary Varian spectrometer (Santa Clara, CA, USA). Fluorescence microscopy (HBO100 ZEISS Fluorescence Microscopy, Carl Zeiss, Jena, Germany) was used for visualizing polymeric microgels, and Zeiss AxioVision software processed fluorescence images. Syringe pumps were sourced from maviTeknik (Mersin, Turkiye).

4.2.2 Microfluidics Channels Fabrication

Photolithography and PDMS molding techniques were employed to create both microfluidics channels, detailed in Figure 4.2a and Figure 4.3. The fabrication began with the cleaning and HMDS treatment of a 4-inch Si wafer, followed by coating with TI prime to enhance adhesion in subsequent steps. The TI prime-coated wafer underwent a brief hotplate bake at 95 °C for 1 minute. Subsequently, the SU-8 2050 negative photoresist was spin-coated onto the wafer to achieve the desired channel thickness. After a pre-bake at 65 °C for 1-minute and a subsequent 20-minute bake at 95 °C, a photo mask featuring the flow-focusing channel design was aligned and brought into contact with the photoresist-coated wafer for UV exposure. Post-exposure, a 5-minute bake at 65 °C and a 10-minute bake at 95 °C followed. Excess and uncured photoresist

were removed using PGMEA, SU-8 developer, and rinsing with IPA and DI water.

Before PDMS casting, the master mold underwent silane vapor treatment in a vacuum desiccator. In a controlled environment, the silicone elastomer base and curing agent were mixed in a 10:1 ratio, poured onto the master mold, degassed, and baked at 65 °C for 2 h The cured PDMS was then peeled off the master mold, and each microchannel was meticulously cut using a razor. Inlets and outlets of the channels were opened using a hand-operated biopsy puncher.

PDMS and glass slide surfaces underwent a 3-minute oxygen plasma treatment in the final steps. Bonding occurred overnight at 65 °C. PTFE tubes were inserted into the microfluidics channel inlets and outlets to facilitate experiments.

4.2.3 Degradable Microgels Fabrication via Microfluidics

Degradable microgels were produced using the W/O emulsion technique within a droplet-based microfluidics setup, as seen in Figure 4.2a. Briefly, a flow-focused microfluidics channel design was employed to generate monodispersed droplets. The channel design has three inlets and one outlet. The side inlets were used to separate the injection of the PDS-group containing copolymer and tetra-arm PEG thiol cross-linker as dispersed phases. The outer inlet was employed for the oil phase/continuous phase. The dispersed phases came together at the intersection and were broken off when they met the continuous phase. After the microdroplet formation, the droplets reached the serpentine channel, which we called the mixing region (Figure 4.2b), where they started cross-linking. They reached the outlet tubing, where they collected into an eppendorf tube. They further undergo washing steps to remove residuals, unreacted monomers, oil, and surfactants.

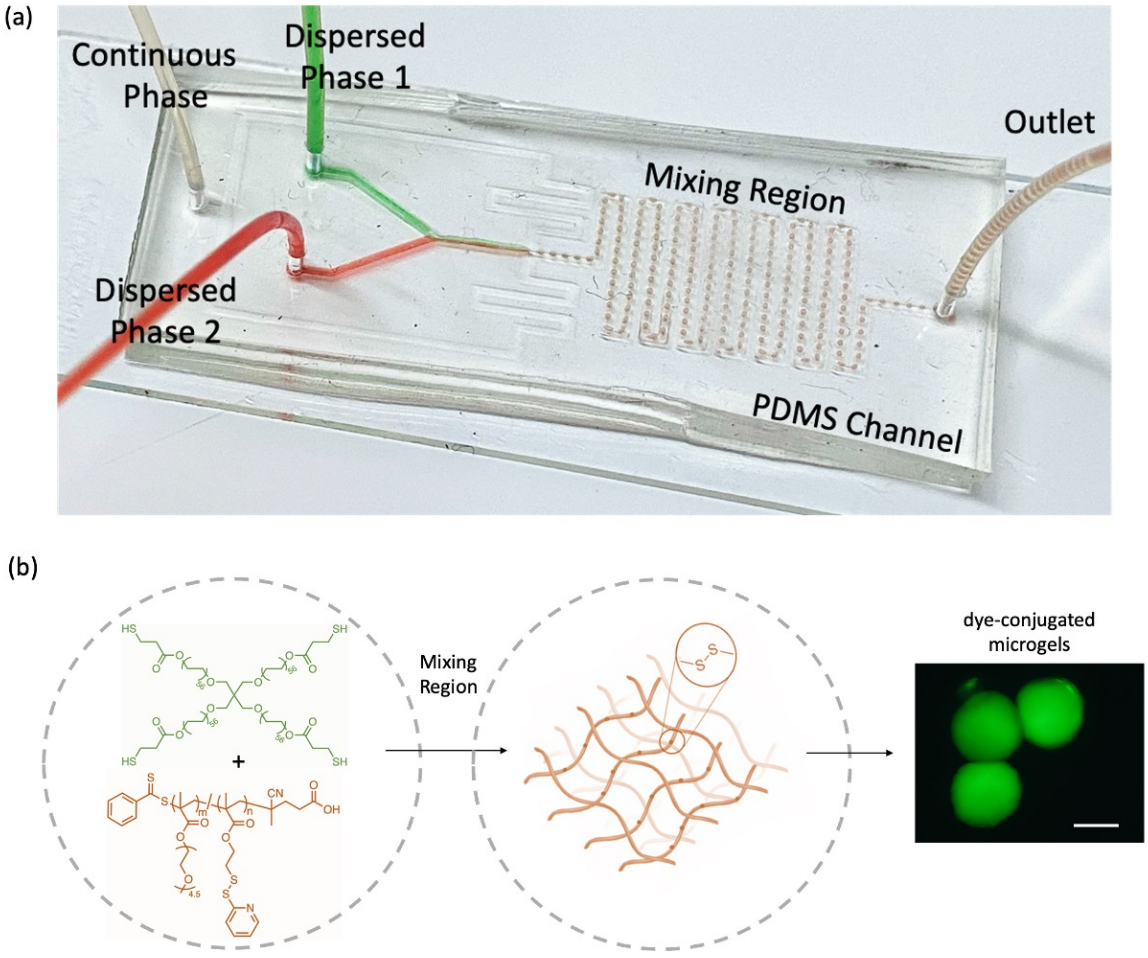

Figure 4.2 (a) Droplet-based microfluidics channel for degradable microgels production, (b) chemical demonstration of the degradable microgels and a fluorescence image of dye-conjugated degradable microgels (Scale 200 μm).

4.2.4 Reducing Agent Carrier Microgels Fabrication via Microfluidics

We employed a separate microgel design to facilitate the reduction of degradable microgels. For this purpose, we intended to utilize HP-β-CD containing microgels, given its biocompatibility and notable encapsulation capacity. We used a Y-shaped microfluidic channel to produce these microgels, and various amounts of HP-β-CD-containing microgels were produced (Figure 4.3).

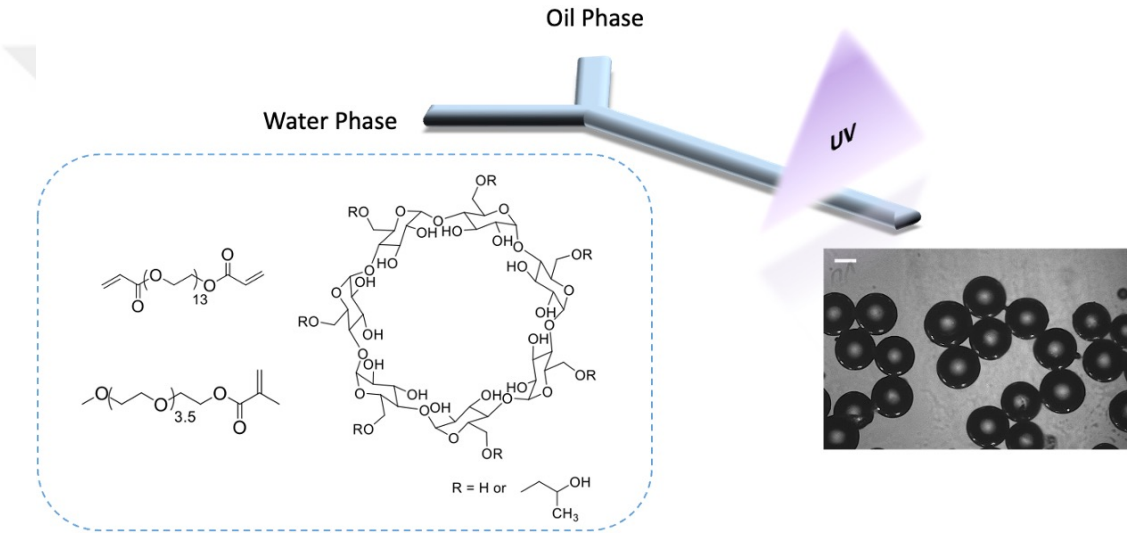

Figure 4.3 Illustration of microfluidics fabrication of HP-β-CD containing non-degradable microgels (Scale 200 μm).

4.2.5 Degradation of Microgels

Microgel degradation was analyzed in the presence of DTT-loaded carrier microgels. Initially, HP-β-CD-containing microgels were loaded with DTT. The degradable microgels were labeled with bodipy-maleimide to assess the degradation profile visually under fluorescence microscopy. Subsequently, both microgels were placed adjacent, and 0.1 ml of DI water was added to them. As the reducing agent-loaded HP-β-CD-containing microgels released their carriers, the liberated DTT initiated the degradation of the degradable microgels.

4.2.6 Encapsulation and Release of Protein

For the protein encapsulation and release studies, FITC-BSA was chosen for the model. FITC-BSA encapsulated into the microgels during the production process in the microfluidics setup. After the complete gelation and washing steps, microgels were placed next to DTT-loaded HP-β-CD-containing microgels, and observed the release profile under the fluorescence microscopy.

4.3 Results and Discussion

4.3.1 Degradable Microgels Fabrication via Microfluidics

To fabricate degradable microgels, we utilized a microfluidics channel design, which allows an in-chip mixing of the copolymer and the cross-linker as seen in Figure 4.2a. We used the outer inlet for the oil injection at a fixed flow rate of 15 μL/min. Side inlets were used to inject PDS-copolymer and tetra-arm PEG thiol into the microfluidics channel at a fixed flow rate of 3 μL/min. Different microgels systems were

Table 4.1

Different equivalents for degradable microgels. MG signifies microgel.

	PDS-copolymer eq.	**Tetra-arm PEG thiol eq.**
MG1	1	1
MG2	2	1
MG3	4	1

fabricated for further evaluation, as seen in Table 4.1. When the cross-linker and copolymer met at the same flow rate at the intersection of the channel, they formed a droplet due to the emulsification. They started to mix while they traveled alongside the serpentine channel and started to cross-link. The obtained microgels were visualized under optical microscopy as soon as they left the outlet tube, as seen in Figure 4.4. Later, the microgels underwent washing to eliminate residual oil and surfactant with

hexane and methanol, respectively.

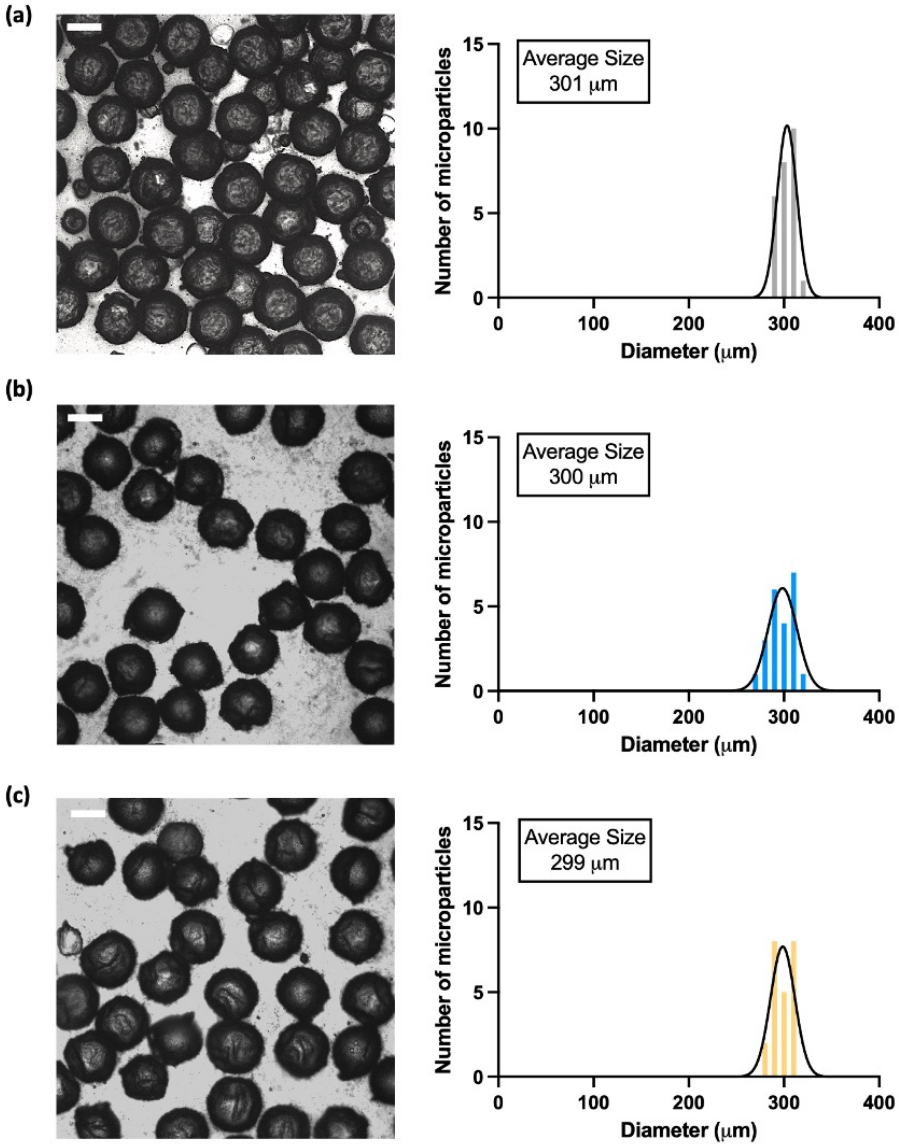

Figure 4.4 Optical microscopy images capturing various degradable microgels were taken immediately upon exiting the outlet tube, along with size distribution graphs. (a) MG1, (b) MG2, (c) MG3 (Scale 200 μm).

SEM images were employed for the characterization of degradable microgels (Figure 4.5). It was observed that the MG3 degradable gel system displayed a lack of stability when subjected to the washing process. This finding suggests a potential challenge in the stability of the MG3 system under such conditions, limiting their usage in further investigation of delivery applications.

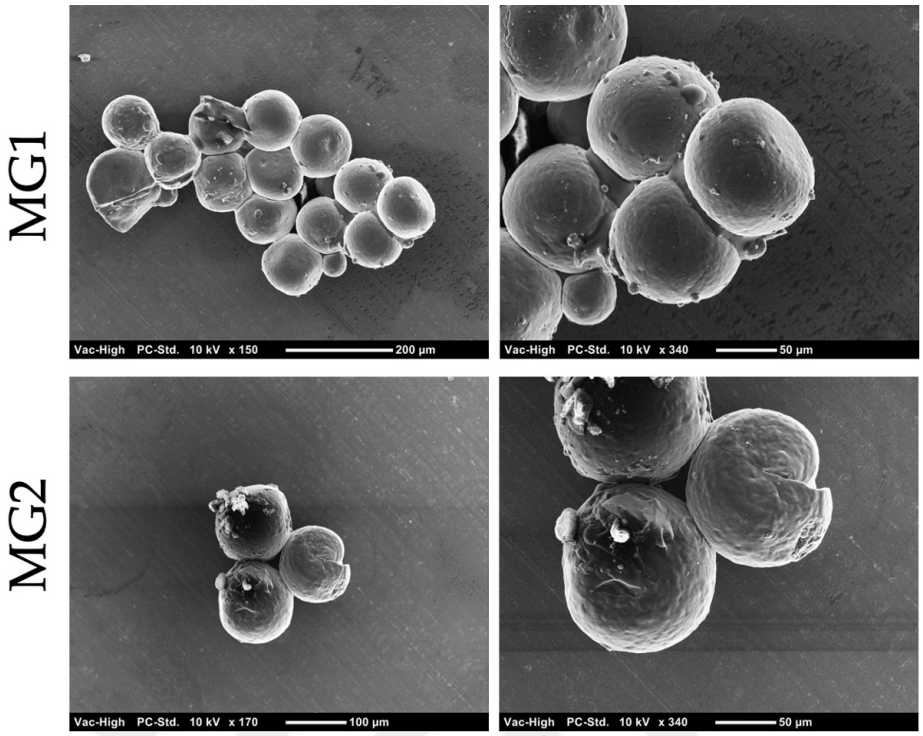

Figure 4.5 SEM images of the degradable gels (MG1 and MG2).

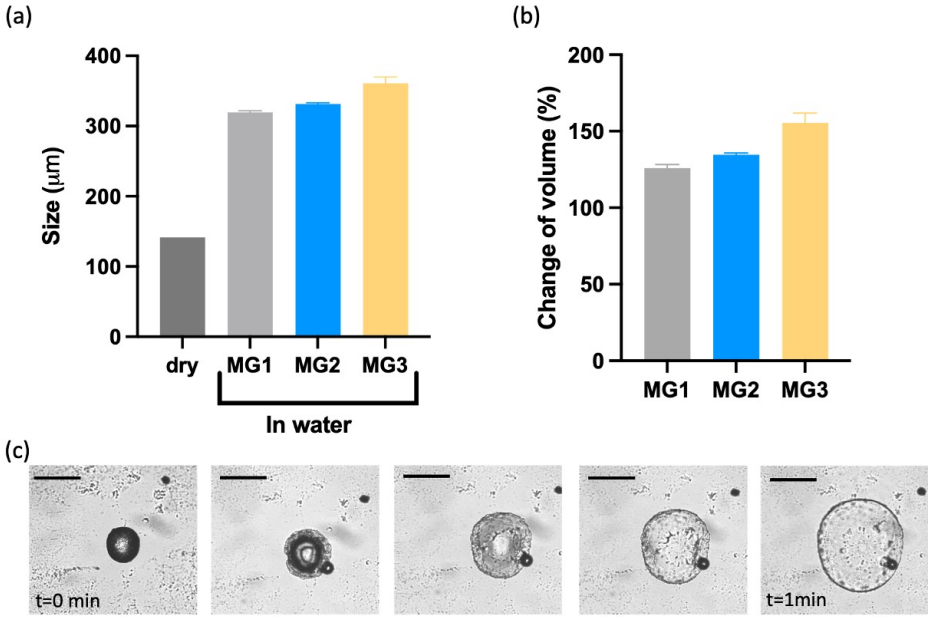

Figure 4.6 (a) Size changes of degradable microgel from dry to wet stage, (b) volume change graph, (c) time-lapse optical microscopy images showing the swelling process (Scale 200 μm).

The swelling characteristics of the acquired microgels were assessed by observing their size alterations from the dry to the wet stage under optical microscopy. The size variations of the microgels exhibited a correlation with the monomer-cross-linker ratios, as seen in Figure 4.6a and b. Figure 4.6c illustrates images captured from the video showcasing the swelling process of a microgel (MG1).

4.3.2 HP-β-CD-containing Microgels Production via Microfluidics

Through a Y-shaped microchannel, we synthesized microgels incorporating HP-β-CD with PEGDA and PEGMEMA monomers. Initially, we fine-tuned the upper limit of HP-β-CD within the polymeric network, ensuring the preservation of both monodispersity and stability of the microdroplets.

Table 4.2

Various ratios for reducing agent carrier microgels.

	PEGDA eq.	**PEGMEMA eq.**	**HP-β-CD eq.**
10%	1	4	0.5
30%	1	4	1.5
50%	1	4	2.5

Different percentages used for the optimization were summarized in Table 4.2. For the production of microgels, flow rates of the dispersed and continuous phased were fixed at 5 μL/min and 15 μL/min, respectively. The microdroplets were cured under the UV light (36-watt) while leaving the outlet tubing. The collected microgels were washed to remove residuals, and their images were captured under optical microscopy as seen in Figure 4.7.

Swelling experiments were performed on HP-β-CD microgels, constituting 50% of the total monomer, to evaluate their porosity and loading capacity. Initially, dry

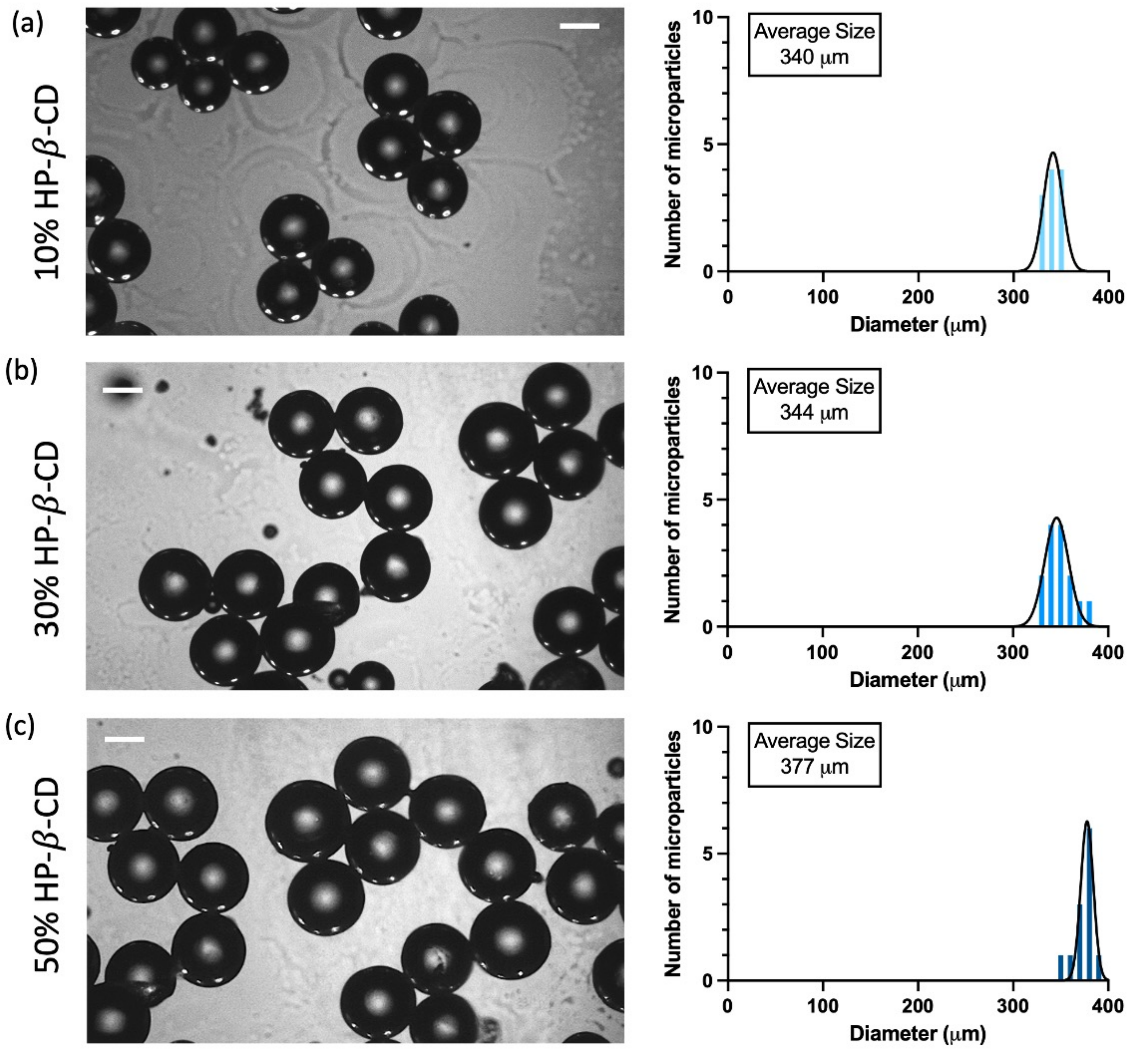

Figure 4.7 Optical images and size distribution of different amount of HP-β-CD containing microgels as reducing agent carrier. (a) 10%, (b) 30%, (c) 50% (Scale 200 μm).

microgels were examined under optical microscopy. Later, 200 μL of DI water was introduced, and images of the swollen microgels were acquired using optical microscopy (Figure 4.8a,b). Then, size and volume change calculations were executed, revealing an average volume change of approximately 79% (Figure 4.8c,d). These experiments showed that the desired amount of the reducing agent can be further loaded to these microgels due to their excellent loading capacity.

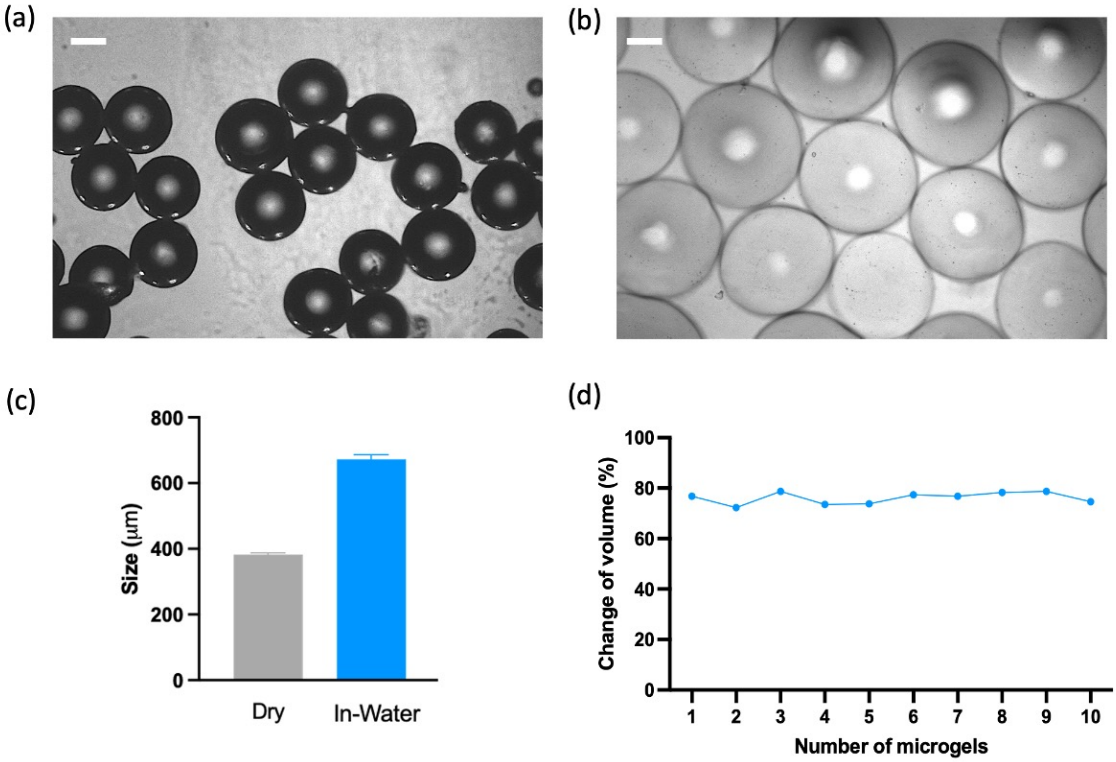

Figure 4.8 (a) HP-β-CD containing microgels at dry stage, (b) HP-β-CD containing microgels in water, (c) size changes from dry to wet stage, (d) percentage change in volume (Scale 200 μm).

Additional characterizations of the microgels containing 50% HP-β-CD were conducted SEM. The visual representations of these characterizations were depicted in Figure 4.9.

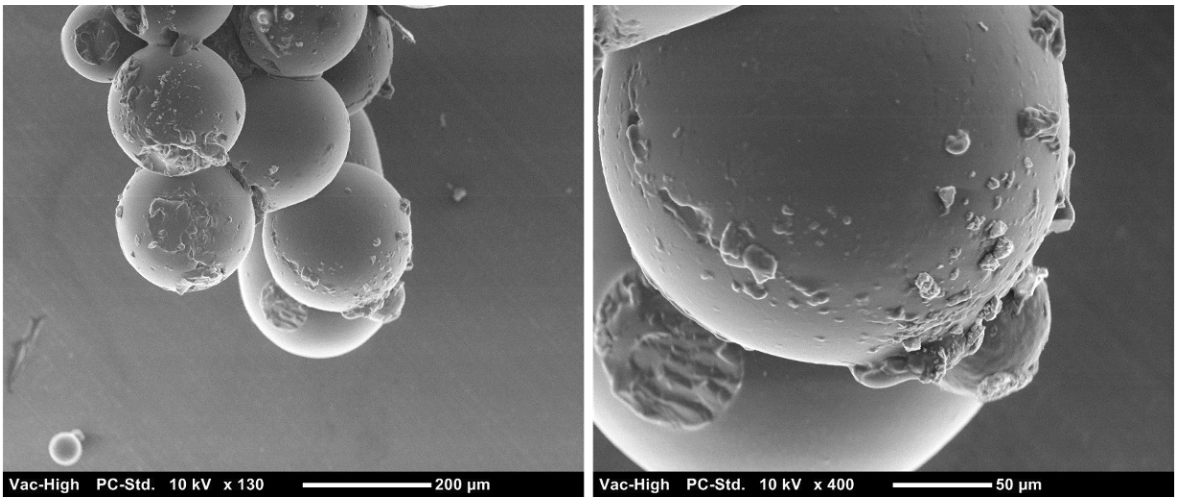

Figure 4.9 SEM images of 50% HP-β-CD-containing microgels.

4.3.3 Degradation of Microgels

Microgels with disulfide bonds are expected to degrade in the presence of a reducing agent like DTT. To illustrate this degradation, we conjugated disulfide-containing microgels (MG1) with a fluorescent dye, bodipy-maleimide. We selected this dye for its insolubility in water. We loaded DTT into the HP-β-CD containing microgels for them to release DTT upon exposure to water in the environment. To prove the concept, we initially loaded an increased amount of DTT (50 mg in 0.1 ml DI water) to 50% HP-β-CD containing microgels. When HP-β-CD containing microgels absorbed all the water, we positioned them next to dye-conjugated degradable microgels. We applied 100 μL water onto the microgels and covered them with a glass slide to obverse the degradation profile under fluorescence and optical microscopy.

Figure 4.10 shows the simultaneously obtained optical and fluorescence images. As seen in the images, DTT is released from the larger microgels, initiating the degradation of bodipy-maleimide conjugated microgels over time. To confirm that the sole cause of microgel degradation is the release of DTT, we replicated the experiments without loading DTT into the microgels containing HP-β-CD. Subsequently, we observed the microgels overtime under the microscopy as seen in Figure 4.11. The findings sug-

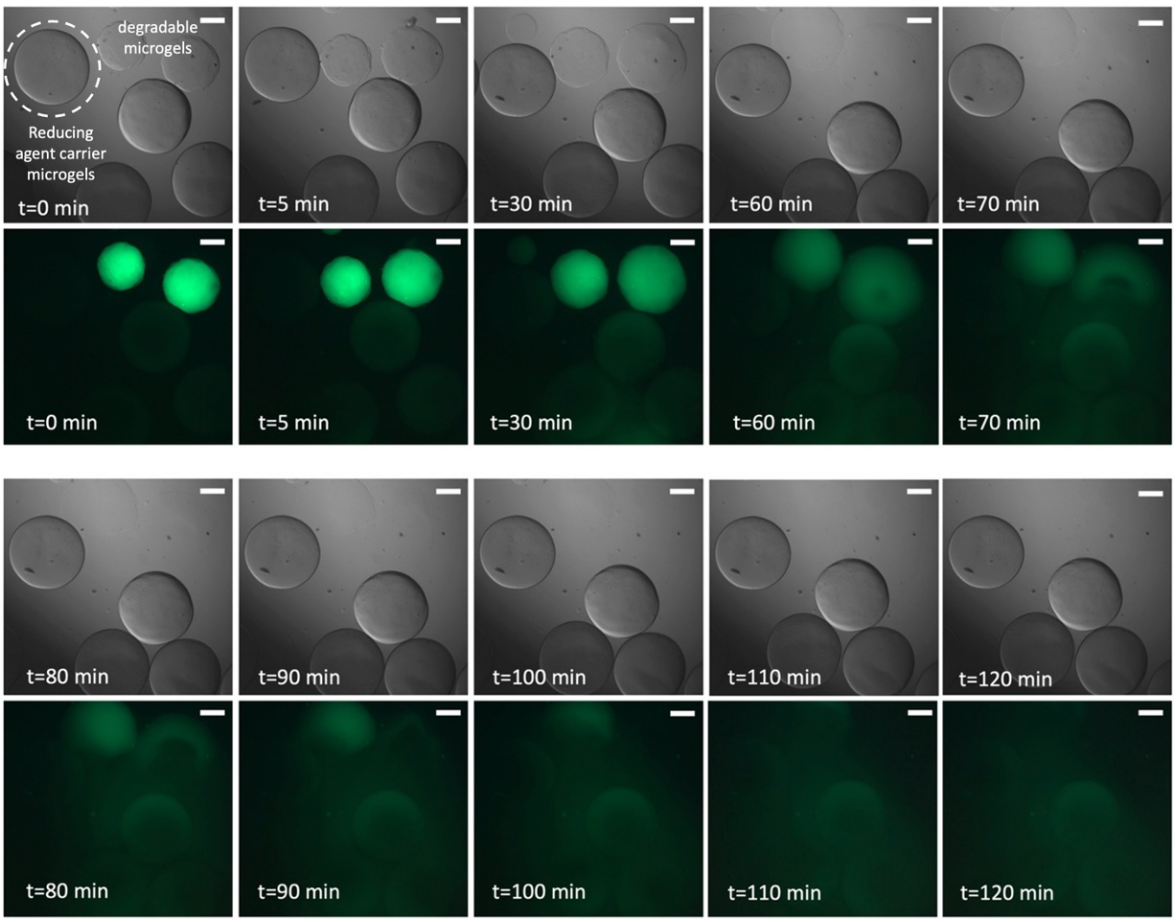

Figure 4.10 Degradation profile of bodipy-maleimide conjugated microgels in the presence of reducing agent-carrier microgels (Scale 200 μm).

gest that both the degradation and subsequent release profile can easily be adjustable by manipulating the number of microgels and the loaded amount of reducing agent to carrier microgels.

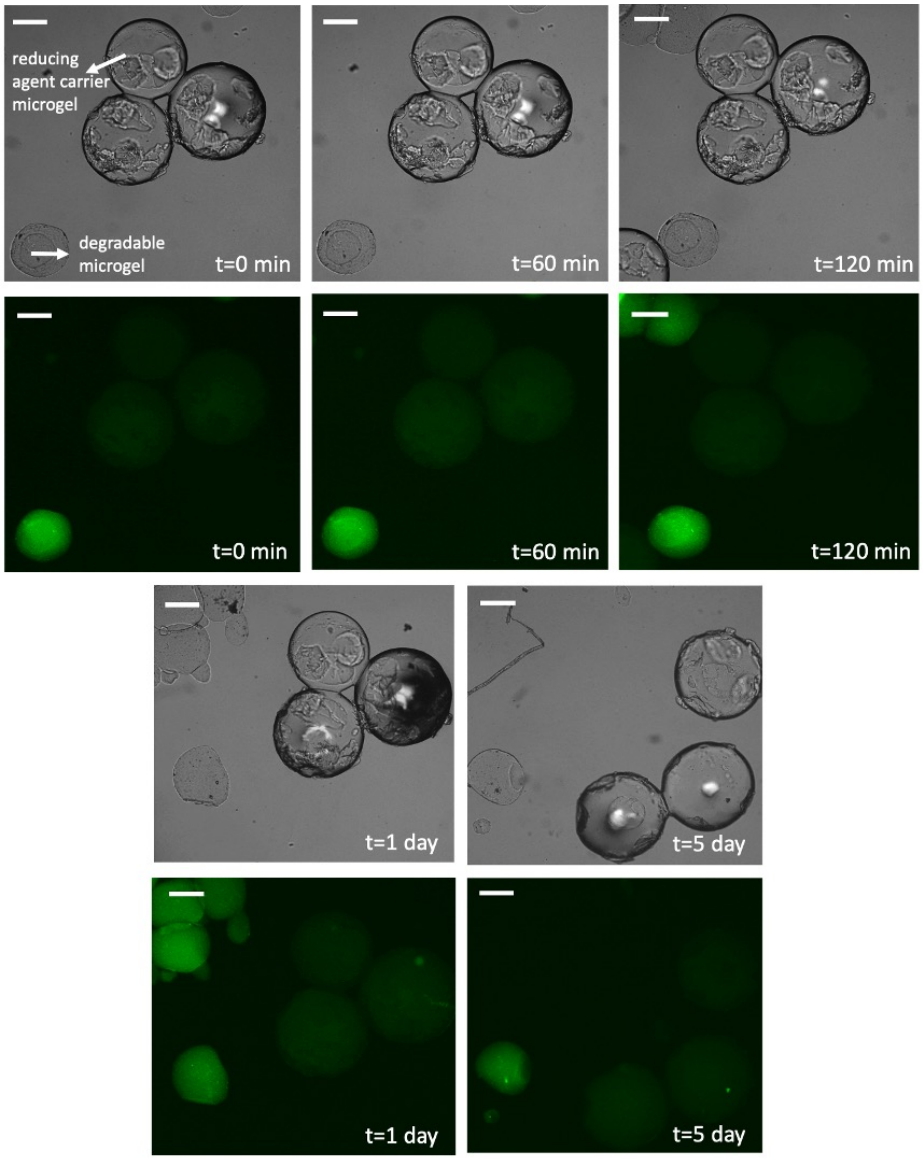

Figure 4.11 Control experiments without loading reducing agent to microgels (Scale 200 μm).

4.3.4 FITC-BSA Encapsulation and Release Studies

FITC-BSA was effectively entrapped within the microgels during their production process in microfluidics. Following the complete gelation process, a thorough washing step was employed to eliminate any remaining oil and surfactant residues, as well as unbound protein. The resulting microgels, encapsulating the dye-conjugated protein, were visualized through fluorescence microscopy, as seen in Figure 4.12.

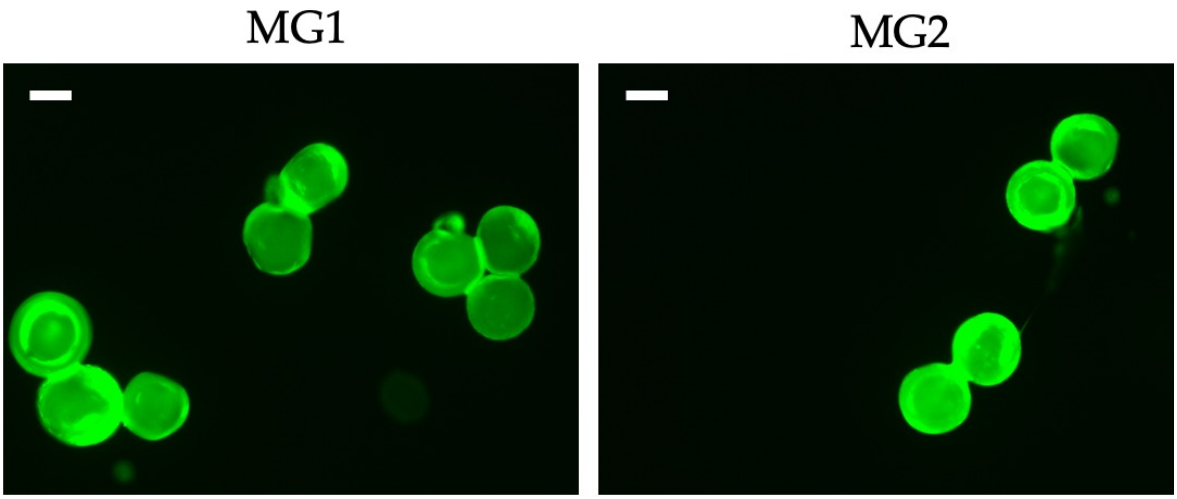

Figure 4.12 Fluorescence images of FITC-BSA encapsulated microgels (Scale 200 μm).

In conducting protein release studies, we initiated by incorporating the reducing agent into microgels containing HP-β-CD, utilizing them as carriers. Subsequently, we performed a rapid washing of these microgels and positioned them next to protein entrapped degradable microgels (MG1). Next, we introduced 100 μL of DI water and covered the setup with a glass slide to observe their behavior under microscopy. The introduction of the reducing agent via carrier microgels triggered the release of the encapsulated protein, facilitated by the degradation of the microgel matrix as observed in Figure 4.13.

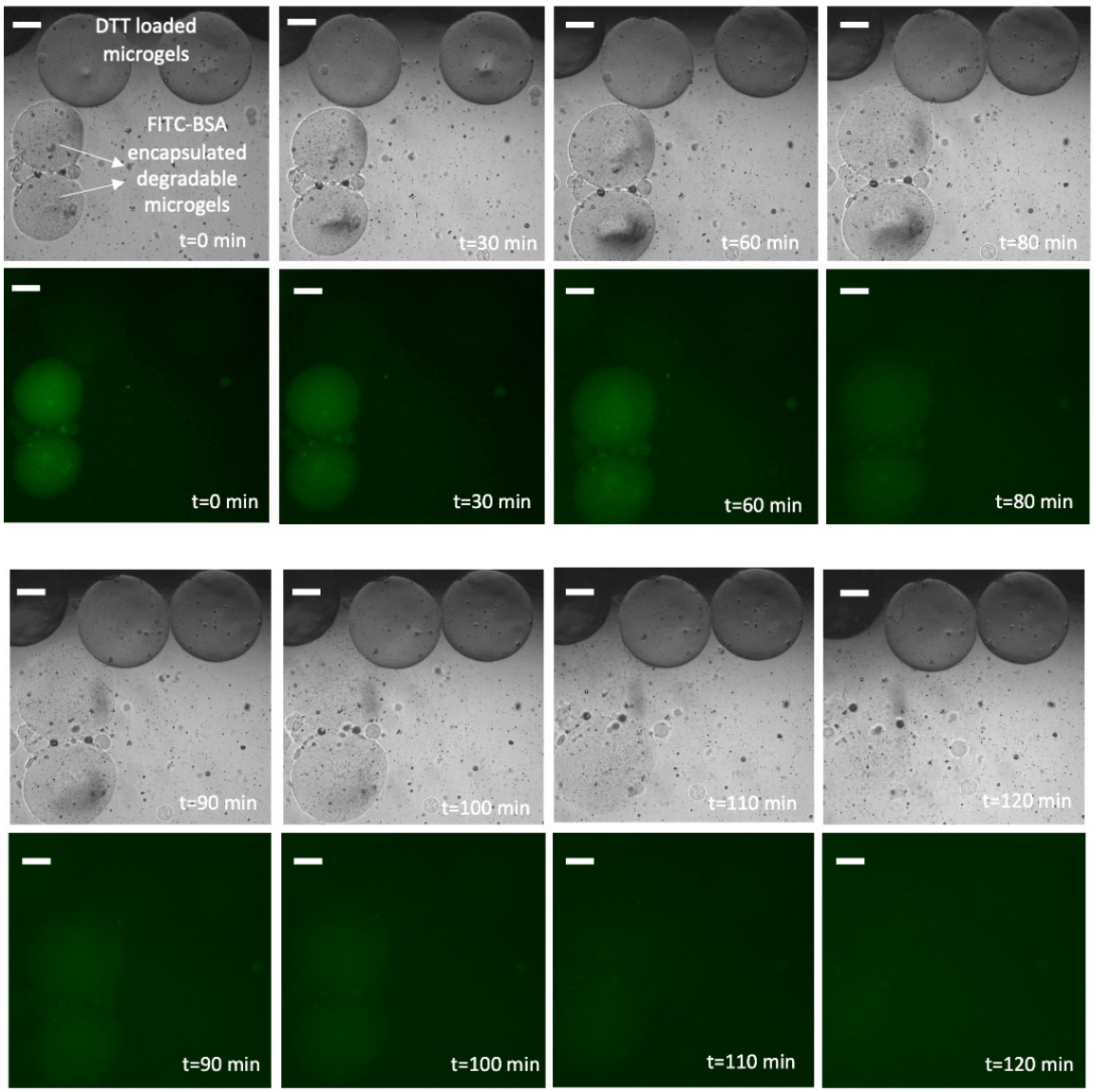

Figure 4.13 Degradation profile of FITC-BSA encapsulated microgels (MG1) in the presence of DTT-loaded microgels (Scale 200 μm).

4.4 Conclusion

We present a straightforward approach for crafting redox-responsive microgels produced via a microfluidic channel. The combination of pyridyl-disulfide group-containing PEG copolymers with tetra-thiol PEG polymers in a microfluidic device results in the formation of microgels. This easy formulation enables the creation of microgels under mild conditions, making it a suitable approach for encapsulating delicate biomolecules with therapeutic significance. The release properties of the encapsulated protein can be precisely and effectively tuned. Notably, the microgels undergo degradation upon encountering thiol-containing reducing agents, triggering the release from another set of biocompatible microgels. This concept has paved the way for injectable microgel systems, significantly advancing drug delivery and biomedical applications. Injectable microgels offer a versatile and minimally invasive approach, enabling precise and controlled delivery of therapeutic agents/proteins. The ability of these microgels to undergo rapid degradation in response to specific triggers, such as thiol-containing reducing agents, enhances their suitability for the on-demand release of encapsulated biomolecules. The injectable nature of these systems opens up possibilities for targeted delivery in vivo, enabling efficient and localized treatment in various medical scenarios. Overall, the advent of injectable microgel systems holds great promise for advancing therapeutic interventions and addressing specific biomedical challenges.

5. MOLECULARLY IMPRINTED POLYMERS FOR BIOMARKER DETECTION

5.1 Introduction

Molecular imprinting is a synthetic methodology that creates artificial recognition units through the polymerization of functional and cross-linking monomers in the presence of the target molecule. In the polymerization process, the target molecule serves as a molecular template. After the polymerization, the target molecule needs to be removed to possess the complementary cavities in shape, size, and position of the functional groups [151, 152]. Herewith, the polymer carries the memory of the target molecule capable of selectively rebinding, as shown in Figure 5.1.

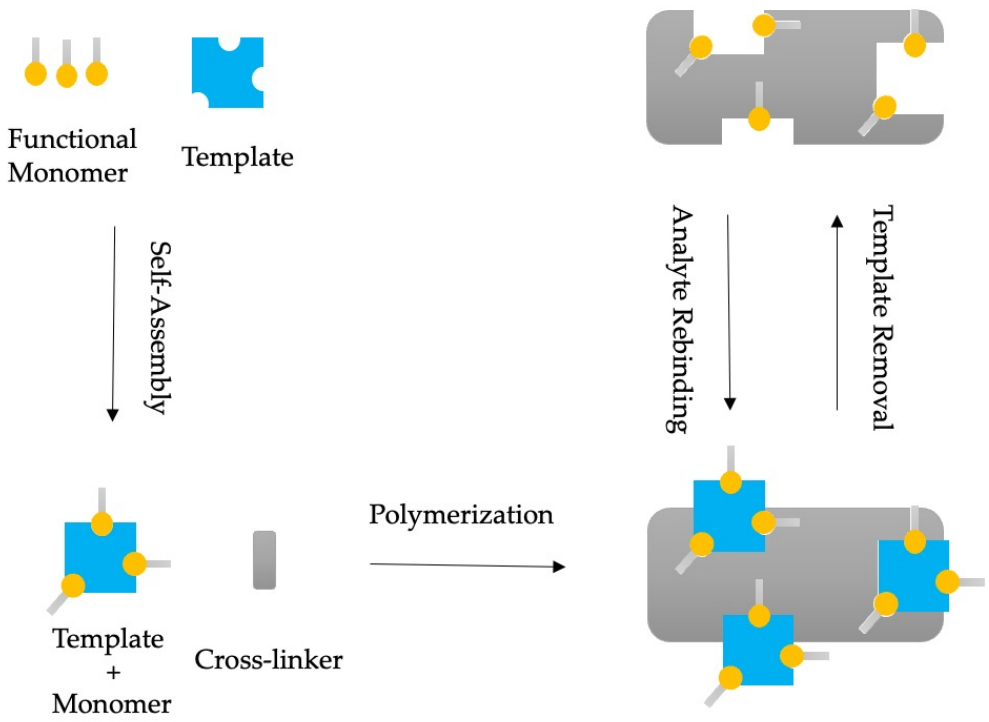

Figure 5.1 Schematic representation for the preparation of the molecularly imprinted polymer.

Molecularly imprinted polymers (MIPs) can be synthesized by different methods depending on the interaction between the template molecule and the functional monomers. This interaction can be either non-covalent [153], like hydrogen bonds, ionic bonds, hydrophobic interactions, Van der Waals forces, or reversible covalent bonds [154]. The non-covalent imprinting approach requires mixing the template molecule and the monomers in an appropriate porogen, which is comparably straightforward for experiments. Still, there will be heterogeneous and non-selective binding sites due to excess free functional monomers and their random associations into the polymeric structure [155]. The covalent imprinting approach is much more complicated since pre-polymerization complexes between the template molecule and functional monomers need to be synthesized, and template removal can be done through either an extraction procedure or chemical cleavage. Despite the time-consuming and complicated nature of the covalent imprinting approach, the advantages of this approach are the creation of more homogenous binding sites by minimizing the number of non-specific sites and the high stability of the polymeric matrix [156]. Some studies demonstrate the benefits of combining covalent and non-covalent approaches [157].

MIPs have found diverse applications, including chemical sensors [158], electrochromatography [159], separations [160], high performance liquid chromatography (HPLC) [161], and solid-phase extraction [50]. These versatile materials have helped progress different fields by using their unique properties. Typically, MIPs are synthesized through the bulk polymerization method. However, this approach necessitates a tedious and time-consuming process involving crushing, grinding, and sieving the obtained polymer. Moreover, the resulting particles exhibit irregular shapes and a heterogeneous distribution of binding sites. Various strategies have been suggested to synthesize spherical MIP particles to overcome these challenges and enhance the efficiency of MIP production. These include techniques such as suspension polymerization, multi-step swelling polymerization, emulsion polymerization, and precipitation polymerization. Until now, various techniques have been employed for the synthesis of MIPs, and past investigations have primarily centered on the imprinting effects, taking into account factors like polymerization temperature, pressure, solvent, and duration. However, limited literature is available comparing polymers generated through different

polymerization methods when targeting specific molecules.

Herein, we first investigate the different monomer, cross-linkers, and their various ratios to optimize the imprinted polymer systems for dopamine detection by bulk polymerization method. Dopamine (DA) is a significant neurotransmitter produced by specific dopaminergic neurons in the brain from the substantia nigra region [162]. The depletion of DA in the central nervous system is defined as a major cause of neurological disorders, specifically Parkinson's disease (PD) [163]. Thereby, the level of DA in biological fluids can be used as a chemical monitor to screen PD and to adjust the ideal therapeutics for patients. After we obtained the best monomer cross-linker system for our target molecule, we utilized different MIP production methods as illustrated in Figure 5.2 to provide a proof-of-concept comparison of the polymeric materials.

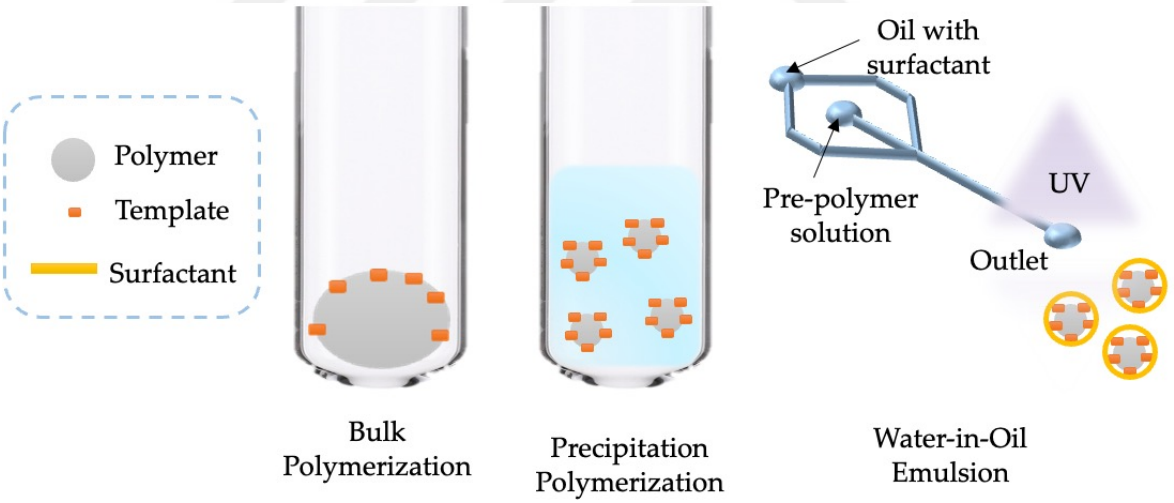

Figure 5.2 Illustration of various fabrication techniques for MIPs.

5.2 Experimental

5.2.1 Materials and Characterization

DA, AAm, BIS, VPBA, DMPA, V-501 were purchased from Sigma Aldrich. All the organic solvents are obtained from Merck.

For the microfluidics setup, we purchased various materials from Sigma Aldrich, including PDMS, HMDS, chlorotrimethylsilane, a negative photoresist (SU-8 2050), PGMEA, glass slides, a biopsy punch (Harris Uni-Core 0.75 mm, USA), and a nonionic surfactant (Span 80). Mineral oil (0.880 kg/L) was obtained from AppliChem, and the adhesion promoter TI prime was acquired from MicroChemicals. PTFE tubes for the microfluidics channels' inlets and outlets were procured from Microfluidic ChipShop (Microfluidic ChipShop, Jena, Germany). The silicon master mold fabrication utilized an EVG 620 semiautomatic contact photolithographic alignment and exposure tool from EV Group (Sankt Florian am Inn, Austria). Plasma treatment of the PDMS device and glass slide was conducted using a laboratory corona treater (BD-20AC, Electro-Technic Products Inc., Chicago, IL, USA).

For in situ photopolymerization, we used a UV light source (36-watt, 365 nm). UV-vis spectra were recorded on a Cary Varian spectrometer (Santa Clara, CA, USA). Optical microscopy (HBO100 ZEISS, Carl Zeiss, Jena, Germany) was employed for visualizing polymeric microgels, and Zeiss AxioVision software processed fluorescence images. Syringe pumps were sourced from maviTeknik (Mersin, Turkiye).

5.2.2 Molecularly Imprinted Polymers (MIPs) Synthesis

MIPs in bulk version were prepared using different functional monomers and cross-linkers as summarized in Table 5.1. Thermal and UV-polymerization methods were applied for each equivalent by simply altering the initiator type. The target molecule and functional monomers were initially combined and subjected to pre-

polymerization/self assembly for 4 h after the mixture was sealed and degassed with nitrogen for 15 minutes. Following the self-assembly, the cross-linkers and initiators were introduced. The mixture was then degassed once more before being subjected to polymerization. While the thermal polymerization was done in the oil bath at 70 °C, a UV light source with a 36-watt power was employed for the UV polymerization. The template removal was performed with an appropriate solvent system until no target molecule was left in the polymeric network, which was detected by UV spectroscopy.

Table 5.1

Various ratios of functional monomers and cross-linkers used for the dopamine imprinted polymer synthesis.

	DA eq.	**MAA eq.**	**EGDMA eq.**	**AAm eq.**	**BIS eq.**	**VPBA eq.**
MIP1	1	4	20	-	-	-
MIP2	1	6	20	-	-	-
MIP3	1	8	20	-	-	-
MIP4	1	8	60	-	-	-
MIP5	1	20	45	-	-	-
MIP6	1	25	30	-	-	-
MIP7	1	-	-	4	16	1
MIP8	1	-	-	4	20	1
MIP9	**1**	**-**	**-**	**1**	**6**	**1**

5.2.3 Rebinding the Target Molecule

The adsorption experiments involved combining 30 mg of the polymeric materials with 1 mL of DA (0.02 mg/mL) in PBS at pH 8. These mixtures were agitated at 37 °C. The remaining concentrations of DA were determined using UV spectroscopy at 280 nm.

5.2.4 Different Fabrication Methods for Dopamine-Imprinted Polymeric Materials

After confirming the best functional monomer-cross-linking ratio, we utilized other fabrication methods for the dopamine-imprinted polymers. We employed precipitation polymerization and W/O emulsion polymerization in the microfluidics channel. First, the DA-imprinted polymer was synthesized through a one-step precipitation polymerization method. All components and reaction conditions in the mixture were identical to those used in bulk polymerization, except for increasing the solvent volume. Later, a flow-focusing microfluidics channel was employed to create W/O emulsions to produce micron-sized DA imprinted polymers. Oil with 10% of Span 80 was utilized as the continuous phase, where the pre-polymer solution was injected as the dispersed phase.

5.3 Results and Discussion

5.3.1 Molecularly Imprinted Polymers (MIPs) Design for Dopamine Template

Following the optimization and testing of various monomer-cross-linker systems, we selected **MIP9** from Table 5.1 to proceed with our comparative experiments.

5.3.1.1 Bulk Polymerization. Bulk imprinted polymers were prepared by using dopamine as the template, AAm and VPBA as functional monomers, BIS as the cross-linker, and water:ethanol (4:1, V:V) as the solvent. DA (0.05 mmol) was dissolved in water: ethanol (0.6 mL) containing AAm and VPBA (0.05 mmol) in a glass vial. The solution was incubated for 4 h to promote self-assembly. VPBA was employed to improve specific DA recognition by leveraging the boronate–catechol interaction [164] and B−N coordination between VPBA and DA [165]. After that, BIS (0.3 mmol) and DMPA (2% of total monomer) were added to the pre-polymerized mixture. The

solution was then sonicated for 10 minutes and purged with nitrogen for 15 minutes. Then, it was put under the UV light source for 30 min. We synthesized two control groups; the first one, non-imprinted polymers (NIP1), was synthesized without adding the template molecule, and the second one, non-imprinted polymers (NIP2), was synthesized without the template and VPBA. The obtained bulk gels can be seen in Figure 5.3.

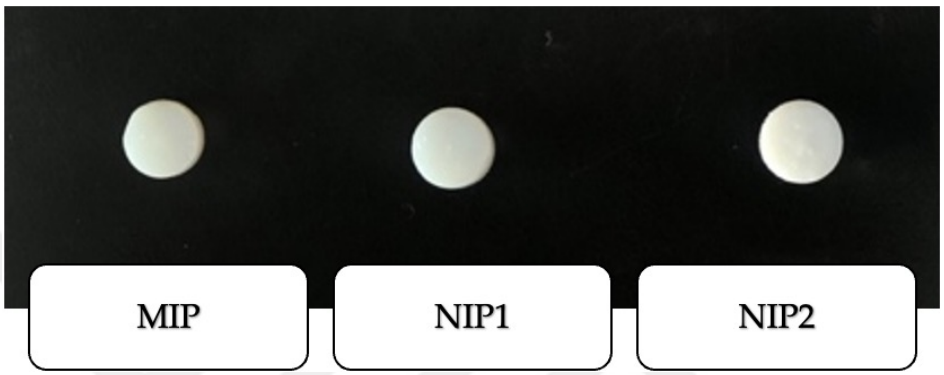

Figure 5.3 Images of the DA-imprinted and non-imprinted bulk polymers.

5.3.1.2 Precipitation Polymerization. The DA (0.05 mmol) as a template and VPBA and AAm (0.05 mmol) as functional monomer were dissolved in water:ethanol (4:1, V:V)(5 mL) in a 10 mL round bottom flask, and then the mixtures were sonicated for 15 min. The sealed mixture was kept 4 h under the magnetic stirring to obtain better self-assembly. Later, the cross-linker, BIS (0.3 mmol), and the initiator, V-501 (2% of total monomer), were added to the mixture, degassed with nitrogen, and put in an oil bath at 70 °C with a continuous magnetic stirring for overnight polymerization. The before and after images of the pre-polymer solution and obtained DA-imprinted nano-sized gels can be seen in Figure 5.4.

5.3.1.3 W/O Emulsion Polymerization in Microfluidics. A flow-focusing microfluidic channel was employed to produce monodispersed micron-sized DA-imprinted microgels. For the dispersed phase, the DA (0.05 mmol) as a template, VPBA and AAm (0.05 mmol) as functional monomer, BIS as the cross-linker, and DMPA as the

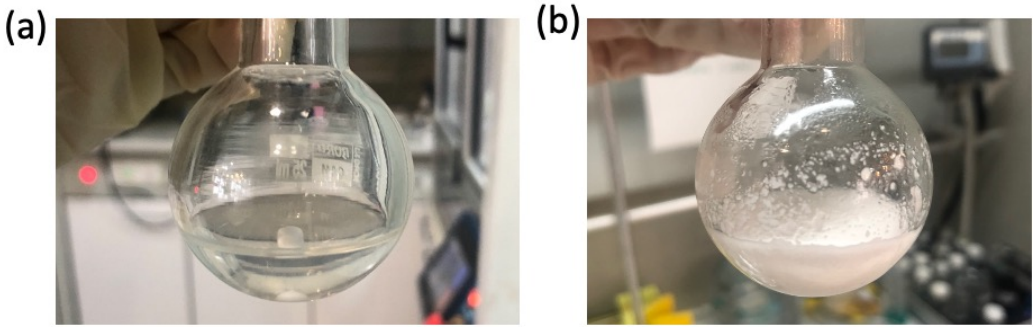

Figure 5.4 (a) Pre-polymer solution, (b) DA-imprinted nanogels produced via precipitation polymerization.

cross-linker were dissolved in 1 ml water:ethanol (4:1, V:V) solvent mixture. For the continuous phase, oil with 10% Span 80 was used. Flow rates were fixed at 5 μL/min for the dispersed phase and 10 μL/min for the continuous phase. Droplet formation occurred at the intersection of the flow-focusing device. As the droplets traveled through the outlet tube, they were exposed to UV light for curing. The obtained DA-imprinted microgels' images were captured with optical microscopy as seen in Figure 5.5a. The average size of the DA-imprinted microgels was measured as 250 μm (Figure 5.5b).

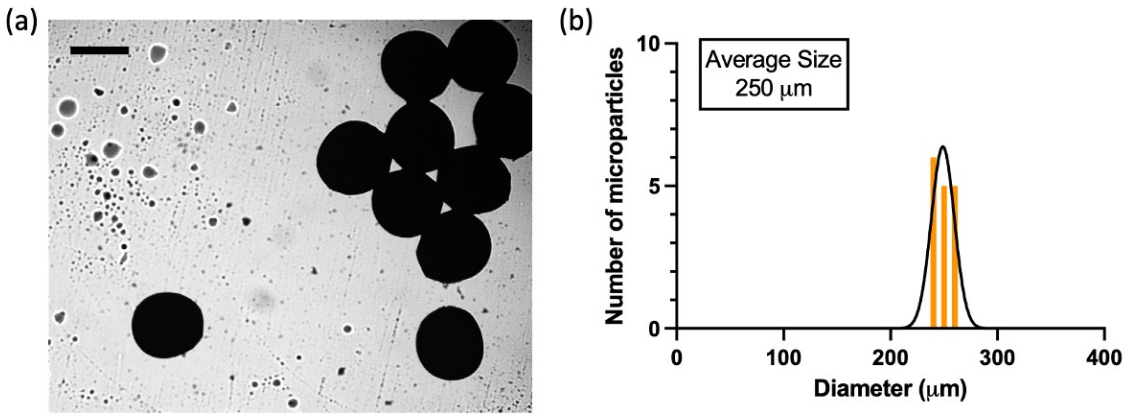

Figure 5.5 (a) DA-imprinted microgels produced via microfluidics (Scale 200 μm), (b) size distribution graph of DA-imprinted microgels.

The DA-imprinted polymers, synthesized through various polymerization techniques, were subsequently subjected to SEM characterization (Figure 5.6).

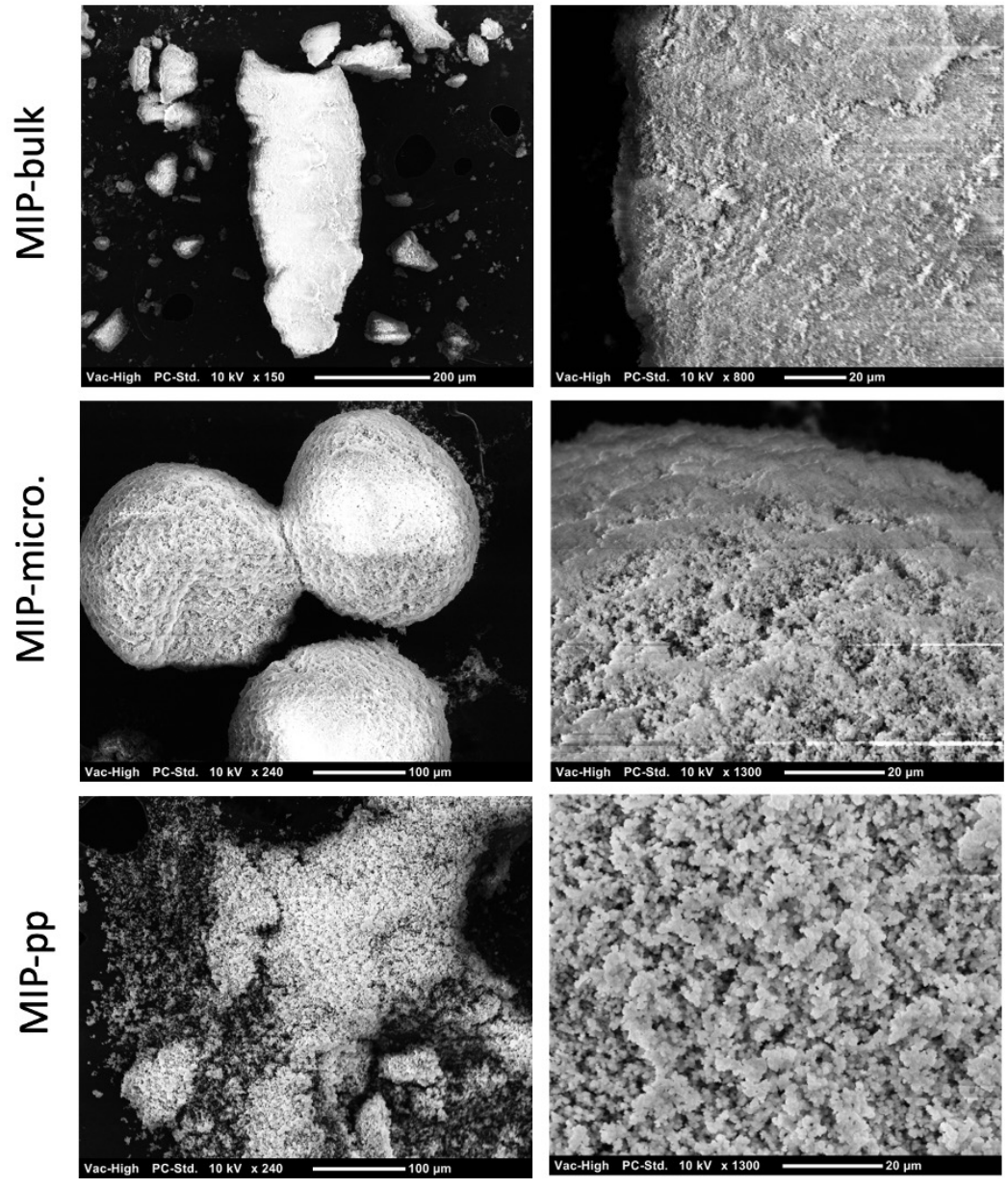

Figure 5.6 SEM images of DA-imprinted polymeric materials synthesized by different methods.

5.3.2 Template Removal

The template dopamine (DA) extraction was carried out using a 0.1 M hydrochloric acid (HCl) solution until no DA peak was detectable in the UV spectroscopy at the absorbance of 280 nm. This template extraction process was uniformly applied to all sizes of DA-imprinted polymeric materials. Subsequently, the polymers were thoroughly washed with DI water, frozen, and lyophilized in preparation for the rebinding experiments.

5.3.3 Dopamine Rebinding

Dopamine rebinding experiments were conducted in PBS with a pH of 7.4. Initially, dopamine solutions (0.02 mg/ml) were prepared for each sample, and their absorbance values were assessed using a UV spectrometer. The 30 mg of each polymeric material was incubated overnight in dopamine solution at room temperature in dark conditions. The solution was then centrifuged, and the supernatant was measured again by a UV spectrometer. The control groups underwent identical procedures, and a dopamine solution without any polymeric materials was incubated under the same conditions. This was done to ascertain whether any decrease in UV absorbance was observed (Figure A.5). Figure 5.7 shows the rebinding performances of different size polymeric materials.

The imprinted microgels obtained through precipitation polymerization demonstrated a better binding capacity when compared to both microgels and bulk counterparts. This observation aligns with expectations, considering that the reduction in the size of the imprinted polymer resulted in an increased surface area. This augmentation in surface area contributed to enhanced molecular recognition and binding efficiency, ultimately yielding a higher binding capacity. Considering each method has its advantages over each other, it is essential to carefully evaluate and select the most suitable approach based on specific requirements, desired outcomes, and the unique characteristics of the situation at hand.

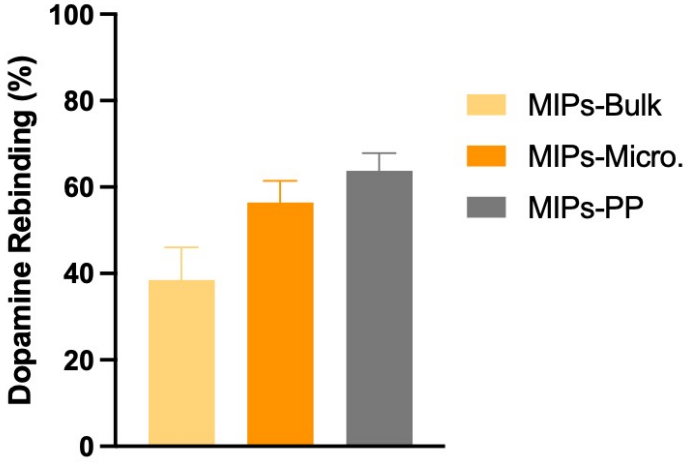

Figure 5.7 Dopamine rebinding results of polymers prepared via different polymerization methods.

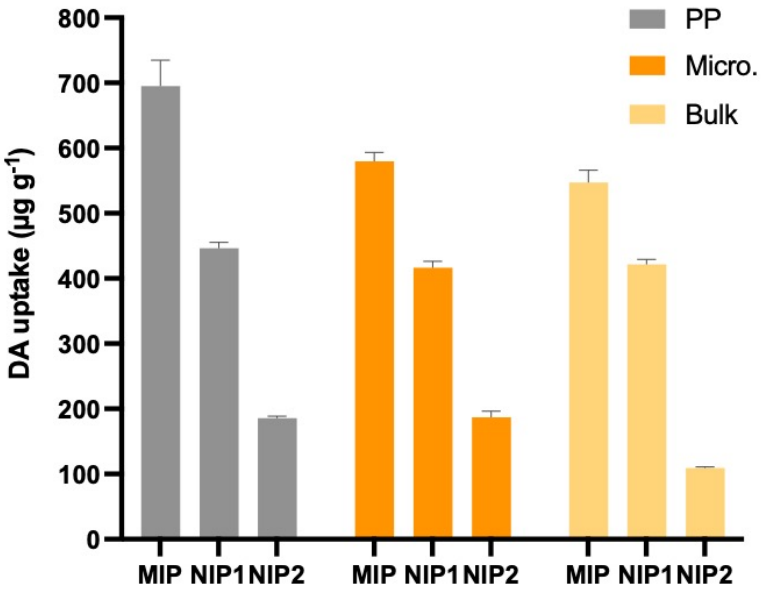

Figure 5.8 Dopamine rebinding results of polymers prepared via different polymerization methods with control groups.

Subsequently, we examined the rebinding capabilities of the control groups, contrasting their performance with that of the imprinted polymers for each polymerization method, as seen in Figure 5.8. Both the control groups demonstrated the non-specific rebinding towards the template molecule. The introduction of boronic acid as a functional group proved pivotal, significantly influencing the final performance. This effect can be attributed to the covalent interaction between dopamine and boronic acid, coupled with the negative charge exhibited by the molecularly imprinted polymeric materials under physiological pH conditions, resulting in remarkable improvements in rebinding performance.

5.3.4 Imprinting Factor (IF) Calculations

Imprinting factors were determined by evaluating the ratios of capacity factors (K) on imprinted and non-imprinted polymers, expressed as in Eq. 5.1.

$$\mathbf{IF} = \mathbf{K}_{mip} \div \mathbf{K}_{nip} \tag{5.1}$$

Here, IF represents the imprinting factor, while Kmip and Knip denote the capacity factors for analytes on the imprinted polymer and the control groups, respectively. The imprinting factor serves as an indicator of selectivity, reflecting the preference of the imprinted polymer over the control polymer for analytes. Consequently, it serves as a quantifiable measure of MIP's affinity and selectivity (Table 5.2).

5.4 Conclusion

In this comprehensive study, our initial focus was adapting various imprinted polymer synthesis procedures tailored for the dopamine template molecule. We sys-

Table 5.2

Imprinting factor values of MIPs prepared by different methods.

	Kmip	**Knip1**	**IF (Kmip/Knip1)**	**Knip2**	**IF(Kmip/Knip2)**
Bulk	0.56	0.43	**1.31**	0.17	**3.15**
Micro.	0.59	0.42	**1.42**	0.19	**3.09**
PP	0.66	0.45	**1.47**	0.18	**3.54**

tematically optimized critical parameters for the synthesis, including ratios, monomer selections, solvent systems, and cross-linking methods. Later, we successfully synthesized dopamine-imprinted polymers via bulk polymerization, precipitation polymerization, and W/O emulsion polymerization methods. To distinguish the efficacy of these methodologies, we compared the adsorption capacities of the DA template molecules. This study allowed us to tailor the synthesis process and provided an understanding of the comparative performance of polymeric materials in different sizes.

6. CONCLUSION

In this dissertation, potential applications of polymeric microgels in diverse biomedical scenarios was explored. A range of polymeric microgels was fabricated employing distinct microfluidics channel configurations. These microgels, in turn, found applications in the bioengineering field, specifically in drug delivery, protein isolation, and biomolecule detection.

The introduction part of the thesis presents an overview of polymeric microgels, explaining their nature and how different methods produce them. Additionally, the thesis offers comprehensive insights into microfluidics, detailing the fabrication of microchannels and their vital role in producing microgels. It also discusses critical examples from previous research that highlight the applications of these microgels in biomedicine. The first chapter introduced a responsive microgel system designed for protein isolation studies. The microgels were fabricated using a flow-focusing microchannel design. This microgel system demonstrated the capability for on-demand protein release by employing thiol-disulfide exchange chemistry. In the second chapter, we engineered microgel systems featuring varied porosities using a microfluidics channel. We synthesized porous microgels by strategically manipulating the monomer systems and incorporating PEG into the polymeric network. These porous microgels were subsequently employed to deliver curcumin, and we conducted in vitro studies to show their effectiveness. The third chapter focused on the *in situ* fabrication of degradable microgels within a microfluidic setup. Degradation occurred in the presence of a reducing agent carried by another microgel model. This study further demonstrated the evaluation of protein delivery. In the final chapter of this thesis, various methods for synthesizing imprinted polymers targeting the dopamine biomarker were explored. The resulting polymers were then compared based on their respective performances in dopamine uptake.

REFERENCES

1. Kazanci, M., "A Review Of Polymeric Smart Materials For Biomedical Applications", *Materials Technology*, Vol. 18, No. 2, pp. 87–93, 2003.

2. Kalirajan, C., A. Dukle, A. J. Nathanael, T.-H. Oh and et al., "A Critical Review on Polymeric Biomaterials for Biomedical Applications", *Polymers*, Vol. 13, No. 17, p. 3015, 2021.

3. Fenton, O. S., K. N. Olafson, P. S. Pillai and et al., "Advances in Biomaterials for Drug Delivery", *Adv. Mater.*, Vol. 30, p. 1705328, 2018.

4. Chambre, L., W. S. Saw, G. Ekineker, L. V. Kiew and et al., "Surfactant-free direct access to porphyrin-cross-linked nanogels for photodynamic and photothermal therapy", *Bioconjugate Chem.*, Vol. 29, No. 12, pp. 4149–4159, 2018.

5. Moro, T., Y. Takatori, K. Ishihara, T. Konno and et al., "Surface grafting of artificial joints with a biocompatible polymer for preventing periprosthetic osteolysis", *Nature Mater.*, Vol. 3, pp. 829–836, 2004.

6. Wang, X., V. Chan and P. R. Corridon, "Acellular Tissue-Engineered Vascular Grafts from Polymers: Methods, Achievements, Characterization, and Challenges", *Polymers*, Vol. 14, No. 22, p. 4825, 2022.

7. Joseph, B., A. George, S. Gopi, N. Kalarikkal and et al., "Polymer sutures for simultaneous wound healing and drug delivery–A review", *International Journal of Pharmaceutics*, Vol. 524, pp. 1–2, 2017.

8. Bolu, B. S., R. Sanyal and A. Sanyal, "Drug delivery systems from self-assembly of dendron-polymer conjugates", *Molecules*, Vol. 23, No. 7, p. 1570, 2018.

9. Altinbasak, I., S. Kocak, A. H. Colby, Y. Alp and et al., "pH-Responsive Nanofiber Buttresses as Local Drug Delivery Devices", *Biomater. Sci.*, Vol. 11, pp. 813–821, 2023.

10. Geckil, H., F. Xu, X. Zhang, S. Moon and et al., "Engineering hydrogels as extracellular matrix mimics", *Nanomedicine*, Vol. 5, No. 3, pp. 469–484, 2010.

11. Song, H.-O., J.-H. Kim, H.-S. Ryu, D.-H. Lee and et al., "Polymeric LabChip Real-Time PCR as a Point-of-Care-Potential Diagnostic Tool for Rapid Detection of Influenza A/H1N1 Virus in Human Clinical Specimens", *PLoS ONE*, Vol. 7, No. 12, 2012.

12. Barhoum, A., O. Sadak, I. A. Ramirez and N. Iverson, "Stimuli-bioresponsive hydrogels as new generation materials for implantable, wearable, and disposable biosensors for medical diagnostics: Principles, opportunities, and challenges", *Advances in Colloid and Interface Science*, Vol. 317, p. 102920, 2023.

13. Nguyen, T. N., V.-D. Phung and V. V. Tran, "Recent Advances in Conjugated Polymer-Based Biosensors for Virus Detection", *Biosensors*, Vol. 13, No. 6, p. 586, 2023.

14. Plamper, F. A. and W. Richtering, "Functional Microgels and Microgel Systems", *Acc. Chem. Res*, Vol. 50, No. 2, pp. 131–140, 2017.

15. Yang, Q., K. Wang, J. Nie, B. Du and et al., "Poly (N-vinylpyrrolidinone) microgels: prepara- tion, biocompatibility, and potential application as drug carriers", *Biomacromolecules*, Vol. 15, No. 6, pp. 2285–93, 2014.

16. Rumyantsev, A. M., R. A. Gumerov and I. I. Potemkin, "A polymer microgel at a liquid–liquid interface: theory vs. computer simulations", *Soft Matter*, Vol. 12, pp. 6799–6811, 2016.

17. Rovigatti, L., N. Gnan, L. Tavagnacco, A. J. Moreno and et al., "Numerical modelling of non-ionic microgels: an overview", *Soft Matter*, Vol. 15, pp. 1108–1119, 2019.

18. Wang, Y., L. Guo, S. Dong, J. Cui and et al., "Microgels in biomaterials and nanomedicines", *Advances in Colloid and Interface Science*, Vol. 266, pp. 1–20, 2019.

19. Kunene, S. C., K.-S. Lin, M.-T. Weng, M. J. C. Espinoza and et al., "Dual stimuli-responsive polymeric microgels for enhanced doxorubicin delivery to hepatocellular carcinoma", *Journal of Drug Delivery Science and Technology*, Vol. 87, p. 104776, 2023.

20. Lifson, M. A., J. A. Carter and B. L. Miller, "Functionalized Polymer Microgel Particles Enable Customizable Production of Label-Free Sensor Arrays", *Anal. Chem.*, Vol. 87, No. 15, pp. 7887–7893, 2015.

21. Xu, S., J. Zhang and E. Kumacheva, "Hybrid polymer-inorganic materials: multiscale hierarchy", *Composite Interfaces*, Vol. 10, No. 4–5, pp. 405–421, 2003.

22. Zhang, Q. M., W. Wang, Y.-Q. Su, E. J. M. Hensen and et al., "Biological Imaging and Sensing with Multiresponsive Microgels", *Chem. Mater.*, Vol. 28, No. 1, pp. 259–265, 2016.

23. Yang, J., B. Huang, Z. Lva and Z. Cao, "Preparation and self-assembly of ionic (PNIPAM-co-VIM) microgels and their adsorption property for phosphate ions", *RSC Adv.*, Vol. 13, pp. 3425–3437, 2023.

24. Izak-Nau, E., S. Braun, A. Pich and R. Göstl, "Mechanically Resistant Poly(N-vinylcaprolactam) Microgels with Sacrificial Supramolecular Catechin Hydrogen Bonds", *Adv. Sci.*, Vol. 9, p. 2104004, 2022.

25. Chen, R., X. Jin and X. Zhu, "Investigation of the Formation Process of PNIPAM-Based Ionic Microgels", *ACS Omega*, Vol. 2, No. 12, pp. 8788–8793, 2017.

26. Lu, B., M. D. Tarn, N. Pamme and T. K. Georgiou, "Tailoring pH-responsive acrylic acid microgels with hydrophobic crosslinks for drug release", *J. Mater. Chem. B*, Vol. 3, pp. 4524–4529, 2015.

27. Li, H., X. Li, P. Jain, H. Peng and et al., "Dual-Degradable Biohybrid Microgels by Direct Cross-Linking of Chitosan and Dextran Using Azide–Alkyne Cycloaddition", *Biomacromolecules*, Vol. 21, No. 12, pp. 4933–4944, 2020.

28. Michel, S. E. S., F. Dutertre, M. L. Denbow, M. C. Galan and et al., "Facile Synthesis of Chitosan-Based Hydrogels and Microgels through Thiol–Ene Photoclick Cross-Linking", *ACS Appl. Bio Mater.*, Vol. 2, No. 8, pp. 3257–3268, 2019.

29. Ma, T., X. Gao, H. Dong, H. He and et al., "High-throughput generation of hyaluronic acid microgels via microfluidics-assisted enzymatic crosslinking and/or Diels–Alder click chemistry for cell encapsulation and delivery", *Applied Materials Today*, Vol. 9, pp. 49–59, 2017.

30. Echeverria, C., S. N. Fernandes, M. H. Godinho, J. P. Borges and et al., "Functional Stimuli-Responsive Gels: Hydrogels and Microgels", *Gels*, Vol. 4, No. 2, p. 54, 2018.

31. Wang, X., D. J. Adlam, R. Wang, A. Altujjar and et al., "Injectable Colloidal Hydrogels of N-Vinylformamide Microgels Dispersed in Covalently Interlinked pH-Responsive Methacrylic Acid-Based Microgels", *Biomacromolecules*, Vol. 24, No. 5, pp. 2173–2183, 2023.

32. Cao, W., P. Ding, H. Fan, Q. Ding and et al., "Carbon Nanomaterials in Temperature-Responsive Poly(N-isopropylacrylamide) Microgels for Controlled Release and Friction Reduction", *ACS Appl. Nano Mater.*, Vol. 6, No. 1, pp. 492–501, 2023.

33. Kharandiuk, T., K. H. Tan, W. Xu, F. Weitenhagen and et al., "Mechanoresponsive diselenide-crosslinked microgels with programmed ultrasound-triggered degradation and radical scavenging ability for protein protection", *Chem. Sci.*, Vol. 13, pp. 11304–11311, 2022.

34. Li, H., R. Luo and K. Y. Lam, "Multiphysics Modeling of Electrochemomechanically Smart Microgels Responsive to Coupled pH/Electric Stimuli", *Macromol. Biosci.*, Vol. 9, pp. 287–297, 2009.

35. Roquero, D. M., O. Smutok, A. Othman, A. Melman and et al., ""Smart" Delivery of Monoclonal Antibodies from a Magnetic Responsive Microgel Nanocomposite", *ACS Appl. Bio Mater.*, Vol. 4, No. 12, pp. 8487–8497, 2021.

36. Jo, S., S. Kim, H. Lee, S. Lee and et al., "Improving cancer chemotherapy through photothermally triggered drug release from poly(N-isopropylacrylamide-co-acrylic acid)/Prussian blue hydrogel", *Materials & Design*, Vol. 233, p. 112243, 2023.

37. Dadsetan, M., K. E. Taylor, C. Yong, Z. Bajzer and et al., "Controlled release of doxorubicin from pH-responsive microgels", *Acta Biomaterialia*, Vol. 9, No. 3, pp. 5438–5446, 2013.

38. Zhang, H., S. Mardyani, W. C. W. Chan and E. Kumacheva, "Design of Biocompatible Chitosan Microgels for Targeted pH-Mediated Intracellular Release of Cancer Therapeutics", *Biomacromolecules*, Vol. 7, No. 5, pp. 1568–1572, 2006.

39. Jung, S.-H., S. Schneider, F. Plamper and A. Pich, "Responsive Supramolecular Microgels with Redox-Triggered Cleavable Crosslinks", *Macromolecules*, Vol. 53, No. 3, pp. 1043–1053, 2020.

40. Jiao, C., F. Obst, M. Geisler, Y. Che and et al., "Reversible Protein Capture and Release by Redox-Responsive Hydrogel in Microfluidics", *Polymers*, Vol. 14, No. 2, p. 267, 2022.

41. Wang, Y., J. Nie, B. Chang, Y. Sun and et al., "Poly(vinylcaprolactam)-Based Biodegradable Multiresponsive Microgels for Drug Delivery", *Biomacromolecules*, Vol. 14, No. 9, pp. 3034–3046, 2013.

42. Volpatti, L. R., M. A. Bochenek, A. L. Facklam, D. M. Burns and et al., "Partially Oxidized Alginate as a Biodegradable Carrier for Glucose-Responsive Insulin Delivery and Islet Cell Replacement Therapy", *Adv. Healthcare Mater.*, Vol. 12, p. 2201822, 2023.

43. Foster, G. A., D. M. Headen, C. González-García, M. Salmerón-Sánchez and et al., "Protease-degradable microgels for protein delivery for vascularization", *Biomaterials*, Vol. 113, pp. 170–175, 2017.

44. Yang, J., Y. Zhu, F. Wang and L. D. et al., "Microfluidic liposomes-anchored microgels as extended delivery platform for treatment of osteoarthritis", *Chemical Engineering Journal*, Vol. 400, p. 126004, 2020.

45. Ye, L., P. A. Cormack and K. Mosbach, "Molecular imprinting on microgel spheres", *Analytica Chimica Acta*, Vol. 435, No. 1, pp. 187–196, 2001.

46. Ullah, B., S. R. Khan, S. Ali and S. Jamil, "Synthesis, parameters, properties and applications of responsive molecularly imprinted microgels: a review", *Reviews in Chemical Engineering*, Vol. 38, No. 6, pp. 703–720, 2022.

47. Orbay, S., O. Kocaturk, R. Sanyal and A. Sanyal, "Molecularly Imprinted Polymer-Coated Inorganic Nanoparticles: Fabrication and Biomedical Applications", *Micromachines*, Vol. 13, No. 9, p. 1464, 2022.

48. Wang, H., J. Yi, D. Velado, Y. Yu and et al., "Immobilization of Carbon Dots in Molecularly Imprinted Microgels for Optical Sensing of Glucose at Physiological pH", *ACS Appl. Mater. Interfaces*, Vol. 7, No. 29, pp. 15735–15745, 2015.

49. Daly, A. C., L. Riley, T. Segura and J. A. Burdick, "Hydrogel microparticles for biomedical applications", *Nat Rev Mater*, Vol. 5, pp. 20–43, 2020.

50. Pichon, V. and K. Haupt, "Affinity Separations on Molecularly Imprinted Polymers with Special Emphasis on Solid-Phase Extraction", *Journal of Liquid Chromatography & Related Technologies*, Vol. 29, pp. 989–1023, 2006.

51. Hudson, A. D., R. Solà, J. T. Ueta, W. Battell, O. Jamieson and et al., "Synthesis of Optimized Molecularly Imprinted Polymers for the Isolation and Detection of Antidepressants via HPLC", *Biomimetics*, Vol. 4, No. 1, p. 18, 2019.

52. Dupin, D., S. Fujii, S. P. Armes, P. Reeve and et al., "Efficient Synthesis of Sterically Stabilized pH-Responsive Microgels of Controllable Particle Diameter by Emulsion Polymerization", *Langmuir*, Vol. 22, No. 7, pp. 3381–3387, 2006.

53. Xu, Q., M. Hashimoto, T. T. Dang, T. Hoare and et al., "Preparation of monodisperse biodegradable polymer microparticles using a microfluidic flow-focusing device for controlled drug delivery", *Small*, Vol. 5, No. 13, pp. 1575–81, 2009.

54. Nichola, J. W., S. T. Koshya, H. Baea, C. M. Hwanga and et al., "Cell-laden microengineered gelatin methacrylate hydrogels", *Biomaterials*, Vol. 31, No. 21, pp. 5536–44, 2010.

55. Panda, P., S. Ali, E. Lo, B. G. Chung and et al., "Stop-flow lithography to generate cell-laden microgel particles", *Lab Chip*, Vol. 8, pp. 1056–1061, 2008.

56. Whitesides, G. M., "The origins and the future of microfluidics", *Nature*, Vol. 442, pp. 368–373, 2006.

57. Gharib, G., I. Butun, Z. Muganli, G. Kozalak and et al., "Biomedical Applications of Microfluidic Devices: A Review", *Biosensors*, Vol. 12, No. 11, p. 1023, 2022.

58. Scott, S. M. and Z. Ali, "Fabrication Methods for Microfluidic Devices: An Overview", *Micromachines*, Vol. 12, No. 3, p. 319, 2021.

59. Seiffert, S., "Functional Microgels Tailored by Droplet-Based Microfluidics", *Macromol. Rapid Commun.*, Vol. 32, pp. 1600–1609, 2011.

60. Seiffert, S., "Microgel Capsules Tailored by Droplet-Based Microfluidics", *ChemPhysChem*, Vol. 14, pp. 295–304, 2013.

61. Farooqi, Z. H., G. T. Vladisavljević, N. Pamme, A. Fatima and et al., "Microfluidic Fabrication and Applications of Microgels and Hybrid Microgels", *Crit. Rev. Anal. Chem.*, pp. 1–15, 2023.

62. Amirifar, L., M. Besanjideh, R. Nasiri, A. Shamloo and et al., "Droplet-based microfluidics in biomedical applications", *Biofabrication*, Vol. 14, p. 022001, 2022.

63. Moragues, T., D. Arguijo, T. Beneyton, C. Modavi and et al., "Droplet-based microfluidics", *Nat Rev Methods Primers*, Vol. 3, p. 32, 2023.

64. Cramer, C., P. Fischer and E. J. Windhab, "Drop formation in a co-flowing ambient fluid", *Chemical Engineering Science*, Vol. 59, No. 15, pp. 3045–3058, 2004.

65. Yobas, L., S. Martens, W.-L. Onga and N. Ranganathana, "High-performance flow-focusing geometry for spontaneous generation of monodispersed droplets", *Lab Chip*, Vol. 6, pp. 1073–1079, 2006.

66. Baret, J.-C., "Surfactants in droplet-based microfluidics", *Lab Chip*, Vol. 12, pp. 422–433, 2012.

67. Herrmann, A., R. Haag and U. Schedler, "Hydrogels and Their Role in Biosensing Applications", *Adv. Healthcare Mater.*, Vol. 10, p. 2100062, 2021.

68. Yu, X., B. Pan, C. Zhao, D. Shorty and et al., "Discovery of Peptidic Ligands against the SARS-CoV-2 Spike Protein and Their Use in the Development of a Highly Sensitive Personal Use Colorimetric COVID-19 Biosensor", *ACS Sens.*, Vol. 8, No. 6, pp. 2159–2168, 2023.

69. Li, H., W. Geng, Z. Qi, W. Ahmad and et al., "Stimuli-responsive SERS biosensor for ultrasensitive tetracycline sensing using EDTA-driven PEI@CaCO3 microcapsule and CS@FeMMs", *Biosensors and Bioelectronics*, Vol. 226, p. 115122, 2023.

70. Mutharani, B., P. Ranganathan, S.-M. Chen and D. V. S. K, "Stimuli-enabled reversible switched aclonifen electrochemical sensor based on smart PNIPAM/PANI-Cu hybrid conducting microgels", *Sensors and Actuators B: Chemical*, Vol. 304, p. 127232, 2020.

71. Stassi, S., E. Fantino, R. Calmo, A. Chiappone and et al., "Polymeric 3D Printed Functional Microcantilevers for Biosensing Applications", *ACS Appl. Mater. Interfaces*, Vol. 9, No. 22, pp. 19193–19201, 2017.

72. Qian, W., Z.-Z. Gu, A. Fujishima and O. Sato, "Three-Dimensionally Ordered Macroporous Polymer Materials: An Approach for Biosensor Applications", *Langmuir*, Vol. 18, No. 11, pp. 4526–4529, 2002.

73. Pourmadadi, M., A. Shamsabadipour, A. Aslani, M. M. Eshaghi and et al., "Development of Polyvinylpyrrolidone-Based nanomaterials for biosensors applications: A Review", *Inorganic Chemistry Communications*, Vol. 152, p. 110714, 2023.

74. Altinbasak, I., M. Arslan, R. Sanyal and A. Sanyal, "Pyridyl disulfide-based thiol–disulfide exchange reaction: shaping the design of redox-responsive polymeric materials", *Polym. Chem.*, Vol. 11, pp. 7603–7624, 2020.

75. Arslan, M., T. N. Gevrek, A. Sanyal and R. Sanyal, "Cyclodextrin mediated polymer coupling via thiol–maleimide conjugation: facile access to functionalizable hydrogels", *RSC Adv.*, Vol. 4, pp. 57834–57841, 2014.

76. Hoyle, C. E., A. B. Lowe and C. N. Bowman, "Thiol-click chemistry: a multifaceted toolbox for small molecule and polymer synthesis", *Chem. Soc. Rev.*, Vol. 39, pp. 1355–1387, 2010.

77. Chen, W., L. A. Shah, L. Yuan, M. Siddiq and et al., "Polymer–paclitaxel conjugates based on disulfide linkers for controlled drug release", *RSC Adv.*, Vol. 5, pp. 7559–7566, 2015.

78. Sun, L., J. Liu and H. Zhao, "Reactive polymeric micelles with disulfide groups in the coronae", *Polym. Chem.*, Vol. 5, pp. 6584–6592, 2014.

79. Choh, S.-Y., D. Cross and C. Wang, "Facile Synthesis and Characterization of Disulfide-Cross-Linked Hyaluronic Acid Hydrogels for Protein Delivery and Cell Encapsulation", *Biomacromolecules*, Vol. 12, No. 4, pp. 1126–1136, 2011.

80. Gaulding, J. C., M. H. Smith, J. S. Hyatt, A. Fernandez-Nieves and et al., "Reversible Inter- and Intra-Microgel Cross-Linking Using Disulfides", *Macromolecules*, Vol. 45, No. 1, pp. 39–45, 2012.

81. Calik, F., *Redox-responsive biodegradable polymeric materials for biomedical applications*, Ph.D. Thesis, Bogazici University, 2022.

82. Conte, M. L., S. Pacifico, A. Chambery, A. Marra and et al., "Photoinduced Addition of Glycosyl Thiols to Alkynyl Peptides: Use of Free-Radical Thiol−Yne Coupling for Post-Translational Double-Glycosylation of Peptides", *J. Org. Chem.*, Vol. 75, No. 13, pp. 4644–4647, 2010.

83. Shepherd, J. L., A. Kell, E. Chung, C. W. Sinclar and et al., "Selective Reductive Desorption of a SAM-Coated Gold Electrode Revealed Using Fluorescence Microscopy", *J. Am. Chem. Soc.*, Vol. 126, No. 26, pp. 8329–8335, 2004.

84. Orbay, S., R. Sanyal and A. Sanyal, "Porous Microgels for Delivery of Curcumin: Microfluidics-Based Fabrication and Cytotoxicity Evaluation", *Micromachines*, Vol. 14, No. 10, p. 1969, 2023.

85. Ebhodaghe, S. O., "A scoping review on the biomedical applications of polymeric particles", *International Journal of Polymeric Materials and Polymeric Biomaterials*, Vol. 72, No. 8, pp. 589–611, 2023.

86. Zheng, J., C. Zhu, X. Xu, X. Wangb and et al., "Supramolecular Assemblies of Multifunctional Microgels for Biomedical Applications", *J. Mater. Chem. B*, Vol. 11, pp. 6265–6289, 2023.

87. Sahiner, N., W. T. Godbey, G. L. McPherson and V. T. John, "Microgel, Nanogel and Hydrogel–Hydrogel Semi-IPN Composites for Biomedical Applications: Synthesis and Characterization", *Colloid. Polym. Sci.*, Vol. 284, pp. 1121–1129, 2006.

88. Agrawal, G. and R. Agrawal, "Functional Microgels: Recent Advances in Their Biomedical Applications", *Small*, Vol. 14, p. 1801724, 2018.

89. Orbay, S. and A. Sanyal, "Molecularly Imprinted Polymeric Particles Created Using Droplet-Based Microfluidics: Preparation and Applications", *Micromachines*, Vol. 14, p. 763, 2023.

90. Wei, Z., S. Wang, H. A. S. Jouni Hirvonen and et al., "Microfluidics Fabrication of Micrometer-Sized Hydrogels with Precisely Controlled Geometries for Biomedical Applications", *Adv. Healthc. Mater.*, Vol. 11, p. 2200846, 2022.

91. Chon, C. H., J. H. Kim, H. On, J. Choi and et al., "A microfluidic application for mass production of drug-loaded polymeric microspheres for a long-acting injectable with IVL-DrugFluidic®, a novel microfluidic microsphere manufacturing platform technology", *OpenNano*, Vol. 12, p. 100153, 2023.

92. Fontana, F., M. P. Ferreira, A. Correia, J. Hirvonen and et al., "Microfluidics as a Cutting-Edge Technique for Drug Delivery Applications", *J. Drug Deliv. Sci. Technol.*, Vol. 34, pp. 76–87, 2016.

93. Trinh, T. N. D., H. D. K. Do, N. N. Nam, T. T. Dan and et al., "Droplet-Based Microfluidics: Applications in Pharmaceuticals", *Pharmaceuticals*, Vol. 16, p. 937, 2023.

94. Li, J. and D. J. Mooney, "Designing Hydrogels for Controlled Drug Delivery", *Nat. Rev. Mater.*, Vol. 1, p. 16071, 2016.

95. Arslan, M., T. N. Gevrek, R. Sanyal and A. Sanyal, "Fabrication of Poly(Ethylene Glycol)-Based Cyclodextrin Containing Hydrogels via Thiol-Ene Click Reaction", *Eur. Polym. J.*, Vol. 62, pp. 426–434, 2015.

96. Arslan, M., T. N. Gevrek, R. Sanyal and A. Sanyal, "Cyclodextrin Mediated Polymer Coupling via Thiol–Maleimide Conjugation: Facile Access to Functionalizable Hydrogels", *RSC Adv.*, Vol. 4, pp. 57834—-57841, 2014.

97. Sartipzadeh, O., S. M. Naghib, F. Haghiralsadat, F. Shokati and et al., "Microfluidic-Assisted Synthesis and Modeling of Stimuli-Responsive Monodispersed Chitosan Microgels for Drug Delivery Applications", *Sci. Rep.*, Vol. 12, p. 8382, 2022.

98. Hoque, J., Y. Zeng, H. Newman, G. Gonzales and et al., "Microgel-Assisted Delivery of Adenosine to Accelerate Fracture Healing", *ACS Biomater. Sci. Eng.*, Vol. 8, pp. 4863–4872, 2022.

99. Saveleva, M. S., M. E. Lobanov, O. I. Gusliakova, V. O. Plastun and et al., "Mucoadhesive Emulsion Microgels for Intravesical Drug Delivery: Preparation, Retention at Urothelium, and Biodistribution Study", *ACS Appl. Mater. Interfaces*, Vol. 15, pp. 25354–25368, 2023.

100. Suhail, M., J. M. Rosenholm, M. U. Minhas, S. F. Badshah and et al., "Nanogels as Drug-Delivery Systems: A Comprehensive Overview", *Ther. Deliv.*, Vol. 10, pp. 697–717, 2019.

101. Degirmenci, A., H. Ipek, R. Sanyal and A. Sanyal, "Cyclodextrin-Containing Redox-Responsive Nanogels: Fabrication of a Modular Targeted Drug Delivery System", *Eur. Polym. J.*, Vol. 181, p. 111645, 2022.

102. Chambre, L., A. Degirmenci, R. Sanyal and A. Sanyal, "Multi-Functional Nanogels as Theranostic Platforms: Exploiting Reversible and Nonreversible Linkages for Targeting, Imaging, and Drug Delivery", *Bioconjugate Chem.*, Vol. 29, pp. 1885–1896, 2018.

103. Malmsten, M., H. Bysell and P. Hansson, "Biomacromolecules in Microgels-Opportunities and Challenges for Drug Delivery", *Curr. Opin. Colloid. Interface Sci.*, Vol. 15, pp. 435–444, 2010.

104. Oh, J. K., D. I. Lee and J. M. Park, "Biopolymer-Based Microgels/Nanogels for Drug Delivery Applications", *Prog. Polym. Sci.*, Vol. 34, pp. 1261–1282, 2009.

105. Özbilenler, C., E. M. Altundağ and M. Gazi, "Synthesis of Quercetin-Encapsulated Alginate Beads with Their Antioxidant and Release Kinetic Studies", *J. Macromol. Sci. Part. A*, Vol. 58, pp. 22–31, 2021.

106. Zhou, X., J. Nie and B. Du, "4-(2-Pyridylazo)-Resorcinol Functionalized Thermosensitive Ionic Microgels for Optical Detection of Heavy Metal Ions at Nanomolar Level", *ACS Appl. Mater. Interfaces*, Vol. 7, pp. 21966–21974, 2015.

107. Durkut, S., "Fe3O4 Magnetic Nanoparticles-Loaded Thermoresponsive Poly (N-Vinylcaprolactam)-g-Galactosylated Chitosan Microparticles: Investigation of Physicochemical, Morphological and Magnetic Properties", *J. Macromol. Sci. Part. A*, Vol. 60, pp. 2181–191, 2023.

108. Gonçalves, A., B. T. Simões, F. V. Almeida, S. N. Fernandes and et al., "Engineering Dual-Stimuli Responsive Poly(Vinyl Alcohol) Nanofibrous Membranes for Cancer Treatment by Magnetic Hyperthermia", *Biomater. Adv.*, Vol. 145, p. 213275, 2023.

109. Klinger, D. and K. Landfester, "Stimuli-Responsive Microgels for the Loading and Release of Functional Compounds: Fundamental Concepts and Applications", *Polymer*, Vol. 53, pp. 5209–5231, 2012.

110. Wang, X., Y. Wu, H. Shang, X. Sun and et al., "Preparation of PH/Light Dual-Responsive Biocompatible Polymer Micelles: Application to Curcumin Delivery", *J. Drug Deliv. Sci. Technol.*, Vol. 86, p. 104652, 2023.

111. Zhu, L., Q. Song and H. Ma, "Synthesis of Hyperbranched Polysiloxane/Poly(N-Isopropylacrylamide) Microgel, Its Stimulus Responsive Behavior and Study for Drug Release", *J. Macromol. Sci. Part. A*, Vol. 60, pp. 18–28, 2023.

112. Sahiner, M., A. S. Yilmaz, R. S. Ayyala and et al., "Biocompatible Glycol Chitosan Microgels as Effective Drug Carriers", *Gels*, Vol. 9, p. 398, 2023.

113. Natalia, F., G. Stoychev, N. Puretskiy, I. Leonid and et al., "Porous Thermo-Responsive PNIPAM Microgels", *Eur. Polym. J.*, Vol. 69, pp. 650–656, 2015.

114. Wen, Z., L. Kang, H. Fu, S. Zhu and et al., "Oral Delivery of Porous Starch-Loaded Bilayer Microgels for Controlled Drug Delivery and Treatment of Ulcerative Colitis", *Carbohydr. Polym.*, Vol. 314, p. 120887, 2023.

115. Dubey, N. C., D. Gaur and B. P. Tripathi, "Responsive Microgels and Microgel Assemblies in Biocatalytic Applications", *J. Polym. Sci.*, Vol. 61, pp. 1730–1748, 2023.

116. Atiyah, N. A., T. M. Albayati and M. A. Atiya, "Functionalization of Mesoporous MCM-41 for the Delivery of Curcumin as an Anti-Inflammatory Therapy", *Adv. Powder Technol.*, Vol. 33, p. 103417, 2022.

117. Al-Hawary, S. I. S., S. A. Jasim, M. M. Kadhim, S. J. Saadoon and et al., "Curcumin in the Treatment of Liver Cancer: From Mechanisms of Action to Nanoformulations", *Phytother. Res.*, Vol. 37, pp. 1624–1639, 2023.

118. Gholipour, F., M. Amini, B. Baradaran, A. Mokhtarzadeh and et al., "Anticancer Properties of Curcumin-Treated Lacto- bacillus Plantarum against the HT-29 Colorectal Adenocarcinoma Cells", *Sci. Rep.*, Vol. 13, p. 2860, 2023.

119. Jiang, L., P. Guo, J. Ju, X. Zhu and et al., "Inhalation of L-Arginine-Modified Liposomes Targeting M1 Macrophages to Enhance Curcumin Therapeutic Efficacy in ALI", *Eur. J. Pharm. Biopharm.*, Vol. 182, pp. 21–31, 2023.

120. Yang, R., S. Zhang, D. Kong, X. Gao and et al., "Biodegradable Polymer-Curcumin Conjugate Micelles Enhance the Loading and Delivery of Low-Potency Curcumin", *Pharm. Res.*, Vol. 29, pp. 3512–3525, 2012.

121. Yeo, S., M. J. Kim, Y. K. Shim, I. Yoon and et al., "Solid Lipid Nanoparticles of Curcumin Designed for Enhanced Bioavailability and Anticancer Efficiency", *ACS Omega*, Vol. 7, pp. 35875–35884, 2022.

122. Zhou, Y., C. Zhou, Y. Zou, Y. Jin and et al., "Multi pH-Sensitive Polymer–Drug Conjugate Mixed Micelles for Efficient Co-Delivery of Doxorubicin and Curcumin to Synergistically Suppress Tumor Metastasis", *Biomater. Sci.*, Vol. 8, pp. 5029–5046, 2020.

123. Zeng, Y., Y. Lv, M. Hu, F. Guo and et al., "Curcumin-Loaded Hydroxypropyl-β-Cyclodextrin Inclusion Complex with Enhanced Dissolution and Oral Bioavailability for Epilepsy Treatment", *Xenobiotica*, Vol. 52, pp. 718–728, 2022.

124. Dhule, S. S., T. F. Patrice Penfornis and, R. Walker and et al., "Curcumin-Loaded-γ-Cyclodextrin Liposomal Nanoparticles as Delivery Vehicles for Osteosarcoma", *Nanomed. Nanotechnol. Biol. Med.*, Vol. 8, pp. 440–451, 2012.

125. Arya, P. and N. Raghav, "In-Vitro Studies of Curcumin-β-Cyclodextrin Inclusion Complex as Sustained Release System", *J. Mol. Struct.*, Vol. 1228, p. 129774, 2021.

126. Khatun, B., P. Baishya, A. Ramtekeb and T. K. Maji, "Study of the Complexation of Structurally Modified Curcumin with Hydroxy- propyl Beta Cyclodextrin and Its Effect on Anticancer Activity", *New J. Chem.*, Vol. 44, pp. 4887–4897, 2020.

127. Heikal, E. J., R. M. Kaoud, S. Gad, H. I. Mokhtar and et al., "Development of Novel PH-Sensitive Eudragit Coated Beads Containing Curcumin-Mesalamine Combination for Colon-Specific Drug Delivery", *Gels*, Vol. 9, p. 264, 2023.

128. Veron, M. G., L. A. Soria, P. D. Perez and M. O. Prado, "Sulfonated PVA Microspheres for Drug Delivery and Simulated Body Fluid Interaction", *J. Macromol. Sci. Part. A*, Vol. 60, pp. 51–62, 2023.

129. Hou, Y., B. Deng, S. Wang, Y. Ma and et al., "High-Strength, High-Water-Retention Hemi-cellulose-Based Hydrogel and Its Application in Urea Slow Release", *IJMS*, Vol. 24, p. 9208, 2023.

130. Józsa, L., G. Vasvári, D. Sinka, D. Nemes and et al., "Enhanced Antioxidant and Anti-Inflammatory Effects of Self-Nano and Microemulsifying Drug Delivery Systems Containing Curcumin", *Molecules*, Vol. 27, p. 6652, 2022.

131. Xin, S., O. M. Wyman and D. L. Alge, "Assembly of PEG Microgels into Porous Cell-Instructive 3D Scaffolds via Thiol-Ene Click", *Chemistry. Adv. Healthc. Mater.*, Vol. 7, p. 1800160, 2018.

132. Behra, M., S. Schmidt, J. Hartmann, D. V. Volodkin and et al., "Synthesis of Porous PEG Microgels Using CaCO3 Microspheres as Hard Templates", *Macromol. Rapid Commun.*, Vol. 33, pp. 1049–1054, 2012.

133. Delbreil, P., X. Banquy and D. Brambilla, "Template-Based Porous Hydrogel Microparticles as Carriers for Therapeutic Proteins", *ACS Bio Med. Chem. Au*, Vol. 3, pp. 252–260, 2023.

134. Agrawal, G., R. Agrawal and A. Pich, "Dual Responsive Poly(N-vinylcaprolactam) Based Degradable Microgels for Drug Delivery", *Part. Part. Syst. Charact.*, Vol. 34, p. 1700132, 2017.

135. Mora-Boza, A., S. G. Ghebrezadik, J. E. Leisen and A. J. García, "Rapid and Facile Light-Based Approach to Fabricate Protease-Degradable Poly(ethylene glycol)−norbornene Microgels for Cell Encapsulation", *Adv. Healthcare Mater.*, Vol. 12, p. 2300942, 2023.

136. Hou, C., Q. Zhang, H. Wang and Y. Li, "Functionalization of PNIPAAm microgels using magnetic graphene and their application in microreactors as switch materials", *J. Mater. Chem.*, Vol. 21, pp. 10512–10517, 2011.

137. Zhao, S., H. Wen, Y. Ou, M. Li and et al., "A new design for living cell-based biosensors: Microgels with a selectively permeable shell that can harbor bacterial species", *Sensors and Actuators B: Chemical*, Vol. 334, p. 129648, 2021.

138. Best, J. P., Y. Yan and F. Caruso, "The Role of Particle Geometry and Mechanics in the Biological Domain", *Adv. Healthcare Mater.*, Vol. 1, pp. 35–47, 2012.

139. Agrawal, G. and R. Agrawal, "Stimuli-Responsive Microgels and Microgel-Based Systems: Advances in the Exploitation of Microgel Colloidal Properties and Their Interfacial Activity", *Polymers*, Vol. 10, No. 4, p. 418, 2018.

140. Wu, Y., S. Wiese, A. Balaceanu, W. Richtering and et al., "Behavior of Temperature-Responsive Copolymer Microgels at the Oil/Water Interface", *Langmuir*, Vol. 30, No. 26, pp. 7660–7669, 2014.

141. Freemonta, T. J. and B. R. Saunders, "pH-Responsive microgel dispersions for repairing damaged load-bearing soft tissue", *Soft Matter.*, Vol. 4, pp. 919–924, 2008.

142. Liu, L., Y.-X. Liu, H. Zhong, X.-R. Li and et al., "Folic acid conjugated palygorskite/Au hybrid microgels: Temperature, pH and light triple-responsive and its application in drug delivery", *Colloids and Surfaces B: Biointerfaces*, Vol. 229, p. 113432, 2023.

143. Zhao, W., R. W. N. Nugroho, K. Odelius, U. Edlund and et al., "In Situ Cross-Linking of Stimuli-Responsive Hemicellulose Microgels during Spray Drying", *ACS Appl. Mater. Interfaces*, Vol. 7, No. 7, pp. 4202–4215, 2015.

144. Wu, Q., T. Su, Y. Maoa and Q. Wang, "Thermal responsive microgels as recyclable carriers to immobilize active proteins with enhanced nonaqueous biocatalytic performance", *Chem. Commun.*, Vol. 49, pp. 11299–11301, 2013.

145. Wang, Q. and M. Libera, "Microgel-modified surfaces enhance short-term osteoblast response", *Colloids and Surfaces B: Biointerfaces*, Vol. 118, pp. 202–209, 2014.

146. Rossow, T., J. A. Heyman, A. J. Ehrlicher, A. Langhoff and et al., "Controlled Synthesis of Cell-Laden Microgels by Radical-Free Gelation in Droplet Microfluidics", *J. Am. Chem. Soc.*, Vol. 134, No. 10, pp. 4983–4989, 2012.

147. Heida, T., O. Otto, D. Biedenweg, N. Hauck and et al., "Microfluidic Fabrication of Click Chemistry-Mediated Hyaluronic Acid Microgels: A Bottom-Up Material Guide to Tailor a Microgel's Physicochemical and Mechanical Properties", *Polymers*, Vol. 12, No. 8, p. 1760, 2020.

148. Sui, X., L. Shui, J. Cui, Y. Xie and et al., "Redox-responsive organometallic microgel particles prepared from poly(ferrocenylsilane)s generated using microfluidics", *Chem.Commun.*, Vol. 50, p. 3058, 2014.

149. Baldwin, A. D., K. G. Robinson, J. Militar, C. D. Derby and et al., "In situ crosslinkable heparin-containing poly(ethylene glycol) hydrogels for sustained anticoagulant release", *J Biomed Mater Res A.*, Vol. 100, No. 8, pp. 2106–2118, 2012.

150. Ghosh, S., S. Basu and S. Thayumanavan, "Simultaneous and Reversible Functionalization of Copolymers for Biological Applications", *Macromolecules*, Vol. 39, No. 17, p. 5595–5597, 2006.

151. Haupt, K., "Imprinted polymers - Tailor-made mimics of antibodies and receptors", *Chem.Commun.*, Vol. 9, pp. 171–177, 2003.

152. Haupt, K., "Peer Reviewed: Molecularly Imprinted Polymers: The Next Generation", *Anal. Chem.*, Vol. 75, No. 17, pp. 376 A–383 A, 2003.

153. Andersson, L., B. Sellergren and K. Mosbach, "Imprinting of amino acid derivatives in macroporous polymers", *Tetrahedron Lett.*, Vol. 25, No. 45, pp. 5211–5214, 1984.

154. Wulff, G., A. Sarhan and K. Zabrocki, "Enzyme-analogue built polymers and their use for the resolution of racemates", *Tetrahedron Lett.*, Vol. 14, No. 44, pp. 4329–4332, 1973.

155. Mosbach, K. and O. Ramström, "The Emerging Technique of Molecular Imprinting and Its Future Impact on Biotechnology", *Nat Biotechnol*, Vol. 14, pp. 163–170, 1996.

156. II, R. J. U., M. Bode and K. D. Shimizu, "Measurement of the continuous distribution of binding sites in molecularly imprinted polymers", *Analyst*, Vol. 125, pp. 1261–1264, 2000.

157. Klein, J. U., M. J. Whitcombe, F. Mulholland and E. N. Vulfson, "Template-Mediated Synthesis of a Polymeric Receptor Specific to Amino Acid Sequences", *Angew. Chemie Int. Ed.*, Vol. 38, No. 13–14, pp. 2057–2060, 1999.

158. Takimoto, K., E. Takano, Y. Kitayama and T. Takeuchi, "Synthesis of Monodispersed Submillimeter-Sized Molecularly Imprinted Particles Selective for Human Serum Albumin Using Inverse Suspension Polymerization in Water-in-Oil Emulsion Prepared Using Microfluidics", *Langmuir*, Vol. 31, No. 17, pp. 4981–4987, 2015.

159. Nilsson, J., P. Spégel and S. Nilsson, "Molecularly imprinted polymer formats for capillary electrochromatography", *Journal of Chromatography B*, Vol. 804, No. 1, pp. 3–12, 2004.

160. Zhou, M., P. Wang, Y. Song, H. Li and et al., "Hybrid hydrogel microspheres loading single-hole hollow imprinted particles for fast and selective uptake of 2′-deoxyadenosine", *Separation and Purification Technology*, Vol. 287, p. 120472, 2022.

161. Kim, K.-S., J.-H. Lee, M. H. Kim and S.-H. Cho, "Preparation and Characterization of Molecularly Imprinted Uniform-sized Poly(4VP-co-EGDMA) Microgels", *Polym J*, Vol. 37, pp. 669–676, 2005.

162. Damier, P., E. Hirsch, Y. Agid and A. Graybiel, "The substantia nigra of the human brain: II. Patterns of loss of dopamine-containing neurons in Parkinson's disease", *Brain*, Vol. 122, No. 8, pp. 1437–1448, 1999.

163. He, R., X. Yan, J. Guo, Q. Xu and et al., "Recent Advances in Biomarkers for Parkinson's Disease", *Front. Aging Neurosci.*, Vol. 10, p. 305, 2018.

164. Liu, L., X. Tian, Y. Ma, Y. Duan and et al., "A Versatile Dynamic Mussel-Inspired Biointerface: From Specific Cell Behavior Modulation to Selective Cell Isolation", *Angew. Chem. Int. Ed.*, Vol. 57, No. 26, pp. 7878–7882, 2018.

165. Ren, L., Z. Liu, Y. Liu, P. Dou and et al., "Ring-Opening Polymerization with Synergistic Co-monomers: Access to a Boronate-Functionalized Polymeric Monolith for the Specific Capture of cis-Diol-Containing Biomolecules under Neutral Conditions", *Angew. Chem. Int. Ed.*, Vol. 121, pp. 6832–6835, 2009.

APPENDIX A. SUPPLEMENTARY DATA

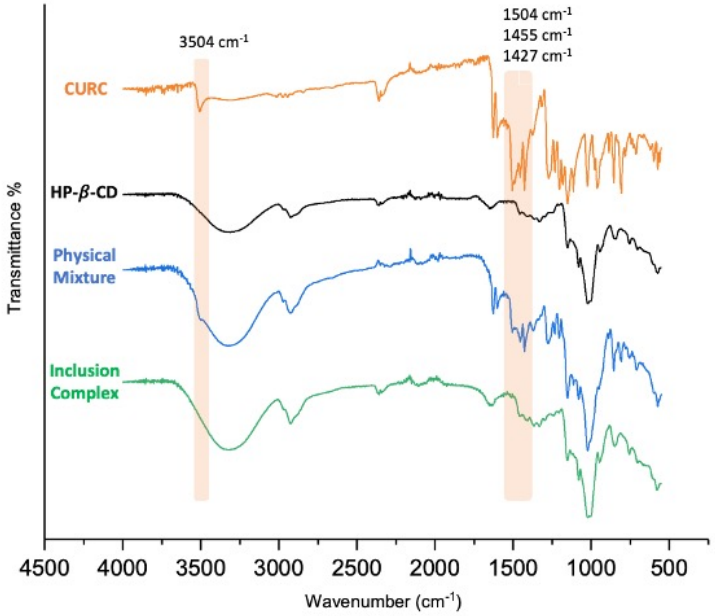

Figure A.1 FT-IR spectra of the components of the Curcumin-HP-β-CD complex inclusion.

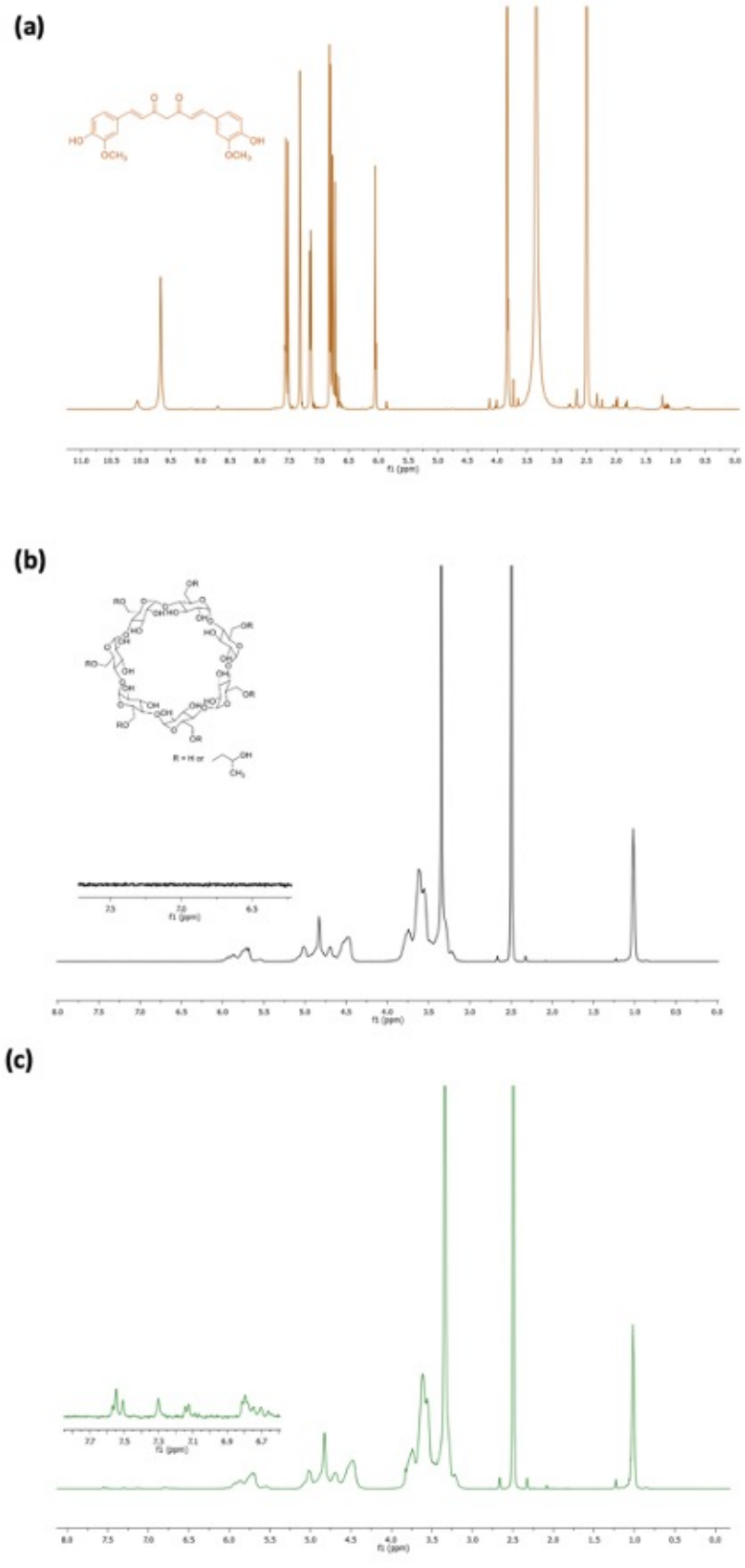

Figure A.2 H-NMR spectrum of the components of the curc/HP-β-CD complex inclusion in DMSO-d6. (a) Curcumin, (b) HP-β-CD and (c) curc/HP-β-CD inclusion complex.

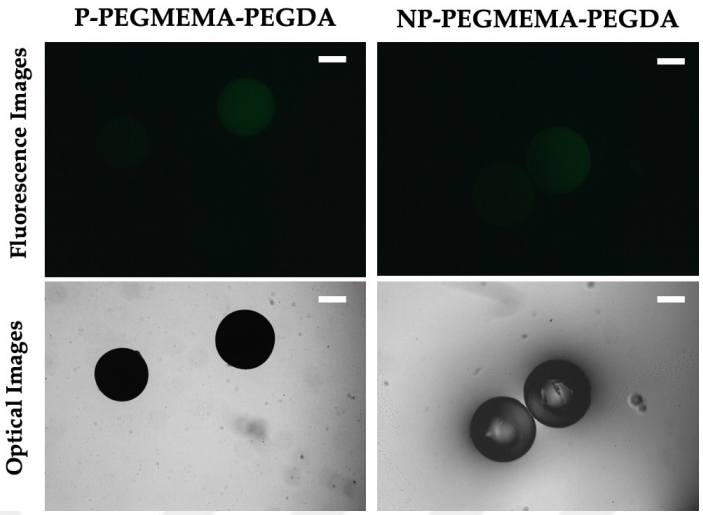

Figure A.3 Microscopy images of microgels after release in cell medium (Scale 200 μm).

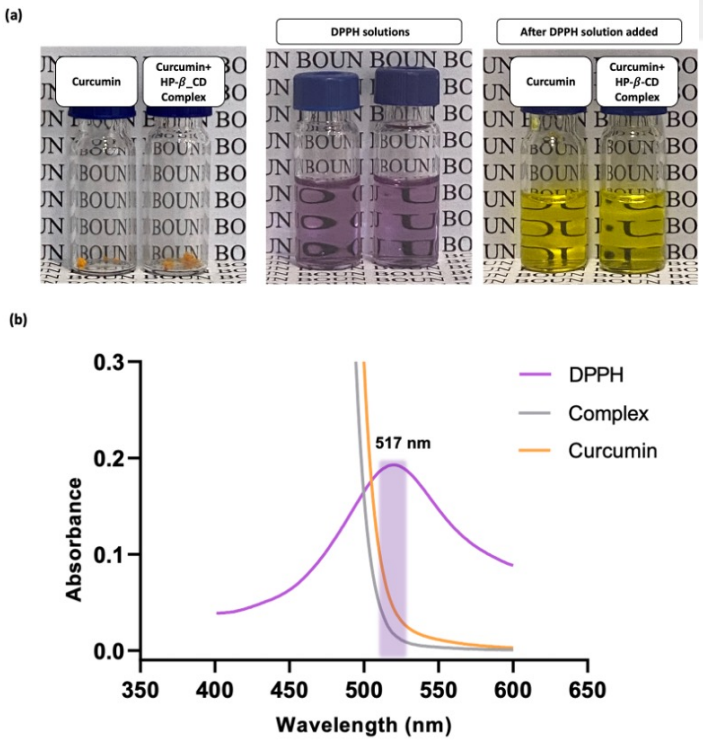

Figure A.4 (a) DPPH solutions introduced to the curcumin and curc/HP-β-CD complex, (b) UV-vis spectra of DPPH solution and DPPH radical scavenging.

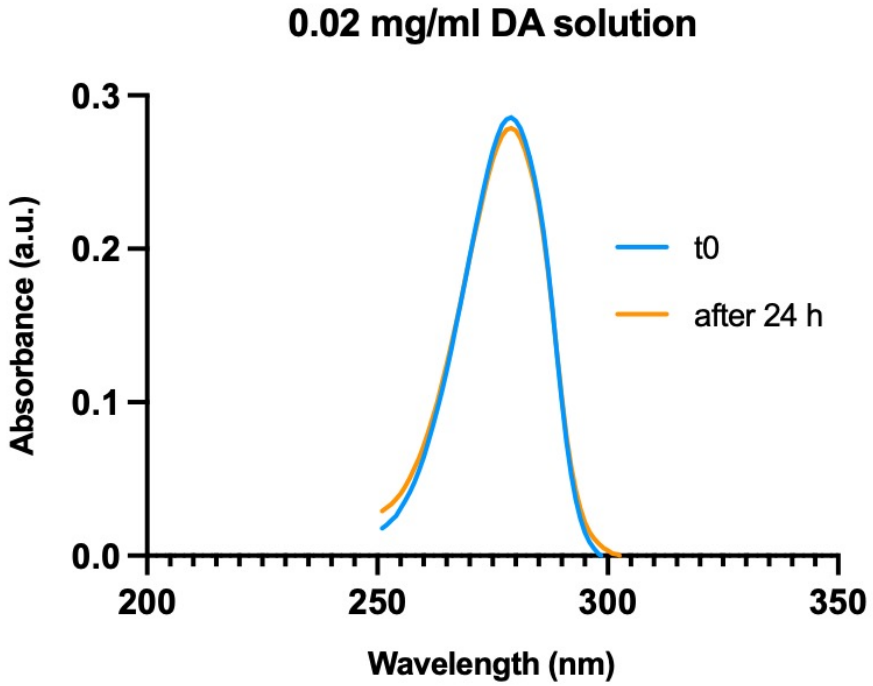

Figure A.5 UV spectra of dopamine solution after 24 h.

APPENDIX B. COPYRIGHT NOTICES

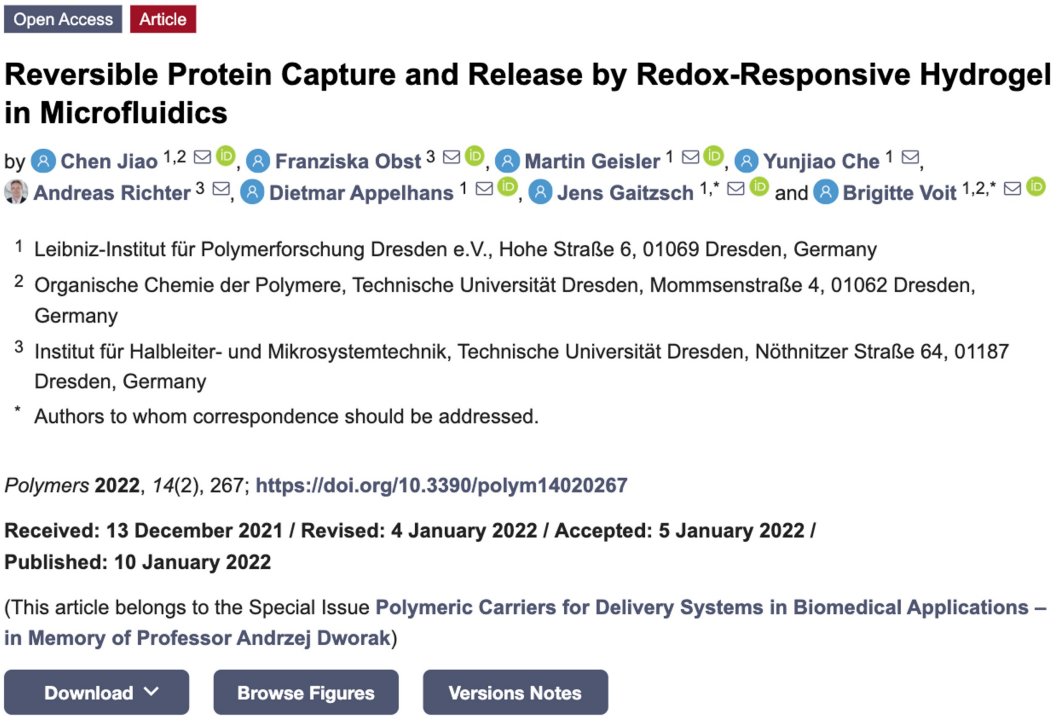

Open Access Article

Reversible Protein Capture and Release by Redox-Responsive Hydrogel in Microfluidics

by Chen Jiao [1,2], Franziska Obst [3], Martin Geisler [1], Yunjiao Che [1], Andreas Richter [3], Dietmar Appelhans [1], Jens Gaitzsch [1,*] and Brigitte Voit [1,2,*]

[1] Leibniz-Institut für Polymerforschung Dresden e.V., Hohe Straße 6, 01069 Dresden, Germany

[2] Organische Chemie der Polymere, Technische Universität Dresden, Mommsenstraße 4, 01062 Dresden, Germany

[3] Institut für Halbleiter- und Mikrosystemtechnik, Technische Universität Dresden, Nöthnitzer Straße 64, 01187 Dresden, Germany

[*] Authors to whom correspondence should be addressed.

Polymers **2022**, *14*(2), 267; https://doi.org/10.3390/polym14020267

Received: 13 December 2021 / Revised: 4 January 2022 / Accepted: 5 January 2022 / Published: 10 January 2022

(This article belongs to the Special Issue **Polymeric Carriers for Delivery Systems in Biomedical Applications – in Memory of Professor Andrzej Dworak**)

Download Browse Figures Versions Notes

© 2022 by the authors. Licensee MDPI, Basel, Switzerland. This article is an open access article distributed under the terms and conditions of the Creative Commons Attribution (CC BY) license (**https://creativecommons.org/licenses/by/4.0/**).

Figure B.1 Copyright permission for Figure 1.3 from Ref. [40].

Order Completed

Thank you for your order.

This Agreement between Ms. Sinem Orbay ("You") and Elsevier ("Elsevier") consists of your license details and the terms and conditions provided by Elsevier and Copyright Clearance Center.

Your confirmation email will contain your order number for future reference.

License Number	5671910000912
License date	Nov 18, 2023

Printable Details

Licensed Content

Licensed Content Publisher	Elsevier
Licensed Content Publication	Chemical Engineering Journal
Licensed Content Title	Microfluidic liposomes-anchored microgels as extended delivery platform for treatment of osteoarthritis
Licensed Content Author	Jielai Yang,Yuan Zhu,Fei Wang,Liangfu Deng,Xiangyang Xu,Wenguo Cui
Licensed Content Date	Nov 15, 2020
Licensed Content Volume	400
Licensed Content Issue	n/a
Licensed Content Pages	1

Order Details

Type of Use	reuse in a thesis/dissertation
Portion	figures/tables/illustrations
Number of figures/tables/illustrations	1
Format	both print and electronic
Are you the author of this Elsevier article?	No
Will you be translating?	No

About Your Work

Title of new work	FABRICATION OF POLYMERIC MICRO-STRUCTURES FOR BIOMOLECULAR SENSING AND ENHANCED THERAPEUTIC DELIVERY
Institution name	Bogazici University
Expected presentation date	Jan 2024

Additional Data

Portions	Figure 1

Requestor Location

Requestor Location	Ms. Sinem Orbay Bogazici University, Kandilli Campus cengelkoy Istanbul, 34684 Turkey Attn: Ms. Sinem Orbay

Tax Details

Publisher Tax ID	GB 494 6272 12

Figure B.2 Copyright permission for Figure 1.4 from Ref. [44].

ACS Publications
Most Trusted. Most Cited. Most Read.

Immobilization of Carbon Dots in Molecularly Imprinted Microgels for Optical Sensing of Glucose at Physiological pH

Author: Hui Wang, Jinhui Yi, David Velado, et al
Publication: Applied Materials
Publisher: American Chemical Society
Date: Jul 1, 2015

Copyright © 2015, American Chemical Society

PERMISSION/LICENSE IS GRANTED FOR YOUR ORDER AT NO CHARGE

This type of permission/license, instead of the standard Terms and Conditions, is sent to you because no fee is being charged for your order. Please note the following:

- Permission is granted for your request in both print and electronic formats, and translations.
- If figures and/or tables were requested, they may be adapted or used in part.
- Please print this page for your records and send a copy of it to your publisher/graduate school.
- Appropriate credit for the requested material should be given as follows: "Reprinted (adapted) with permission from {COMPLETE REFERENCE CITATION}. Copyright {YEAR} American Chemical Society." Insert appropriate information in place of the capitalized words.
- One-time permission is granted only for the use specified in your RightsLink request. No additional uses are granted (such as derivative works or other editions). For any uses, please submit a new request.

If credit is given to another source for the material you requested from RightsLink, permission must be obtained from that source.

BACK CLOSE WINDOW

Figure B.3 Copyright permission for Figure 1.5 from Ref. [48].

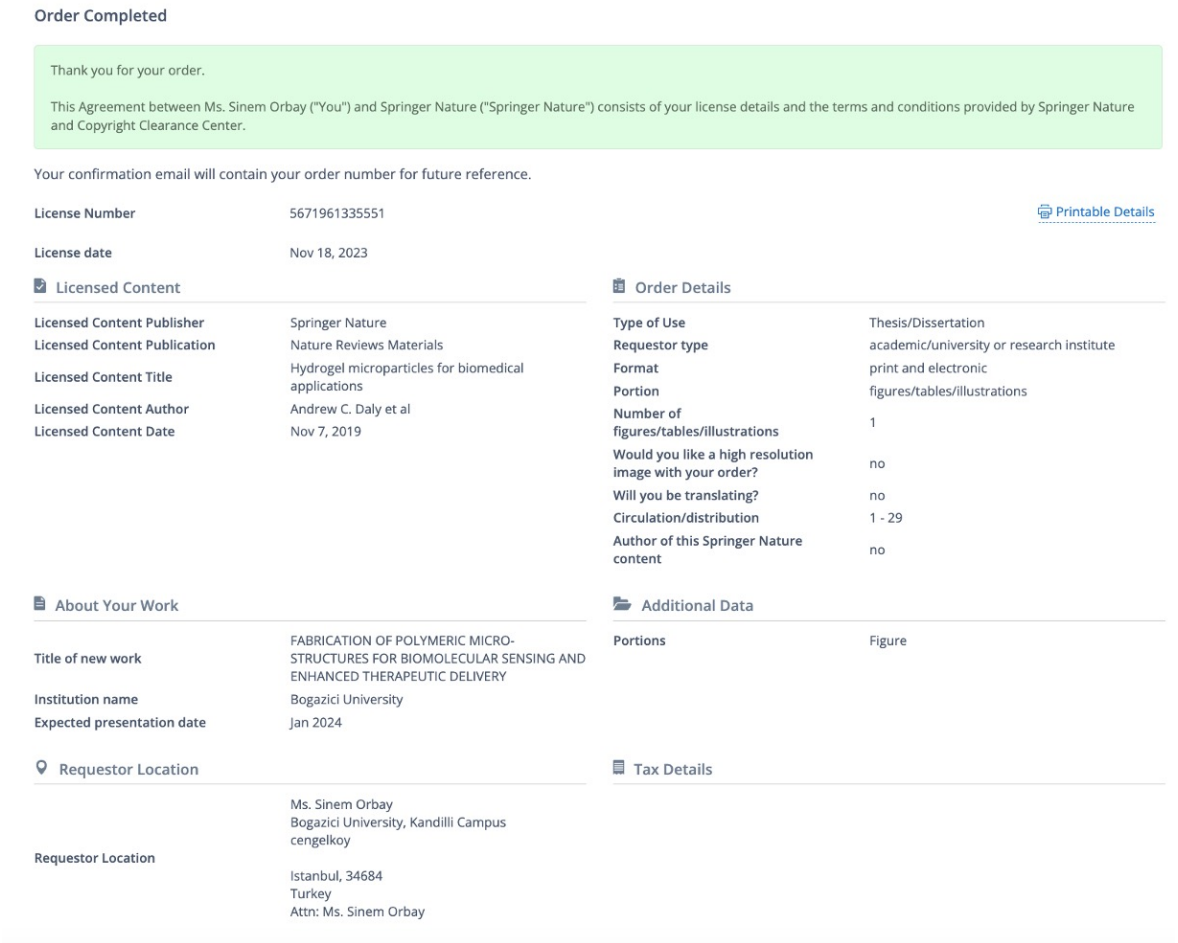

Order Completed

Thank you for your order.

This Agreement between Ms. Sinem Orbay ("You") and Springer Nature ("Springer Nature") consists of your license details and the terms and conditions provided by Springer Nature and Copyright Clearance Center.

Your confirmation email will contain your order number for future reference.

License Number	5671961335551
License date	Nov 18, 2023

Printable Details

Licensed Content

Licensed Content Publisher	Springer Nature
Licensed Content Publication	Nature Reviews Materials
Licensed Content Title	Hydrogel microparticles for biomedical applications
Licensed Content Author	Andrew C. Daly et al
Licensed Content Date	Nov 7, 2019

Order Details

Type of Use	Thesis/Dissertation
Requestor type	academic/university or research institute
Format	print and electronic
Portion	figures/tables/illustrations
Number of figures/tables/illustrations	1
Would you like a high resolution image with your order?	no
Will you be translating?	no
Circulation/distribution	1 - 29
Author of this Springer Nature content	no

About Your Work

Title of new work	FABRICATION OF POLYMERIC MICRO-STRUCTURES FOR BIOMOLECULAR SENSING AND ENHANCED THERAPEUTIC DELIVERY
Institution name	Bogazici University
Expected presentation date	Jan 2024

Additional Data

Portions	Figure

Requestor Location

Requestor Location	Ms. Sinem Orbay Bogazici University, Kandilli Campus cengelkoy Istanbul, 34684 Turkey Attn: Ms. Sinem Orbay

Tax Details

Figure B.4 Copyright permission for Figure 1.6 from Ref. [49].

Open Access Review

Biomedical Applications of Microfluidic Devices: A Review

by Ghazaleh Gharib [1,2,3,*], İsmail Bütün [1], Zülâl Muganlı [1], Gül Kozalak [1,3], İlayda Namlı [1], Seyedali Seyedmirzaei Sarraf [1], Vahid Ebrahimpour Ahmadi [1], Erçil Toyran [1], Andre J. van Wijnen [4] and Ali Koşar [1,2,3,5,*]

[1] Faculty of Engineering and Natural Science, Sabanci University, Istanbul 34956, Turkey
[2] Sabanci University Nanotechnology Research and Application Centre (SUNUM), Istanbul 34956, Turkey
[3] Center of Excellence for Functional Surfaces and Interfaces for Nano Diagnostics (EFSUN), Faculty of Engineering and Natural Sciences, Sabanci University, Istanbul 34956, Turkey
[4] Department of Biochemistry, University of Vermont, 89 Beaumont Avenue, Burlington, VT 05405, USA
[5] Turkish Academy of Sciences (TÜBA), Çankaya, Ankara 06700, Turkey
[*] Authors to whom correspondence should be addressed.

Biosensors **2022**, *12*(11), 1023; **https://doi.org/10.3390/bios12111023**

Received: 23 September 2022 / Revised: 30 October 2022 / Accepted: 8 November 2022 / Published: 16 November 2022

(This article belongs to the Special Issue **Microfluidics for Detection and Analysis**)

Download Browse Figures Versions Notes

© 2022 by the authors. Licensee MDPI, Basel, Switzerland. This article is an open access article distributed under the terms and conditions of the Creative Commons Attribution (CC BY) license (**https://creativecommons.org/licenses/by/4.0/**).

Figure B.5 Copyright permission for Figure 1.7 from Ref. [57].

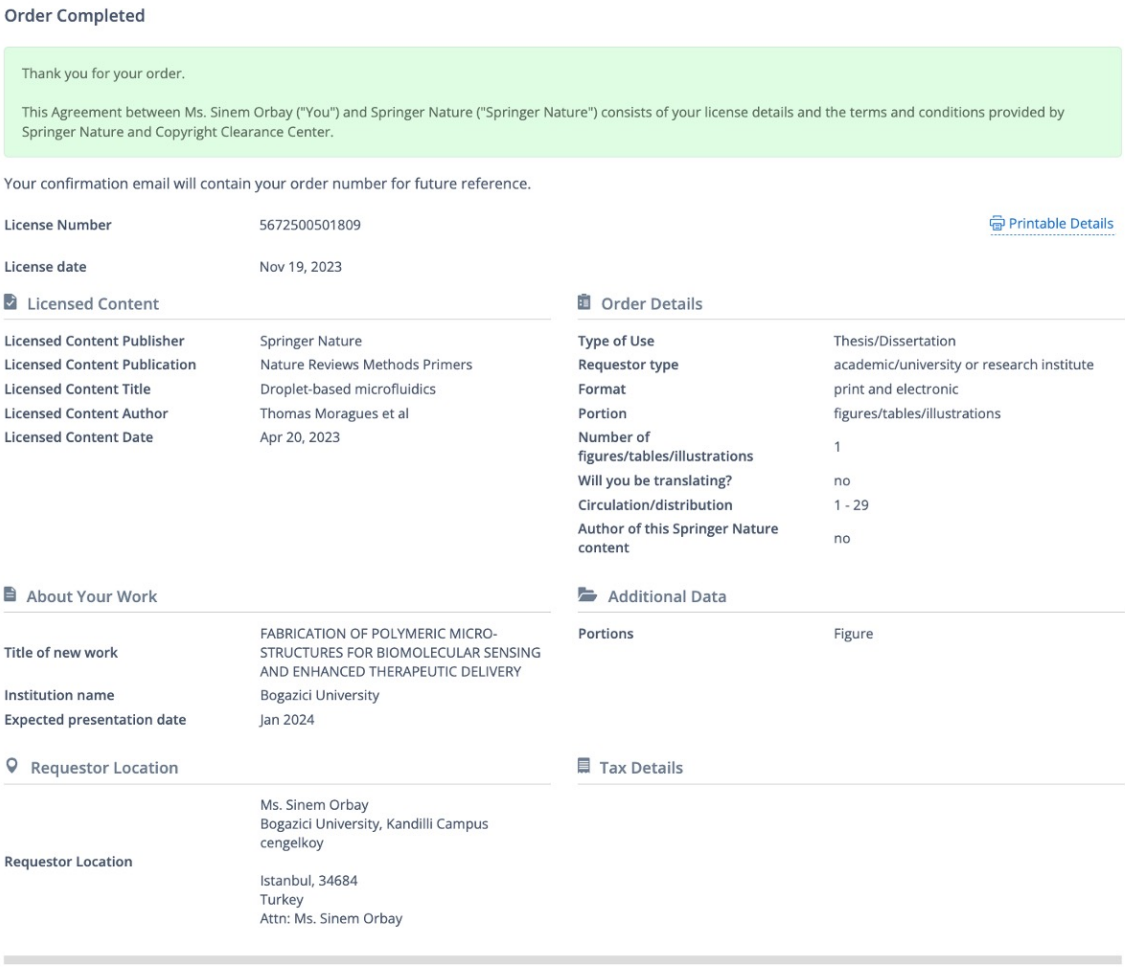

Order Completed

Thank you for your order.

This Agreement between Ms. Sinem Orbay ("You") and Springer Nature ("Springer Nature") consists of your license details and the terms and conditions provided by Springer Nature and Copyright Clearance Center.

Your confirmation email will contain your order number for future reference.

License Number	5672500501809
License date	Nov 19, 2023

Printable Details

Licensed Content

Licensed Content Publisher	Springer Nature
Licensed Content Publication	Nature Reviews Methods Primers
Licensed Content Title	Droplet-based microfluidics
Licensed Content Author	Thomas Moragues et al
Licensed Content Date	Apr 20, 2023

Order Details

Type of Use	Thesis/Dissertation
Requestor type	academic/university or research institute
Format	print and electronic
Portion	figures/tables/illustrations
Number of figures/tables/illustrations	1
Will you be translating?	no
Circulation/distribution	1 - 29
Author of this Springer Nature content	no

About Your Work

Title of new work	FABRICATION OF POLYMERIC MICRO-STRUCTURES FOR BIOMOLECULAR SENSING AND ENHANCED THERAPEUTIC DELIVERY
Institution name	Bogazici University
Expected presentation date	Jan 2024

Additional Data

Portions	Figure

Requestor Location

Requestor Location	Ms. Sinem Orbay Bogazici University, Kandilli Campus cengelkoy Istanbul, 34684 Turkey Attn: Ms. Sinem Orbay

Tax Details

Figure B.6 Copyright permission for Figure 1.12 from Ref. [63].

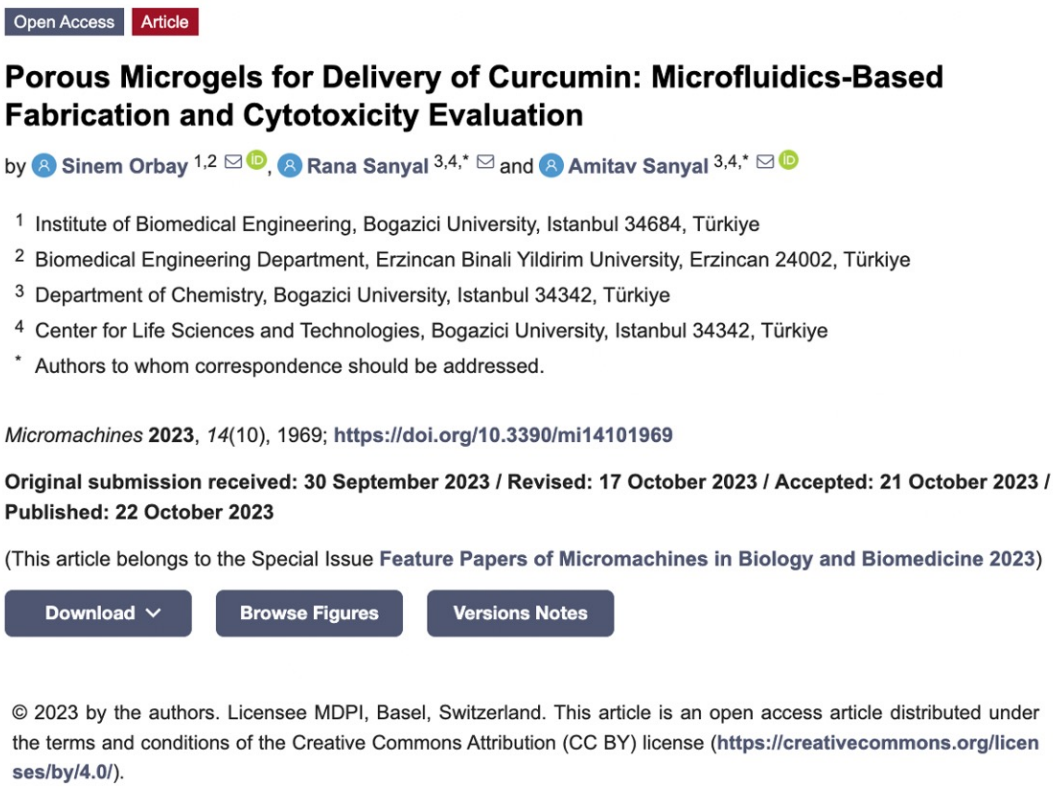

Open Access Article

Porous Microgels for Delivery of Curcumin: Microfluidics-Based Fabrication and Cytotoxicity Evaluation

by Sinem Orbay [1,2], Rana Sanyal [3,4,*] and Amitav Sanyal [3,4,*]

[1] Institute of Biomedical Engineering, Bogazici University, Istanbul 34684, Türkiye
[2] Biomedical Engineering Department, Erzincan Binali Yildirim University, Erzincan 24002, Türkiye
[3] Department of Chemistry, Bogazici University, Istanbul 34342, Türkiye
[4] Center for Life Sciences and Technologies, Bogazici University, Istanbul 34342, Türkiye
[*] Authors to whom correspondence should be addressed.

Micromachines **2023**, *14*(10), 1969; **https://doi.org/10.3390/mi14101969**

Original submission received: 30 September 2023 / Revised: 17 October 2023 / Accepted: 21 October 2023 / Published: 22 October 2023

(This article belongs to the Special Issue **Feature Papers of Micromachines in Biology and Biomedicine 2023**)

Download Browse Figures Versions Notes

© 2023 by the authors. Licensee MDPI, Basel, Switzerland. This article is an open access article distributed under the terms and conditions of the Creative Commons Attribution (CC BY) license (**https://creativecommons.org/licenses/by/4.0/**).

Figure B.7 Copyright permission for Chapter 3 [84].